WIM-based Modelling of Traffic Load Scenarios for Extreme Load Effects in Long-span Bridges

Doctoral Thesis

Doctoral thesis performed by:
Xuejing Wang

Directors:
Prof. Dr. Joan Ramon Casas
Prof. Dr. Xin Ruan

Doctoral program:
Construction Engineering

Barcelona, Spain
July, 2023

UNIVERSITAT POLITÈCNICA DE CATALUNYA
BARCELONATECH
Departamento de Ingeniería Civil y Ambiental

UNIVERSITAT POLITÈCNICA DE CATALUNYA
BARCELONATECH

PhD program in Construction Engineering

WIM-based Modelling of traffic Load Scenarios for Extreme Load Effects in Long-span Bridges

Doctoral thesis by:

Xuejing Wang

Thesis advisor:

Joan Ramon Casas, Xin Ruan

Department of Civil and Environmental Engineering

Barcelona, July, 2023

Acknowledgments

Across the campus, spring is showing up as trees and flowers bloom. In this season of new beginnings, I've finished my PhD thesis. The journey started with worries and doubts, but they turned into a deep understanding of my topic. Every word written is a symbol of the hard work I've put in over the last few years, and the guidance I've received from many supervisors and friends.

I want to first thank my supervisor, Prof. Joan Ramon Casas and Prof. Xin Ruan. They introduced me to the field of bridges and helped me with every step of my thesis. Their profound knowledge, exacting standards, and vast practical experience will serve as an enduring source of inspiration and learning in my future pursuits. I wish to express my earnest appreciation and respect to them both.

Next, I want to thank Prof. Xiaoying Zhou from Southeast University and Dr. Junyong Zhou from Guangzhou University. Their help and guidance while writing my thesis was invaluable. Their excitement for exploring different fields and their deep love for engineering has inspired me. I'm truly grateful to them.

During my time as a doctoral student, I have been the beneficiary of the nurturing environment provided by the doctoral office of the Universitat Politècnica de Catalunya, its pristine campus, and its conducive academic atmosphere. I wish to express my heartfelt gratitude and deep respect to the staff and students of the university.

My gratitude also extends to my colleagues: Hang Su, Tian Peng, Zeren Jin, Yue Li, Yiping Mai, Jun Song, Yi Wei, and Xinying Zhao. Their help with my research and their dedication to learning have set a great example for me.

I must acknowledge my husband, Dr. Mingyang Zhang, for his unwavering support, encouragement, and guidance in my academic endeavors. His presence in my life has been a beacon, dissipating the fog of uncertainty and doubt.

Finally, I want to thank my parents for their love and support. They've been there for me when I needed them most. I hope finishing this thesis brings them as much happiness as they've given me.

Abstract

The traffic live load is one of the most important variable actions for the design of new and the assessment of existing bridges. Due to the spatial and temporal high randomness and various weights of vehicle loading, there are massive loading scenarios during bridge operation. It is challenging to model all the actual values of traffic load on bridges in a deterministic way. Probabilistic concepts were widely employed to consider the numerous sources of uncertainty in the traffic model. Meanwhile, the measured traffic data captured by Weigh-in-Motion (WIM) technologies has been widely used in the traffic load simulation.

The WIM data has made it possible to analyze the traffic load of a specific site. However, previous traffic load models have shortcomings when it comes to representing the complicated spatial distribution of traffic loads on the bridge deck quantitatively. The probability of the spatial distribution pattern of vehicles on long-span bridge decks provoking maximum load effect (LE) is vital for assessing bridge safety and also helps to understand the performance of bridges under vehicular loading.

This Ph.D. thesis proposes a probabilistic model for vehicle scenarios leading to extreme load effects (LEs (maximum-response-per-day event)) for long-span bridges. Meanwhile, a Bayesian inference-based approach for its updating according to the actual traffic conditions was developed with the objective of taking into consideration the changing characteristic of traffic, both in density and weight of the heavy vehicles. This thesis mainly contains three aspects of research.

Firstly, a probabilistic Gaussian mixture model for heavy vehicle scenarios on the bridge deck under free-flow condition is proposed for long-span bridges based on collected WIM data. A non-stationary Poisson process is utilized to simulate the uneven occurrence of heavy vehicles in different lanes, and it is assumed that they are located within the artificially defined cells on the bridge deck. Then, Nataf transformation is employed to consider the correlation of gross vehicle weights (GVWs) within close range in the same lane. The Monte Carlo method is employed with the proposed probabilistic model for modeling complex spatial distributions of heavy vehicles.

Secondly, due to the fact that the traffic conditions are affected by the surroundings and will typically vary and also unpredictably change during the lifetime of long-span bridges, the prior site-specific traffic load spatial distribution model and its updated posterior version considering actual traffic conditions via Bayesian inference are proposed. A Bayesian inference approach is developed for the updating of spatial load distribution in the extremes LE scenarios utilizing the particle filter (PF). The updated load profile and corresponding load intensity for different traffic states proposed in this thesis, can be the basis to define accurate traffic load models for long-span bridges.

Finally, the application of the proposed methodology to a real bridge is presented. The effects of correlation in GVWs and stationarity of vehicle distribution location on the structural responses are investigated and discussed. The load responses calculated by the proposed model and Monte Carlo method for different effects are compared with the values derived from the code model. The results show that with the increase of the correlation level of the neighboring GVWs, the simulated responses are more prone to get extreme values, which means an increasing probability of the most unfavorable spatial distribution of on-bridge vehicles. The same results are also found under the non-stationary simulation state for vehicle location. The non-stationary Poisson process provides an efficient, highly feasible method, which is also on the safe side, for simulating the vehicle spatial distribution for specific effects. Meanwhile, by employing the Bayesian inference approach for the updating of spatial load distribution, the traffic load response of long-span bridges in operation can be accurately estimated while considering the changes in traffic states. It shows the superior performance in describing complex spatial distribution updating problems for traffic load modeling.

Keywords: Long-span bridges; Traffic load model; Extreme load effect; Heavy vehicle scenarios; Gross vehicle weight; Vehicle spatial distribution; Bayesian inference; Particle filter;

Resumen de la Tesis

La sobrecarga de tráfico es una de las acciones variables más importantes en el diseño de puentes nuevos y la evaluación de los existentes. Debido a la enorme variabilidad tanto espacial como temporal y los distintos tipos y pesos de los vehículos, existen una infinidad de escenarios de carga de tráfico durante la etapa de servicio. Es inviable intentar modelizar todas las posibles combinaciones y escenarios de manera determinista. Por ello, los métodos probabilísticos se han utilizado ampliamente para poder considerar las numerosas incertidumbres presentes en un modelo de sobrecarga de tráfico. Por otro lado, información relativa al tráfico obtenida mediante técnicas de pesaje en movimiento (weigh-in-motion, WIM) se han utilizado también de manera profusa en la simulación de la acción del tráfico.

La técnica WIM ha hecho posible el análisis de las acciones de tráfico en un entorno específico. Sin embargo, los modelos de tráfico existentes presentan problemas cuando se trata de modelizar la complicada distribución de las cargas de los vehículos en el puente de manera cuantitativa con el objetivo de obtener valores máximos de respuesta. La probabilidad de distribuciones espaciales de los vehículos dentro del tablero de un puente de gran luz, provocando un valor máximo de un determinado esfuerzo o deformación, resulta vital para calcular su seguridad estructural, a la vez que sirve de ayuda para comprender la respuesta de dichos puentes frente a la acción del tráfico.

En la presente tesis doctoral se propone un modelo probabilista de distribución de vehículos en el tablero de un puente de gran luz que dan lugar a valores extremos de la respuesta en esfuerzos y flechas (máxima respuesta diaria). Por otra parte, se propone también utilizar inferencia Bayesiana para la actualización del mismo de acuerdo con las condiciones reales de tráfico de un determinado lugar con el objetivo de acomodar el modelo a las situaciones cambiantes del tráfico, tanto en volumen como en distribución de pesos de los vehículos pesados. Por ello, la tesis contiene 3 aspectos principales:

En primer lugar, se define un modelo probabilístico mixto Gaussiano para los escenarios de vehículos pesados en el tablero de puentes de gran luz en condiciones de tráfico fluído, basado en datos reales de tráfico obtenidos de WIM. Se propone un proceso estocástico de Poisson no estacionario para simular la no uniformidad en la distribución de vehículos pesados en distintos carriles y dentro del mismo carril, asumiendo que los mismos se sitúan en determinadas posiciones dentro del tablero. A continuación, se utiliza una transformación de Nataf para tener en cuenta la correlación de pesos de vehículos pesados (GVW) entre vehículos cercanos en el mismo carril. El modelo propuesto se combina con el método de Monte Carlo para simular las complejas distribuciones espaciales de los vehículos en el puente.

En segundo lugar y dado que las condiciones actuales de tráfico en un puente en particular están afectadas por distintos factores y variarán durante la vida útil del puente, el modelo “a priori” de

distribución espacial de tráfico para el puente en concreto, así como el modelo actualizado “a posteriori” se obtienen mediante inferencia Bayesiana utilizando el método de filtro de partículas (PF). El modelo actualizado de distribución espacial del tráfico así como la intensidad de la carga propuestos en esta tesis son la base para desarrollar modelos de tráfico futuros más precisos para el caso particular de puentes de gran luz.

Finalmente, se aplica la metodología propuesta al caso de un puente real. Los efectos de la correlación de pesos en los vehículos pesados, así como la estacionariedad o no de la distribución de dichos pesos dentro del tablero son estudiados. Los valores característicos de respuesta máxima para determinadas variables obtenidos mediante el modelo propuesto y la simulación de Monte Carlo se comparan con los que se prescriben tanto en el código de acciones en China como en Estados Unidos y Europa. Los resultados ponen de manifiesto que los valores máximos de respuesta aumentan con el incremento de la correlación entre pesos de vehículos pesados cercanos. Asimismo, se obtiene valores máximos superiores si se supone un proceso de tipo Poisson no estacionario para la distribución espacial de los vehículos pesados. Por ello, dicho proceso se considera como el más preciso, y del lado seguro, para la simulación de la distribución espacial de vehículos pesados. Por otro lado, a través de la inferencia Bayesiana para la actualización de dicha distribución espacial, se puede estimar de manera precisa la respuesta frente al tráfico teniendo en cuenta las variaciones en las características del mismo.

Palabras clave: puentes de gran luz, modelo de sobrecarga de tráfico, respuesta máxima, vehículo pesado, distribución espacial de tráfico, inferencia Bayesiana, Filtro de partículas

TABLE OF CONTENTS

Acknowledgments V

Abstract VI

Resumen de la Tesis VIII

TABLE OF CONTENTS X

LIST OF TABLES XIII

LIST OF FIGURES XIV

CHAPTER 1 Introduction ***1***

1.1 Motivation 1

1.2 Objectives 2

1.3 Thesis organization 4

CHAPTER 2 State of the art ***6***

2.1 Vehicle load measurement 6

2.2 Traffic load modeling 9

2.3 Site-specific traffic load model and its updating 11

2.4 Identifying gaps in the existing research 12

CHAPTER 3 Probabilistic model of traffic scenarios for extreme LEs in long-span bridges ***15***

3.1 Introduction 15

3.2 Model of heavy vehicle distribution 15

3.3 Description of scenarios of extreme LE based on WIM Data 18

3.4 Modeling of vehicle location distribution by Poisson process 23

3.5 Modeling of heavy vehicles weight 25

3.5.1 GMM and determination of components number 25

3.5.2 Correlation of heavy vehicles and Nataf transformation 26

3.6 Extreme value theory for the return period extrapolation 29

3.7 Conclusions 29

CHAPTER 4 Application of extreme response scenario probabilistic model ***31***

4.1 Introduction 31

4.2 Description of the cable-stayed bridge 31

4.3 Scenarios of extreme LE 32

4.3.1 Heavy vehicle location distribution 33

4.3.2 Heavy vehicle weight and parameters 36
4.3.3 Monte Carlo simulation of the scenarios model 36
4.4 Impacts of ignoring light vehicles and moving vehicle-centroid into cell on LE 40
4.5 Impacts of stationarity and correlation in vehicle weight on extreme LE 45
4.6 Comparison of load model effect with Design Codes 48
4.7 Conclusions 51
CHAPTER 5 Validation and extended applications of the scenario probabilistic model 52
5.1 Introduction 52
5.2 Validation of the proposed model 53
5.2.1 Validation of loading scenarios 53
5.2.2 Validation of LEs 55
5.3 Congestion scenario simulation by the proposed model 60
5.4 Conclusions 72
CHAPTER 6 Site-specific traffic load model of long-span bridges via Bayesian updating 73
6.1 Introduction 73
6.2 Definition of the site-specific traffic load model 74
6.3 Effect of the shape of influence line of long-span bridges in the load model 75
6.4 Selection of the form of the site-specific load model 78
6.5 Selection of load intensity 80
6.6 Bayesian approach for updating traffic scenarios 81
6.7 Conclusions 89
CHAPTER 7 Application of the site-specific traffic model and its Bayesian updating 90
7.1 Application of Bayesian inference for updating the vehicle spatial distribution of extreme scenarios 90
7.2 Traffic load model updated for different traffic states 95
7.3 Conclusions 103
CHAPTER 8 Conclusions and future research 104
8.1 Conclusions 104
8.2 Future research 106
References 107
Appendix 1. List of acronyms 115
Appendix 2. Results for each effect in the case study 116
Appendix 3. Extended application of the proposed extreme response scenario probabilistic model 129

LIST OF TABLES

TABLE 3-1 ACCURACY AND FILTRATION CRITERIA OF WIM DATA. 19
TABLE 4-1 THE PARAMETERS OF POISSON PROCESSES FOR VEHICLE LOCATION MODEL (VEH) (EFFECT 1). 33
TABLE 4-2 PARAMETER OF SIMULATED GMM (TONNES). 36
TABLE 4-3 COMPARISON OF THE RESPONSES DERIVED FROM SIMULATION LOAD AND CODES FOR DIFFERENT EFFECTS OF THE INVESTIGATED BRIDGE. 51
TABLE 5-1 ACCURACY AND FILTRATION CRITERIA OF WIM DATA. 54
TABLE 5-2 PARAMETER COMPARISON OF SIMULATED AND ORIGINAL GMM (TONNES). 54
TABLE 5-3 COMPARISON OF POISSON PARAMETERS FROM THE PROPOSED MODEL AND SIMULATED WIM DATA (ARTIFICIAL WIM DATA BY CA METHOD) (ALL LANES) (VEH). 54
TABLE 6-1 LOAD FORMS FOR THE OVERALL DESIGN IN DIFFERENT CODES. 79
TABLE 6-2 CORRECTION FACTORS FOR DIFFERENT LES AND TRAFFIC CONDITIONS. 81
TABLE 7-1 CORRECTION FACTORS FOR DIFFERENT LES AND TRAFFIC CONDITIONS. 100
TABLE 7-2 LOAD INTENSITY AND LOAD FORM SCHEMATIC DIAGRAM OF TRAFFIC MODEL FOR DIFFERENT STRUCTURAL EFFECTS. 102
TABLE 7-3 TOTAL LOAD ON BRIDGE DECK OF PROPOSED TRAFFIC MODEL. 102

LIST OF FIGURES

FIGURE 1-1 THE BRIEF LOGIC OF THE THESIS. 3
FIGURE 3-1 (A) VEHICLE DISTRIBUTION OF SCENARIOS OF EXTREME LE; (B) HEAVY VEHICLE DISTRIBUTION WITH CELL STRUCTURE OF SCENARIOS OF EXTREME LE MODEL; (C) CELL NUMBERING AND MATHEMATICAL REPRESENTATION. 17
FIGURE 3-2 MODELLING PROCESS OF EXTREME RESPONSE SCENARIO. 18
FIGURE 3-3 A SAMPLE OF VEHICLE SCENARIO OF EXTREME LE. 20
FIGURE 3-4 STATISTICS OF CELLS OCCUPIED BY HEAVY VEHICLES IN (A) NORMAL PROBABILITY PAPER; (B) INNER LANES; (C) OUTER LANES. 22
FIGURE 3-5 SAMPLE DATA AND MODELLING OF GVW IN (A) NORMAL PROBABILITY PAPER; (B) INNER LANES; (C) OUTER LANES. 23
FIGURE 3-6 PROBABILITIES OF A CELL TO BE OCCUPIED BY A HEAVY VEHICLE IN A MAXIMUM LE SCENARIO OF (A) INNER LANES; (B) OUTER LANES (EFFECT 1). 24
FIGURE 4-1 CONFIGURATION OF THE LONG-SPAN CABLE-STAYED BRIDGE WITH THE INFLUENCE LINE OF EFFECT AFC (UNIT: M). 32
FIGURE 4-2 POISSON DISTRIBUTION PARAMETERS FOR EACH CELL AND THE AVERAGE VALUES FOR DIFFERENT INTENSITY LEVEL AREAS OF (A) INNER LANES; (B) OUTER LANES. 34
FIGURE 4-3 CELL CLASSIFICATION OF LOAD INTENSITY LEVEL ACCORDING TO STATISTICS. 34
FIGURE 4-4 SAMPLES OF SIMULATED HEAVY VEHICLES DISTRIBUTION FOR (A) NON-STATIONARY PROCESS; (B) STATIONARY PROCESS. 35
FIGURE 4-5 RELATIONSHIP BETWEEN AIC AND NUMBER OF COMPONENTS. 36
FIGURE 4-6 SIMULATION SAMPLES OF GVWS FROM DIFFERENT CORRELATION LENGTH *D* FOR OUTER LANE. 37
FIGURE 4-7 SIMULATED SAMPLES OF SCENARIOS FOR (A) STATIONARY PROCESS LOCATION DISTRIBUTION; (B) NON-STATIONARY PROCESS LOCATION DISTRIBUTION 39
FIGURE 4-8 IMPACT ON LE BY IGNORING LIGHT VEHICLES. 41
FIGURE 4-9 RELATIVE ERROR OF LE CAUSED BY MOVING VEHICLES INTO CELL: (A) NORMAL PROBABILITY PAPER; (B) HISTOGRAM. 42
FIGURE 4-10 ERROR BOXPLOT OF MOVING HEAVY VEHICLES INTO CELLS (CELL LENGTH = 20 M). 43
FIGURE 4-11 ERROR BOXPLOT OF MOVING HEAVY VEHICLES INTO CELLS (CELL LENGTH = 10 M). 43
FIGURE 4-12 EXTREME RESPONSE SCENARIOS FOR DIFFERENT EFFECTS WITH DIFFERENT CELL LENGTHS. 44
FIGURE 4-13 PROBABILITY DENSITY AND FITTING OF THE SIMULATION RESULTS FOR NON-STATIONARY AND STATIONARY PROCESSES WHEN THE GVWS ARE UNCORRELATED: (A) GUMBEL PROBABILITY PAPER; (B) HISTOGRAM. 45
FIGURE 4-14 SIMULATED CDFS OF EXTREMUM OF AXIAL FORCE FOR NON-STATIONARY PROCESS (A) GUMBEL PROBABILITY PAPER; (B) OVERALL CDF; (C) TAIL BEHAVIOR. 47
FIGURE 4-15 QUANTILE VALUE OF EFFECT EXTREMUM OF SIMULATED DATA BY (A) NON-STATIONARY PROCESS; (B) STATIONARY PROCESS. 48
FIGURE 4-16 RATIO OF SIMULATED EXTREME RESPONSE TO CHINESE CODE VALUE FOR DIFFERENT EFFECTS WITH *D* = 100 M AND NON-STATIONARY PROCESS. 49
FIGURE 5-1 COMPARISON OF THE UPPER TAIL OF EFFECT 1 FROM PROPOSED MODEL AND SIMULATED WIM DATA (ARTIFICIAL WIM DATA BY CA METHOD). 56
FIGURE 5-2 COMPARISON OF THE UPPER TAIL OF EFFECT 2 FROM PROPOSED MODEL AND SIMULATED WIM DATA (ARTIFICIAL WIM DATA BY CA METHOD). 56
FIGURE 5-3 COMPARISON OF THE UPPER TAIL OF EFFECT 3 FROM PROPOSED MODEL AND SIMULATED WIM DATA (ARTIFICIAL WIM DATA BY CA METHOD). 57

FIGURE 5-4 COMPARISON OF THE UPPER TAIL OF EFFECT 4 FROM PROPOSED MODEL AND SIMULATED WIM DATA (ARTIFICIAL WIM DATA BY CA METHOD). 57
FIGURE 5-5 COMPARISON OF THE UPPER TAIL OF EFFECT 5 FROM PROPOSED MODEL AND SIMULATED WIM DATA (ARTIFICIAL WIM DATA BY CA METHOD). 58
FIGURE 5-6 BOX PLOT OF GROSS WEIGHT ON BRIDGE DECK OF SCENARIO OF MAXIMUM-PER-DAY EVENT FROM PROPOSED MODEL AND SIMULATED WIM DATA. 59
FIGURE 5-7 HISTOGRAM OF OCCURRENCE TIME OF THE EXTREME SCENARIOS. 61
FIGURE 5-8 THE AVERAGE HOURLY TRAFFIC AND RATIO OF RESPONSE TO D60 FOR EXTREME SCENARIOS DURING DAYTIME. 61
FIGURE 5-9 THE GVW DISTRIBUTION OF HIGH HOURLY TRAFFIC VOLUME SCENARIOS. 62
FIGURE 5-10 THE (A) AVERAGE SPEED HISTOGRAM; (B) TRAFFIC FLOW HISTOGRAM FOR EACH HOUR; (C) GVW DISTRIBUTION HISTOGRAM OF THE GENERATED CONGESTED TRAFFIC. 63
FIGURE 5-11 THE PROBABILITY OF OCCURRENCE OF VEHICLES IN EACH CELL ON THE OUTER LANES. 65
FIGURE 5-12 PROBABILITIES OF A CELL TO BE OCCUPIED BY A VEHICLE IN AN EXTREME RESPONSE SCENARIO AND CONGESTED FLOW. 66
FIGURE 5-13 DATA AND FITTING OF GVW IN (A) NORMAL PROBABILITY PAPER; (B) INNER LANES; (C) OUTER LANES. 67
FIGURE 5-14 SAMPLES OF EXTREME RESPONSE SCENARIOS OF CONGESTION FLOW (LOAD EFFECT 1). 68
FIGURE 5-15 COMPARISON OF IGNORING LIGHT VEHICLES AND NOT IGNORING LIGHT VEHICLES OF A CONGESTION SCENARIO. 69
FIGURE 5-16 SAMPLES OF SIMULATED CONGESTION SCENARIOS BY THE PROPOSED MODEL. 70
FIGURE 5-17 PROBABILITY DENSITY OF THE RATIO OF LE FROM SIMULATED CONGESTION SCENARIOS TO CHINESE CODE VALUE. 71
FIGURE 6-1 FLOWCHART OF THE MODELING PROCEDURE OF SITE-SPECIFIC TRAFFIC LOAD MODEL. 74
FIGURE 6-2 CONFIGURATION OF THE SUTONG BRIDGE WITH THE INFLUENCE LINES OF THREE EFFECTS (UNIT: M). 76
FIGURE 6-3 OCCURRING PROBABILITY OF HEAVY VEHICLE IN THE EXTREME SCENARIOS ON THE OUTER LANE FOR DIFFERENT EFFECTS OF A LONG-SPAN CABLE-STAYED BRIDGE WITH A MAIN SPAN OF 1088 M. 78
FIGURE 6-4 DIFFERENT VEHICLE SEQUENCE LOAD FORMS. 79
FIGURE 6-5 PROCEDURE OF PF FOR UPDATING SPATIAL RANDOM FIELDS BASED ON OBSERVED DATA. 87
FIGURE 6-6 SMOOTHING PROCESS OF SAMPLES FOR SPATIAL UPDATING. 88
FIGURE 6-7 SCHEMATIC PLOT OF THE RESAMPLING PROCESS. 89
FIGURE 7-1 CONFIGURATION OF THE LONG-SPAN CABLE-STAYED BRIDGE WITH THE INFLUENCE LINES OF FIVE EFFECTS AND DEFINITION OF THE 3 DIFFERENT INTENSITY AREAS (UNIT: M). 91
FIGURE 7-2 OBSERVATION VECTOR ON THE BRIDGE DECK AND MATRIX Λ REPRESENTING THE OBSERVED LOCATIONS ON THE LANES. 94
FIGURE 7-3 DISTRIBUTION OF VEHICLE LOAD INTENSITY FOR OUTER LANE BEFORE AND AFTER UPDATING USING FOUR TRAFFIC STATES. 95
FIGURE 7-4 EFFECT RATIO TO D60 FROM OBSERVED DATA WITH DIFFERENT AADT GENERATED BY CA METHOD. 97
FIGURE 7-5 PDF OF GVWS FROM OBSERVED DATA WITH DIFFERENT GVWS DISTRIBUTION GENERATED BY CA METHOD. 97
FIGURE 7-6 UPDATED LOAD FORM PROFILE OF TRAFFIC MODEL FOR FIVE EFFECTS AND AADT EQUAL TO 100000. 98
FIGURE 7-7 RESPONSE RATIO OF UPDATED RESULTS TO ORIGINAL SCENARIO FOR DIFFERENT TRAFFIC STATES. 99
FIGURE 7-8 INFLUENCE OF GVW STATISTICAL DISTRIBUTION ON THE RESPONSE RATIO OF UPDATED RESULTS TO ORIGINAL SCENARIO. 100
FIGURE 7-9 TOTAL LOAD ON THE BRIDGE DECK OF THE PROPOSED TRAFFIC MODEL AND D60. 102

CHAPTER 1 Introduction

1.1 Motivation

The structural performance and durability of long-span bridges are negatively impacted by external loads, environmental factors, and the degradation of materials over time. These issues lead to costly maintenance and performance improvement efforts for bridge structures (Chen et al., 2017). Statistical data reveals that 26% of the 610,000 bridges in service in the United States exhibit structural defects, costing $76 billion annually for maintenance and repair; Almost 50% of the 1,000,000 bridges in the European Union have been in service for over 50 years, thereby demanding considerable annual financial commitments towards their maintenance; In Australia 70% of the 26,000 bridges have been in service for more than 40 years, requiring significant maintenance investments totalling A$18 billion annually (Zhu, 2017). Over the past three decades, China has witnessed extensive bridge construction and become the country with the largest number of bridges in the world, reaching more than 1 million, leading to a progressive rise in operation and maintenance expenses. Improving the assessment accuracy of bridges is of great significance to reduce severe damage to bridge structures, preventing structural failures, extending service life, and optimizing management and maintenance costs.

For the assessment and management of long-span bridges, vehicle load is a very crucial variable load because its substantial uncertainty and high load level can pose many challenges to structural safety. In recent years, researchers have conducted many studies around vehicle load models for long-span bridges, especially site-specific vehicle load models that directly affect the structural response of bridges. Soriano et al. (2017) found that one heavy truck, two trucks traveling side by side or following in the same lane will provide the largest response of multi-lane bridges with spans less than 60 m. Meanwhile, the research of Caprani et al. (2008) shows that it is not realistic to believe that two trucks events drive the design of short to medium-span bridges. Clearly four trucks events play an important role. However, long-span bridges have more diverse and complicated extreme response scenarios (Guo & Caprani, 2019; Hwang & Kim, 2019; Chen & Wu, 2011; Xu et al., 2012). Meanwhile, the changes in the temporal-spatial characteristics of traffic loads are not always reasonably considered in the design specifications due to the rapid

development of transportation industry. Several traditional traffic load models as stated in codes were primarily developed for bridges with small or medium spans (Ruan et al., 2017; Enright & O'Brien, 2013; Nowak et al., 2010). Based on the above consensus, researchers have developed simulations and modeling of site-specific traffic flows for long-span bridges, while many researchers found that the congestion state is the most critical factor affecting the structural effects of long-span bridges (Ruan et al., 2017; Lipari et al., 2017; Getachew & O'Brien, 2007; He et al., 2022; Caprani, 2012; Guo & Caprani, 2019; Hwang & Kim, 2019).

In summary, previous studies have confirmed that the traditional traffic load models derived for short and medium-span bridges are not applicable to site-specific traffic assessment of long-span bridges. Also, most of the current site-specific load models for long-span bridges have been devoted to simulating site-specific traffic flows, and a significant portion of the studies have focused on congested traffic flows. Few studies have been conducted on vehicular load extreme response scenarios of free flow on the bridge deck. Extreme response scenario refers to the on-bridge deck vehicles distribution, which can induce extreme response values for structural effects. The reason for the focus on free-flow is that the author found that certain free-flowing traffic with low volumes and high vehicle weight levels (usually readily available at night) are equally important for the safety assessment of long-span bridges, but lack the attention they deserve.

Therefore, it is essential to focus on the site-specific traffic load-based vehicular load scenarios on bridge deck that can induce extreme response values for structural effects for long-span bridges, and develop the extreme response scenarios of vehicular load for free-flow conditions to improve their performance assessment. Additionally, the rapid advancements in sensor and computer technologies have enabled accurate traffic data measurement, making precise estimation of bridge vehicle load responses a research priority (Leahy et al., 2015; O'Brien et al., 2015).

1.2 Objectives

Based on the identified gaps and problems in the existing models of traffic load for long-span bridges, as summarized in the previous section and fully presented in the state of the art (chapter2), the objective of this work is to propose a probabilistic model for extreme response scenarios of vehicular load on bridge deck in free-flow conditions for long-span bridges, then, construct a site-specific traffic load model based on the simulation results of the probabilistic model, and the

updating method for this site-specific model is also proposed. The detailed objectives of this thesis are presented as follows:

Objective 1: To develop a probabilistic load model for heavy-vehicle extreme response scenarios leading to extreme LEs on long-span bridges. To implement the proposed method to simulate vehicle scenarios corresponding to maximum-response-per-day events under free-flow traffic conditions. Ensure the applicability of the proposed scenario probabilistic model to long-span bridge assessment by focusing on free-flow traffic conditions.

Objective 2: A site-specific traffic load model is proposed based on the simulation results of the probabilistic model in Objective 1. The model is effective in deriving the maximum LEs for long-span bridges during the reference period when free-flow traffic conditions are considered.

Objective 3: To develop a Bayesian inference approach for model updating, enabling the site-specific traffic load model to adapt to changing traffic conditions and provide more accurate predictions of maximum LEs.

The brief logic of the thesis is shown in Figure 1-1.

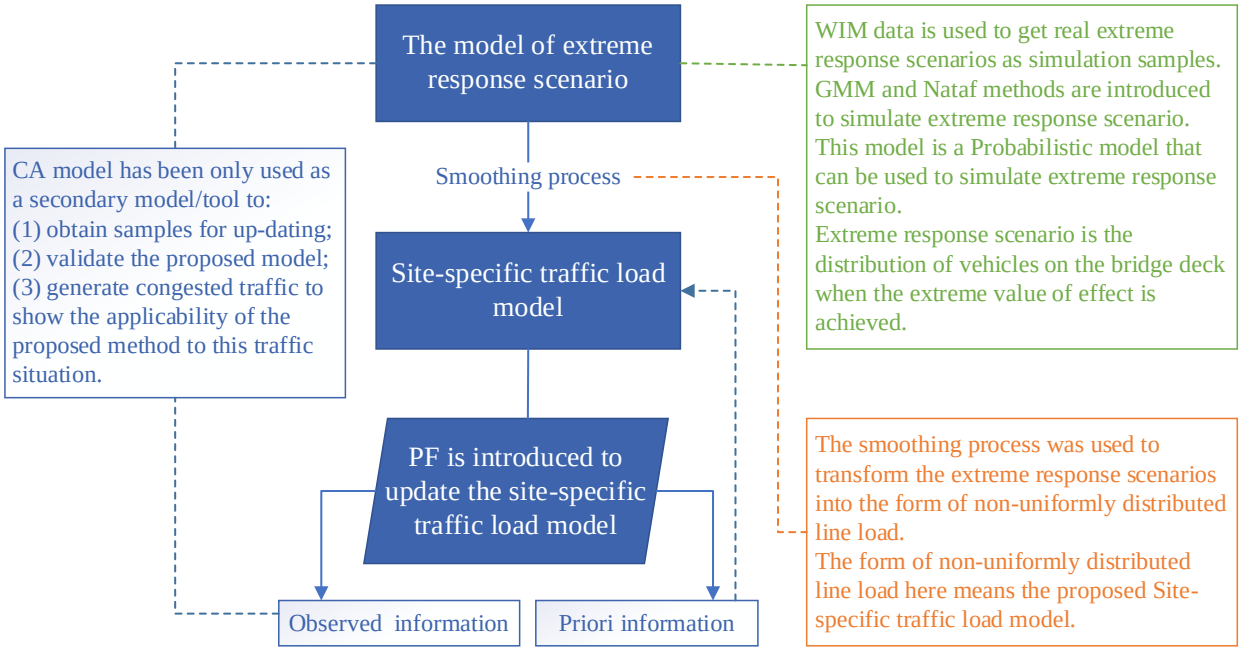

Figure 1-1 The brief logic of the thesis.

1.3 Thesis organization

Based on the proposed objectives and the corresponding methodology, this thesis is organized into eight chapters. Each chapter is thought to deal with particular topics related to the above objectives: state of the art, probabilistic model of traffic scenarios for extreme LEs in long-span bridges, application of extreme response scenario probabilistic model, validation and extended applications of the scenario probabilistic model, site-specific traffic load model of long-span bridges via Bayesian updating, and application of the site-specific traffic model and its Bayesian updating. The summary content of each chapter is as follows:

Chapter 2 is the state of the art. Firstly, the development of the vehicle load measurement technique is presented. Secondly, the state of the knowledge of the traffic load modeling method is comprehensively reviewed, and site-specific traffic load model and its updating is illustrated. Lastly, the gaps are detected according to the relate literature review.

Chapters 3 proposes a probabilistic model for vehicle distribution simulation of extreme response scenarios on the bridge deck, resulting in extreme LEs.

In Chapter 4, the proposed extreme response scenario model is applied to a real bridge. The numerical study is carried out on a long-span cable-stayed bridge to investigate the effects of correlation in GVWs and stationarity of vehicle distribution location on the structural responses. The load responses calculated by the proposed model and Monte Carlo method for different effects are compared with the values derived from code model.

In Chapter 5, the proposed extreme response scenario model is validated and applied to congested traffic flow to demonstrate the applicability of the model to congested traffic situations too, and to show that free flow and congested flow are of similar importance for the safety of long-span bridges.

Chapter 6 presents a site-specific traffic load model to derive the maximum LEs within a reference period for long-span bridges based on the simulation results of the extreme response scenario model proposed in Chapter 3. Then, Chapter 6 develops a Bayesian inference-based approach for the updating of the site-specific traffic load model according to the actual traffic conditions.

In Chapter 7, the proposed site-specific load model and its updating method are applied to a real bridge. The updated load profile and corresponding load intensity for different traffic states can be used as a reference for accurate traffic load assessment of long-span bridges under free-flow traffic.

Finally, in Chapter 8, the conclusions are given based on the above chapter analysis. In addition, the future research works are presented.

CHAPTER 2 State of the art

2.1 Vehicle load measurement

Advancements in measurement technology have facilitated real-time monitoring and early warning systems for bridge condition assessment. Historically, vehicle load and information measurements were acquired through rudimentary observation techniques. Manual observation methods were employed to gather traffic flow data, such as traffic volume and composition for specific road sections, while integral scales provided overall vehicle weight information (Cheng et al., 2006). However, these approaches were labor-intensive and failed to capture details such as axle weight and vehicle speed.

The subsequent evolution of static weighing technology enabled the measurement of vehicle information, including axle weight, vehicle weight, and wheelbase. Despite providing accurate data, static load-bearing methods necessitated stationary vehicles on weighing platforms, resulting in inefficiency and potential traffic congestion on busy road sections. Moreover, the large scale of static weighing platforms often led to overloaded vehicles taking alternate routes or unloading prior to inspection, compromising the authenticity of the acquired vehicle data.

Contemporary dynamic weighing methods have emerged, offering varying degrees of accuracy and application scopes, contingent upon the type and precision of the sensors employed (Jiang et al., 2011; Yang et al., 2006). In China, curved plate and weighing platform-based dynamic weighing systems rely on the principle that as a vehicle axle traverses the weighing platform, the resistance strain gauges within the platform's sensors form multiple sets of bridges that lose balance, generating an instantaneous unbalanced output signal. Analog-to-digital converters transform the signal into electrical signals, which are then processed to identify axle weight and axle distance information. These dynamic weighing systems also have some minor drawbacks such as: the quartz dynamic weighing system addresses these limitations by directly generating electrical signals under sensor pressure as a result of axle action, with signal amplification yielding axle weight and additional information.

The aforementioned dynamic weighing system is extensively employed in contemporary domestic highway weighing and charging systems. It is characterized by limitations on vehicle speed, extended operational life, and data accuracy suitable for charging systems. In this dynamic weighing system, vehicles traverse the weighing platform at a specific speed, resulting in a brief tire interaction time with the platform. The force exerted on the platform stems not only from the actual axle weight but also from numerous interfering factors, such as vehicle speed, vibration, and road surface irregularities.

The rapid development of modern sensing systems, including piezoelectric and fiber optic sensors, has facilitated their integration into dynamic weighing systems. This has enabled the accurate measurement of axle weight, wheelbase, vehicle weight, vehicle speed, as well as various traffic and vehicle information, such as vehicle spacing and time intervals, without impacting vehicle operation. This system, known as the Weigh in Motion (WIM) system, can measure vehicle and traffic flow data more precisely under high-speed vehicle operation conditions. The utilization of piezoelectric sensors offers a high signal-to-noise ratio, extended service life, and excellent impact resistance. Although road surface leveling and other factors may affect the measurement accuracy, the precision of the acquired data is sufficient for vehicle load response research in the field of dynamic vehicle weighing.

In 1992, the European Federation of Highway Systems Research Laboratories initiated the COST323 program in accordance with the European Commission for Transport procedural framework. Focusing on dynamic load monitoring of vehicles in motion, the primary objective of the program was to study, improve, and promote WIM technology. By 1998, 19 countries had joined the COST323 organization, and the accuracy of WIM data had improved significantly. Due to its ability to capture comprehensive traffic flow and vehicle load data, WIM technology is highly valued in load and load response research. Scholars have explored wheel weight signal detection, noise removal, and wheel weight value identification techniques to enhance the WIM system's measurement accuracy. Additionally, studies have investigated the installation of WIM systems on highway sections to enable comprehensive vehicle information monitoring systems, supporting overload management and extreme vehicle traffic congestion prediction. Research has also been conducted to calculate the damage state of bridges and highway pavements using measured WIM

data, predict the structures' remaining lifespan, and develop reinforcement management and maintenance strategy (Enright et al., 2013; Xia et al., 2014).

Although WIM technology can obtain accurate vehicle information due to efficient sensing systems, installing WIM systems on all highway sections is cost-prohibitive and impractical, and the equipment's durability for field use is limited. Bridge weigh in motion (BWIM) is a dynamic weighing system that measures a bridge's structural response under vehicle loading, using strain data to solve for vehicle axle weights and other information as an inverse problem. Moses (1979) first proposed the BWIM technique, which employed strain gauges to measure the strain history of a vehicle at the measurement point as it passed over a bridge. In conjunction with axle detection devices installed on the road, this method recorded the number of axles and vehicle speed to reconstruct complete vehicle information.

The BWIM technique first obtains the strain time course at the measurement point by calibrating the structural impact line using a standard vehicle passing over the bridge. The strain response time course under any traffic condition is then obtained based on this information, and the number of vehicles, vehicle type, and vehicle weight are inferred using certain principles and algorithms (Hitchcock et al., 2012; Chen et al., 2009; Wang et al., 2013). The BWIM technique offers several advantages over the WIM method: 1) high weighing accuracy for gross weight, but not as good performance as WIM for axle weight measurement; 2) vehicles can pass freely, with minimal impact from travel speed on measurement results; 3) no interference with traffic or road surfaces, and no need for traffic restrictions on the bridge deck during installation (require traffic restrictions on the roads underneath the bridge). However, BWIM technology also faces certain challenges, such as: the measurement data is significantly affected by the signal-to-noise ratio of the equipment.

Both WIM and BWIM technologies are unable to precisely determine the specific distribution of vehicles on a bridge or highway. Dynamic image recognition technology can process and analyze dynamic images captured from highway videos to identify the exact location and model of a vehicle, including parameters such as the number of axles, wheelbase, vehicle length, distance, license plate number, and others. By utilizing static vehicle data from toll stations and simulating the distribution of vehicle weight and axle weight, complete vehicle load and traffic flow information can be obtained. Currently, image recognition technology is in its early stages within the field of vehicle load research. Studies (Yu 2021; Bai 2021; Chen et al. 2013) have explored

violation vehicle monitoring, license plate information recognition, and vehicle identification on Sutong Bridge using image recognition technology, providing a foundation for its application in vehicle research.

WIM, BWIM, and image recognition are the primary methods for measuring vehicle and traffic loads. These technologies not only serve as data sources for traffic engineering management, vehicle overload control, bridge and highway pavement structure damage analysis, and lifespan prediction, but also contribute to the development of intelligent highway monitoring systems.

2.2 Traffic load modeling

The traffic live load is one of the most important variable actions for the assessment of existing bridges. Due to the spatial and temporal high randomness and various combinations of vehicle loads, there are massive loading scenarios during bridge operation. Therefore, it is challenging to model all of the actual values of traffic load on bridges in a deterministic way. Probabilistic concepts were widely employed to consider the numerous sources of uncertainty in the traffic model. In the literature on traffic load simulation, the measured traffic data which is usually captured by WIM technologies, has been widely used. WIM is a technology that can capture the free-flow traffic characteristics of a vehicle sequence without interfering with the traffic operation (Hallenbeck & Weinblatt 2004). The WIM data has made it possible to analyze the traffic load of a specific site (Chen et al. 2018; Getachew & O'Brien 2007; Leahy et al. 2015; O'Brien et al. 2015; Ruan et al. 2017; Anitori, Casas & Ghosn 2017; 2018). Monte Carlo method, as a common simulation method, is able to utilize the probability parameters deduced from WIM records and generate massive traffic scenarios, including vehicle combinations that were not recorded throughout the duration of measurement (Ruan et al. 2017; Enright & O'Brien 2013).

The changes in the temporal-spatial characteristics of traffic loads are not always reasonably considered in the design specifications due to the rapid development of transportation industry. Several traditional traffic load models as stated in codes were primarily developed for bridges with small or medium spans (Ruan et al. 2017; Enright & O'Brien 2013; Nowak, Lutomirska & Sheikh Ibrahim 2010). The codes include D60 (Ministry of Communications and Transportation [MOCAT], 2015), American Association of State Highway and Transportation Officials (AASHTO 2004), BS5400 (BSI, 2006), and Eurocode (EN, 2003). It should be noted that

AASHTO has extended the validity of the design live load, and the load model HL-93 is now used for all span lengths (Nowak, Lutomirska & Sheikh Ibrahim 2010). Nevertheless, the extension does not mean it is an accurate reflection of the actual traffic loading. The traffic load model for small and medium-span bridges may not be appropriate to be directly used for long-span bridges, or at least needs to be periodically updated based on current traffic before being applied to long-span bridges. For example, the Eurocode provides a set of comprehensive methods for traffic load representation on bridges with loaded length not exceeding 200 m (although it has been applied to several longer bridges, it is extremely conservative).

Therefore, numerous studies have been already devoted to the study of traffic LEs for long-span bridges and evaluating the applicability of traffic models in current codes to these bridges. Because the corresponding dominating traffic distribution scenarios are notably distinct, the responses to traffic load of bridges with long-loaded length are different from those with medium or small-loaded length (Caprani 2013; O'Brien 2012; Caprani, O'Brien & McLachlan 2008; Chen & Cai 2007). The traffic load of long-span bridges is governed by high-volume traffic or congestion. Because the span is long and there are numerous vehicles on several lanes, the influence of groups of trucks (platooning) is important for the structural assessment of long-span bridges (Chen & Wu 2011; Xu, Chen & Xia 2012). Due to the characteristic of influence lines of short and medium-span bridges, the maximum response of multi-lane bridges with short and medium-span is determined by several close traveling heavy trucks (Soriano, Casas & Ghosn 2017; Caprani et al. 2008). Comparatively, long-span bridges have more diverse and complicated extreme response scenarios.

Based on the long-term WIM data and congestion situation, Hwang and Kim, 2019 proposed a multi-lane load model for long-span bridges and found that the LE by the proposed congested model shows comparable values to AASHTO LRFD or Honshu-Shikoku bridge design code. Guo & Caprani (2019) focused on load patterning on long-span bridges and proposed a rational and practical load patterning method based on both congested and free-flow traffic. They suggested that the design model for long-span bridges can be obtained by reducing traffic load levels currently specified in the codes. Meanwhile, the cellular automaton (CA) method was a widely used tool to simulate the traffic flow (Ruan et al. 2017). With the aid of the CA method, complex

movements of vehicles, such as speed changes, lane changes, etc. (Ruan et al. 2017) can be simulated, and the generated long-term LEs can be utilized in the structural assessment.

2.3 Site-specific traffic load model and its updating

Bridge structures are subjected to various loads during the long-term service period such as dead, traffic, wind, and earthquake loads. Particular attention was devoted to traffic loads owing to the bridges suffering from them every day, not like winds or earthquakes. Traffic loads involve considerable uncertainties and variability. The main source of uncertainty are the traffic conditions (i.e., site-specific traffic) at the bridge location (Kim & Song 2019; Roberts & Shepard 2000). Therefore, it is necessary to consider the site-specific traffic conditions of the bridge when evaluating the traffic LEs, especially for long-span bridges, for which the effect is greatly affected by groups of trucks rather than by several heavy vehicles as it happens in short and medium-span bridges (Ruan et al. 2017; Caprani, O'Brien & McLachlan 2008; Caprani 2013; Chen & Wu 2011; O'Brien, Hayrapetova & Walsh 2012; Soriano, Casas & Ghosn 2017; Xu, Chen & Xia 2012).

For a site-specific traffic load model considering extreme scenarios, the traffic parameters are time-varying. Updating the model according to the actual traffic parameters is crucial. The Bayesian inference technique offers a possibility to reduce the uncertainty in parameter estimation and prediction. Updating methodology can be employed within the Bayesian framework. The posterior probability distributions are acquired by integrating the existing information represented by a prior probabilistic model with newly observed data. Recently, Kim and Song (2021) developed a Bayesian inference methodology to update the probabilistic model parameters of bridge traffic loads given new observed data concerning the traffic environment, which allowed a more reasonable and accurate estimation of traffic parameters and LEs. Although used in many engineering applications (Pang et al. 2021; Kelly & Smith 2009), the applications of Bayesian method in the prediction of bridge extreme traffic LEs are still scarce and most of the cases are only used to update the response extremes for traffic loads, neglecting to update the scenarios for the spatial distribution of heavy vehicles on the bridge deck. In research using simulated traffic LEs, O'Brien et al. (2015) used the Bayesian method and found that its prediction capabilities varied depending on the type of LEs. Leahy et al. (2015) evaluated the site-specific LEs of bridges using the Bayesian method with GVW information collected from 19 sites as prior data. Yu & Cai (2019) and Yu et al. (2019) developed a Bayesian approach to predict the traffic LEs with fast

updates using the observed strain response. The changes in the traffic environment of a long-span bridge over its lifetime also require developing a model capable of estimating the site-specific traffic loads.

2.4 Identifying gaps in the existing research

The existing research on the limitations of operating costs and equipment durability of the WIM system necessitates the development of a simulation process for traffic flow. This process should be based on data obtained from the WIM system during a specific time period and should be capable of determining the extreme load response and corresponding traffic scenarios, such as the most critical maximum-per-day event, that may occur during a required return period (Ruan et al. 2017). Notwithstanding, the majority of previous studies primarily focus on the extreme LEs of long-span bridges, with insufficient attention given to the characteristics of the spatial distribution of vehicles when extreme responses are obtained.

Also, previous traffic load models exhibit limitations in accurately representing the complex spatial distribution of traffic loads on bridge decks. The probability of spatial distribution patterns of vehicles on long-span bridge decks, which can provoke maximum LEs, is important for assessing bridge safety and understanding their performance under vehicle loads (Chen et al. 2019). During operational periods, the formation of platoons, or groups of heavy vehicles, may pose significant risks to the safety of long-span bridges. The proportion of heavy vehicles in traffic flow has a more substantial impact on the structural effect than the traffic flow itself (Lipari, Caprani & O'Brien 2017). Moreover, diverse spatial patterns of vehicle distribution yield varying LEs, depending on the influence line/surface of the effect in question. Concurrently, traditional simulation methods have concentrated more on traffic flow or congestion sequences simulation rather than directly modelling the spatial distribution of vehicles on the bridge deck when extreme values are obtained, rendering them inefficient and costly, particularly when computing extreme responses over extended reference periods.

The focus on traffic flow or congestion sequences simulation, while disregarding the characteristics of the spatial distribution of vehicles that may lead to extreme response values (especially for free flow traffic), renders traditional simulation methods both inefficient and costly in terms of computational effort required for obtaining extreme responses over long reference time

periods. In light of the limitations of conventional vehicle load models in spatial distribution modeling, Chen et al. (2019) proposed a probabilistic approach for modeling the spatial distribution of heavy vehicles on long-span bridges using an undirected graphical method. The authors noted that exploring all potential spatial arrangements of vehicles on bridge decks could result in a combinatorial explosion, making it challenging to compute the empirical probability of each possible spatial vehicle distribution pattern. This highlights the need for research on vehicle spatial distribution modeling and the development of efficient computational inference algorithms. Nevertheless, the proposed method by Chen et al. (2019) predominantly simulates standard vehicle spatial distribution scenarios, paying scant attention to maximum-response-per-day events, which hold significant implications for structural performance evaluation.

In this thesis, a probabilistic model for vehicle scenarios leading to extreme LEs (maximum-response-per-day event) for long-span bridges is proposed. The definition of these vehicle scenarios is the vehicle spatial distribution at the moment when the maximum effect is obtained. For the simulation of vehicle location on the bridge deck, the stationary and non-stationary Poisson process is introduced for both outer lanes and inner lanes. With the non-stationary process, the uneven spatial distribution of the vehicle loads on bridge deck can be simulated. The proposed method is able to take into consideration multiple lanes and complex spatial distribution of vehicle scenarios corresponding to maximum-response-per-day event under free-flow traffic. While congestion scenarios are indeed critical to the safety of long-span bridges, as demonstrated later in the thesis, the author has found that free flow can also threaten the safety of this type of bridges in specific scenarios and is of equal research value. For each day, a full day traffic data is passed through the influence line to identify the loading event that is critical for the corresponding LE. The vehicle distribution on the lane corresponding to the maximum response among the samples of 86400 seconds in one day is selected as one sample for the proposed model. Regarding the efficiency of the proposed method, which must be considered in the modeling process of the new model, the benefit is evident. In fact, the total time of the traditional method to obtain one-week six-lane traffic flow is about 0.7 to 1 hour (Ruan et al. 2017). With the one-week traffic flow, seven extreme LEs traffic scenarios can be obtained. Comparatively, applying the proposed method, it takes less than one second to simulate seven sets of traffic scenarios of maximum-response-per-day event. Meanwhile, this thesis develops a site-specific traffic load model based on the simulation results of the probabilistic model of extreme response scenarios. Then, a Bayesian

inference-based approach for the updating of the site-specific traffic model according to the actual traffic conditions. The two proposed models are demonstrated under free-flow traffic conditions, which are also critical to long-span bridge assessment.

CHAPTER 3 Probabilistic model of traffic scenarios for extreme LEs in long-span bridges

3.1 Introduction

The importance and benefits of using a site-specific load model for assessing existing bridges and designing new bridges have been widely recognized (Ruan et al. 2017; Anitori, Casas & Ghosn 2018; Enright, Carey & Caprani 2013). This is because site-specific traffic loads provide critical information for bridge maintenance and design, as the behaviors of bridge components under such traffic can be better understood (Frangopol & Liu 2007; Gao et al. 2022). However, despite the significant uncertainties associated with traffic loads and the fact that they can vary depending on site-specific traffic conditions, the design code and maintenance strategies for long-span bridges do not currently take into account the actual traffic conditions and uncertainties (Kim & Song 2019). Therefore, it is essential to develop a probabilistic traffic model that can accurately reflect the actual traffic environments of long-span bridges. In this chapter, a probabilistic model of extreme response scenario that can express the characteristics of site-specific traffic flow for long-span bridge is developed. The probabilistic model of extreme response scenario is a model that can simulate the distribution of heavy vehicles on the bridge deck when the extreme response is obtained. In the following, without specific claim, scenario refers to extreme response scenario which can be simulated by the proposed model.

3.2 Model of heavy vehicle distribution

To develop a model for scenarios of extreme LE, it is necessary to develop a spatial distribution model of heavy vehicles on the bridge deck. There are two key issues associated with heavy vehicles to be resolved: the first is their locations on the deck, and the second is their weights. In this paper, the bridge deck is divided into $n \times m$ cells according to the lane and specific constant cell length, dl, wherein m means the number of cells along the longitudinal direction of the bridge and n is the number of lanes. dl is determined according to the statistical data of the length of heavy vehicles. According to Chen et al. (2019), the average length of large vehicles is 15.13 m.

Based on the measured WIM data, the total wheelbase (i.e., the distance from the first axle to the last axle) of the multi-axle vehicle shows a peak value of 17.5 m. Considering the influences of the front and rear overhang of the vehicle, and the distance between the vehicles while driving, the length of the cell should be slightly longer than the wheelbase. Therefore, the length of the cells is taken as 20 m as shown in Figure 3-1 **(b)**. The shaded part shown in Figure 3-1 **(b)** represent one cell. When the loaded length of the bridge is *L* as shown in Figure 3-1 **(a)**, its longitudinal cell number *m* satisfies **Equation (3-1)**.

$$L < m * dl \leq L + dl \tag{3-1}$$

For the convenience of modeling, the influence of light vehicles on loading effect is ignored (which means removing all light vehicles, the removal is applied to the calculation of the response and also to the simulation of the spatial position); and the centroid of heavy vehicles is moved (i.e., the loading location of each heavy vehicle is moved from the original position to the closest cell center in the same lane). The simplified process is illustrated in Figure 3-1. Meanwhile, it is assumed that only one heavy vehicle can be accommodated in one cell. If there are two heavy vehicles distributed in the same cell, the vehicle with the farther centroid can be moved to the adjacent cell.

Referring to the concepts of CA, each cell of a lane has two states: either empty or occupied by a heavy vehicle (Ruan et al. 2017). With a large amount of observation data, the state of each cell becomes random. Considering the presence of a vehicle in the cell as an event, the cell states can be regarded as the occurrence or non-occurrence of events in a random process. Then the event can be described as a binary random variable as shown in **Equation (3-2)**. The value 0 means the cell is empty, and 1 means the cell is occupied by one heavy vehicle.

$$\Lambda_{i,j} = 1\ (occupied)\ or\ 0\ (empty), \quad i = 1,2,\cdots,m \quad j = 1,2,\cdots,n \tag{3-2}$$

where *i* and *j* represent the *i*-th cell in lane *j*, as shown in Figure 3-1 **(c)**. The presence or absence of vehicles in the cells is defined as a binary random variable. The state of cells on the *n*-th lane is described as the random vector as shown in **Equation (3-3)**, also shown in the dotted box in Figure 3-1 **(c)**:

$$\mathbf{\Lambda} = (\Lambda_1, \Lambda_2, \cdots, \Lambda_m) \tag{3-3}$$

For instance, the location of heavy vehicles on the *n*-th lane in the extreme response scenarios can be described by a Poisson process, as **Equation (3-4)**, according to Figure 3-1 **(c)**.

$$\mathbf{\Lambda} = (0,0,1,\dots\dots,1) \tag{3-4}$$

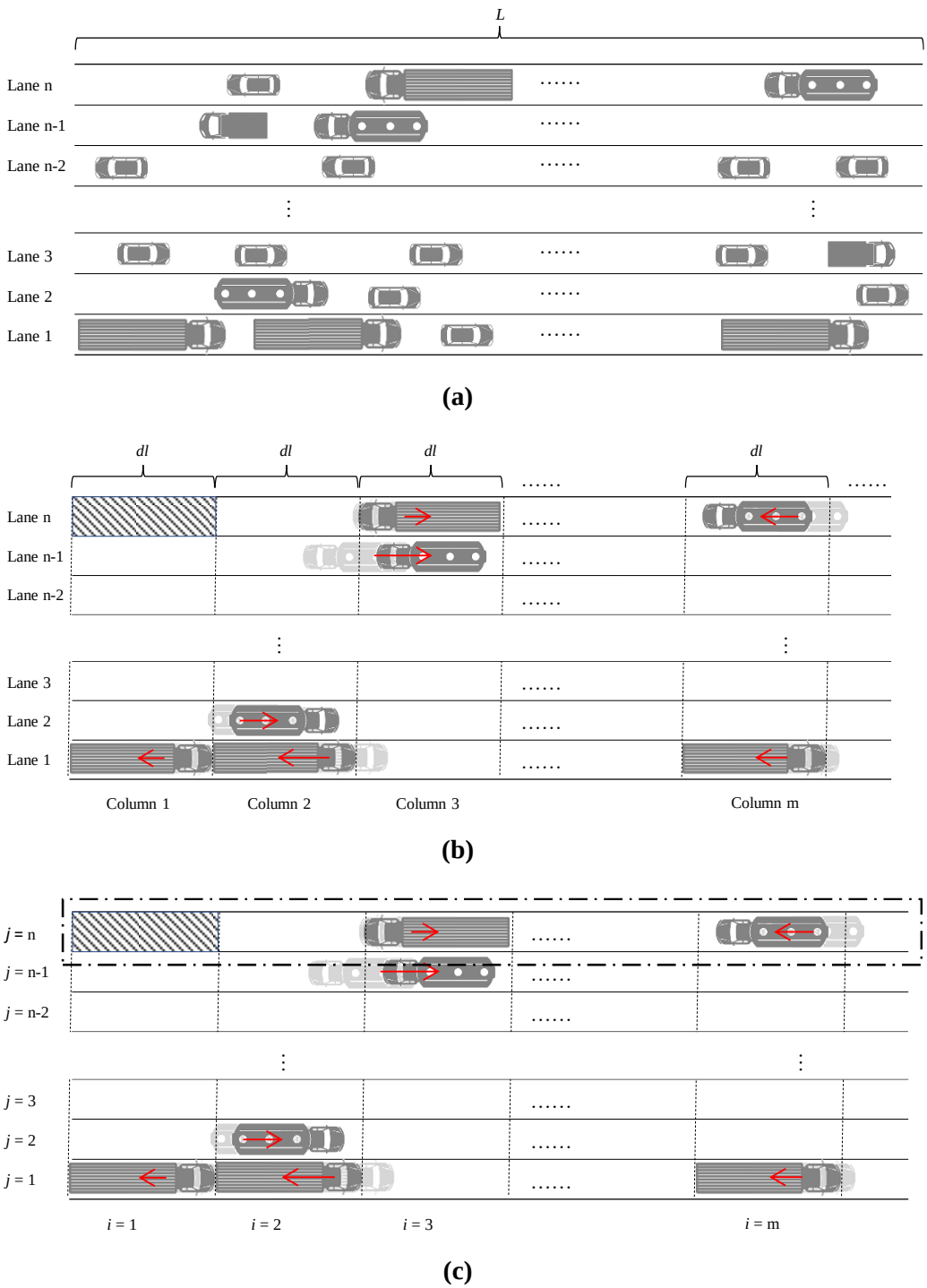

Figure 3-1 (a) Vehicle distribution of scenarios of extreme LE; (b) Heavy vehicle distribution

with cell structure of scenarios of extreme LE model; (c) Cell numbering and mathematical representation.

Then, multiplying corresponding elements of this location vector and the GVW vector simulated by Gaussian mixture model (GMM) and Nataf method, the scenarios of heavy vehicles in the bridge can be modeled probabilistically as shown in Figure 3-2.

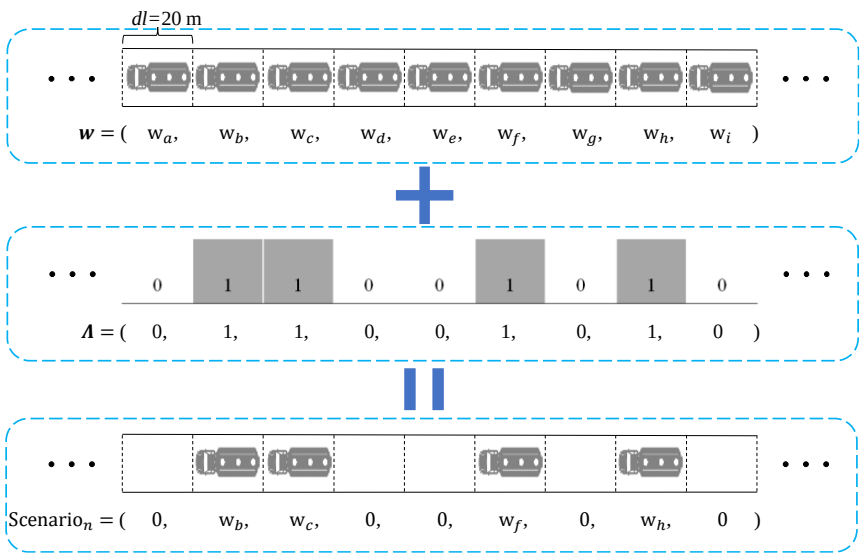

Figure 3-2 Modelling process of extreme response scenario.

3.3 Description of scenarios of extreme LE based on WIM Data

The WIM data used in this study was collected during 423 days in 2014 to 2015 from a six-lane highway located in Zhejiang Province, China. This highway is a principal pass way connecting Hangzhou Bay and the surrounding cities and has been in service for over 10 years. Traffic data from six unidirectional lanes were measured. The accuracy and filtration criteria on raw data are shown in Table 3-1 (Ruan et al. 2017). After filtration, the daily traffic volume is approximately 16,500-50,000, which is representative of multi-lane traffic level in China. Data containing 11,055,095 vehicles with 28,034,398 axles, both cars and trucks, were collected. The WIM data can represent free-flow traffic state after analysis, and this consistent 423-day WIM data were used as the basis for building the proposed scenario model and also the basis for simulating data used for validation.

Table 3-1 Accuracy and filtration criteria of WIM data.

Ordinal	1	2	3	4	5	6	7
Item	Arrival time	Axle number	Lane number	Velocity	GVW	Axle weight	Axle spacing
Accuracy	0.1 s	Positive integer	Positive integer	0.1 km/h	0.01 t	0.01 t	0.01 m
Filtration criteria	/	{2,3,4,5,6}	{1,2,3,4,5,6}	⩾10 km/h	⩾0.5 t & ⩽200 t	⩾0.1 t & ⩽80 t	⩾0.6 m & ⩽20 m
Note	Vehicles with axle number more than 6 are no more than 0.17%. Velocity below 10 km/h cannot be measured correctly by the WIM system. GVW below 0.5 t is not correct, and that more than 200 t generally no exists. Axle weight below 0.1 t is not correct, and that more than 80 t generally no exists. Axle spacing should be larger than lowest tyre diameter e.g., 0.6 m, and axle spacing more than 20 m in trailer generally no exists. Ordinals 1-7 are essential for the construction of vehicle sequences. Axle number = number of axle weight Axle number = number of axle spacing + 1 GVW = sum of all axle weights						

To simulate the passing of vehicle sequences from WIM data collected in a road section through a certain bridge length requires some assumptions. One is to assume that the monitoring station is set at a certain distance from one side of the bridge in such a way that the obtained WIM data is also valid for the bridge; the second is to assure that the vehicles maintain their velocities when crossing the bridge. As the proposed extreme response scenario model is a spatial model rather than a temporal model, the constant vehicle speed of the WIM data is assumed only to obtain static samples of the extreme response scenario under free-flow conditions, without considering rules such as overtaking and lane changing of the traffic flow. Then, according to the arriving time and velocity of a certain vehicle and also the location of the monitoring station (the location recording the arriving time of the vehicle), the time history of the vehicle when passing the bridge can be obtained.

With the aid of the influence surface/line method, the LEs of long-span bridges can be calculated from data collected by WIM system. In this paper, the structural effects are calculated every second for 423 consecutive days. The maximum load response can be fitted by GEV distribution according to the extreme value theory. The block maximum approach, which divides a long series of data sets into blocks, can be used to determine the GEV parameters (Kim & Song, 2019). Then, using the set of maximum data, the highest value from each block may be used to estimate the parameters of the GEV distribution (Gnedenko, 2017). The maximum data of traffic field for each hour, day,

week, and year was utilized in several research to match the GEV distribution (O'Brien et al., 2015). In this thesis, the block size is chosen as 1-day, daily differences in scenarios caused by parameters such as traffic flow are ignored. Since the traffic characteristics evolve from year to year, a Bayesian approach needs to be introduced to update the extreme response scenario based site-specific traffic model, so the yearly maximum value cannot be selected as the block size. The maximum response among the samples of 86400 seconds in every day is selected as one sample for the proposed model. Within one second, the total vehicle number and vehicle weight on the bridge deck will not change significantly. Also, the considered parameters of the proposed probabilistic model are the number of heavy vehicles on the lane and the GVWs on the lane, which will only change very slightly in a second. In Zhou's research (Zhou, 2018), it was assumed based on the findings of a related study (Davis 2003), that the driving reaction time is no shorter than 1 s and that the relevant driving mechanisms become complicated when it exceeds 1 s. Therefore, 1 s was chosen as the time step in this thesis for calculating the response, according to Zhou's research. One vehicle scenarios example of extreme LE of the axial force of the longest cable (AFC, Effect 1) is illustrated in Figure 3-3. The following figures and tables without special remarks are the results of Effect 1. The total scenarios of extreme LE consist of 423 samples.

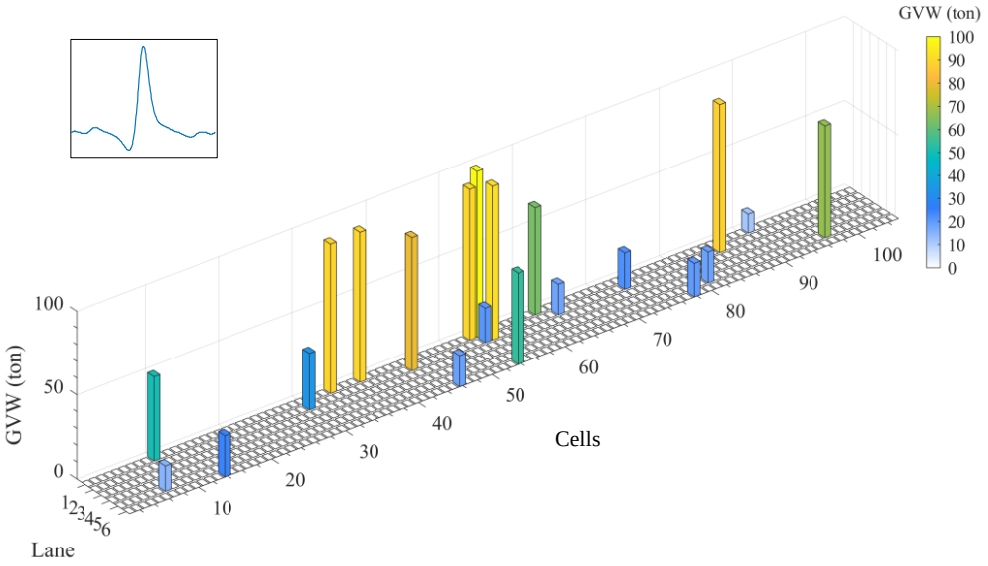

Figure 3-3 A sample of vehicle scenario of extreme LE.

Figure 3-4 (a) displays the differences between the distribution functions in inner lanes and outer lanes of the statistical results of cells occupied by heavy vehicles on the probability paper. The outer lane is defined as the outermost lane in each direction. Both the leftmost and rightmost lanes

of a road are outer lanes. The remaining lanes are defined as the inner lanes. For example, for a 6-lane road, lanes 1 and 6 are the outer lanes and lanes 2 to 5 are the inner lanes. Figure 3-4 **(b)** and **(c)** show the statistical results of cells occupied by heavy vehicles per lane for scenarios of extreme LE, which is the database of the following Poisson simulation. There are significant differences in occupied cells over the outer lanes (i.e., slow lane) and inner lanes (i.e., fast lane), which is consistent with vehicle driving habits. The average number of occupied cells along the whole loaded length is 1.9356 for inner lanes, and 4.6537 for outer lanes. The average number of cells occupied by heavy trucks in the inner lane is much smaller than for the outer lane, because the heavy vehicles over 10 tonnes prefer to drive on the outer lane. Since the bridge has six lanes, the average total number of cells occupied by heavy vehicles on the whole bridge deck under extreme response scenario may up to 1.9356×4 + 4.6537×2 = 17.0498. Due to the significant statistical differences in the distribution of heavy vehicles between lanes, it is necessary to model the different lanes separately.

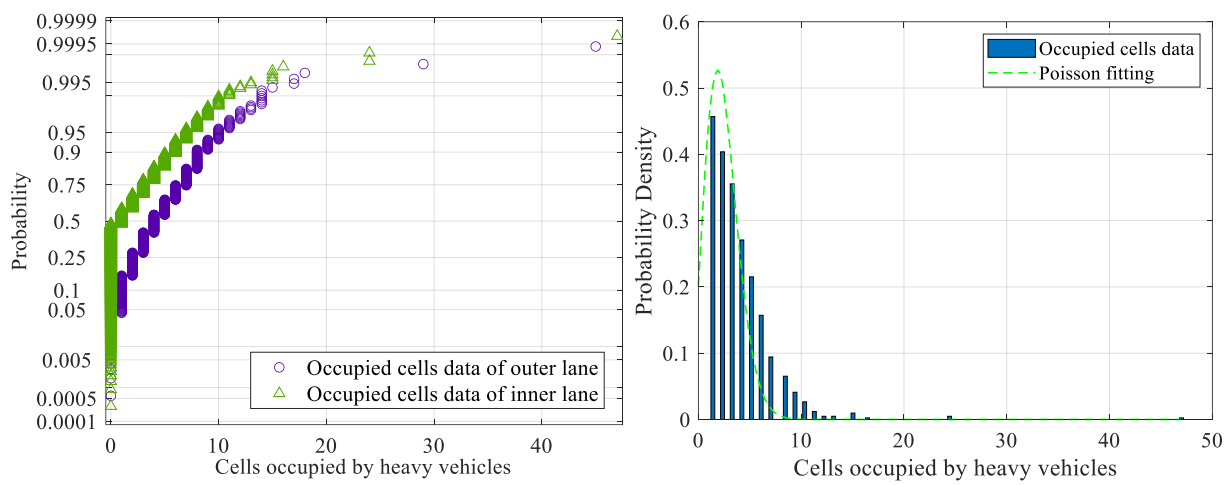

(a) **(b)**

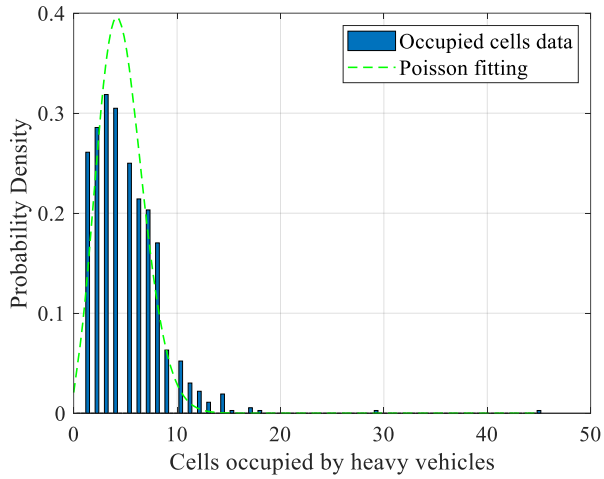

(c)

Figure 3-4 Statistics of cells occupied by heavy vehicles in (a) normal probability paper; (b) inner lanes; (c) outer lanes.

Figure 3-5 (a) displays the differences between the distribution functions in inner lanes and outer lanes of the GVWs on the probability paper. Figure 3-5 **(b)** and **(c)** show the histogram and fitting of the GVWs for inner and outer lanes. It can be seen that the observed GVW in the scenarios of extreme LE for heavy vehicle follows a typical multimodal distribution. Meanwhile, there is not significant differences in GVW between inner and outer lanes.

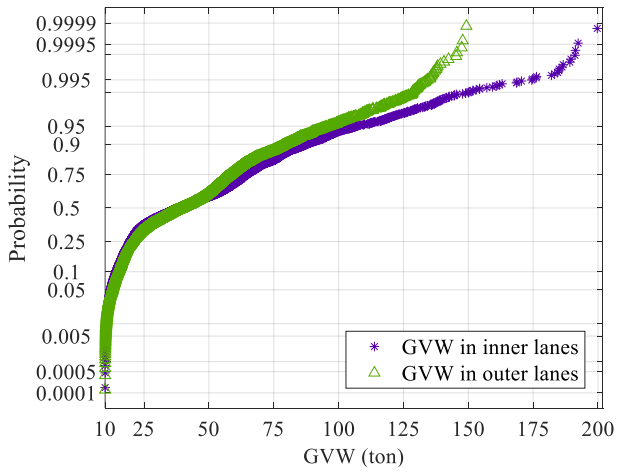

(a)

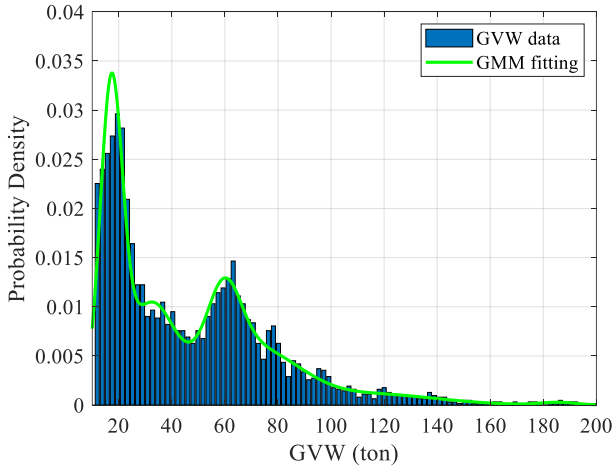

(b)

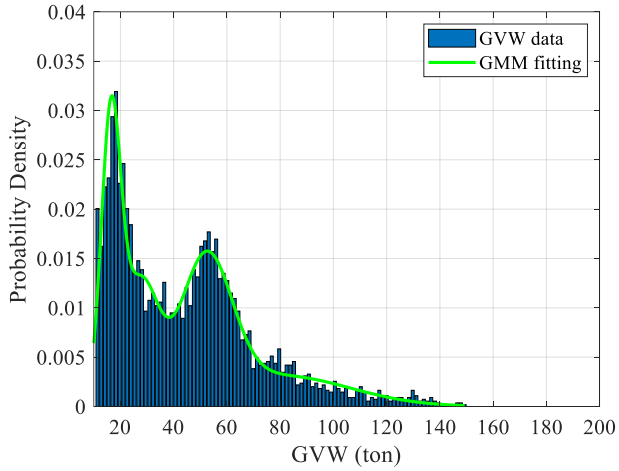

(c)

Figure 3-5 Sample data and Modelling of GVW in (a) normal probability paper; (b) inner lanes; (c) outer lanes.

3.4 Modeling of vehicle location distribution by Poisson process

A number of random process models have been used for modeling serial vehicle location or vehicle load, such as filtered compound Weibull process and filtered compound Poisson process (Guo, Li & Zhao 2016). In this paper, a suitable probabilistic distribution needs to be chosen to fit the occupancy state of the cells on a particular lane. A Poisson distribution is a probability distribution used in statistics to illustrate how many times an event is expected to occur during a certain period or within a certain area. It is a distribution of count. Poisson distributions are frequently used to analyze independent events that happen at a consistent rate within a certain time or region. Poisson process is also widely used in various fields to simulate the number of occurrences of specific events within a certain region or time frame (Kioumarsi et al. 2016; Li, Wang & Zhang 2016). According to the traffic simulation results shown in Figure 3-4, the Poisson process is adopted to develop a simple and reasonable model for the spatial distribution of heavy vehicle in one lane. The number of occurrences of cells occupied by vehicles within a certain loaded length $(0, L]$ is n. The specific meaning of n as a Poisson distribution parameter is that the event of a vehicle appearing in a cell occurs n times in a certain loaded length (e.g., a given lane). Then, the probability of n can be determined by **Equation (3-5)**:

$$Pr(T_L = n) = \frac{(\lambda L)^n exp(-\lambda L)}{n!}, \quad n = 0, 1, 2, \ldots \tag{3-5}$$

where $Pr(\cdot)$ is the occurrence probability of the event, and λ represents the mean occurrence rate of the cells occupied by vehicles. For a stationary vehicle distribution process, λ is constant over the loading location, the units of λ should be vehicles per unit length.

In addition to the stationary process, the location distribution of vehicles can also be considered as a non-stationary process. In Figure 3-6, the X-axis represents the cell location on the whole length of the investigated bridge, totally containing 105 cells. For a specific LE, the occurrence rate of cells occupied by heavy vehicles, represented by the Poisson parameter $\lambda(l)$, can be assumed to vary by location, influenced by the shape of the influence line. Maximum effects are obtained when vehicles are situated in areas with the highest values of the influence line. Because the probability of occurrence is determined by the location of the cell in the lane, as shown in Figure 3-6, $\lambda(l)$ can be calculated by **Equation (3-6)**:

$$\lambda(l) = \lambda_0(l) \cdot \theta \tag{3-6}$$

where $\lambda_0(l)$ represents the average level of the occurrence rate of occupied cell, and θ reflects the variation along the loading location.

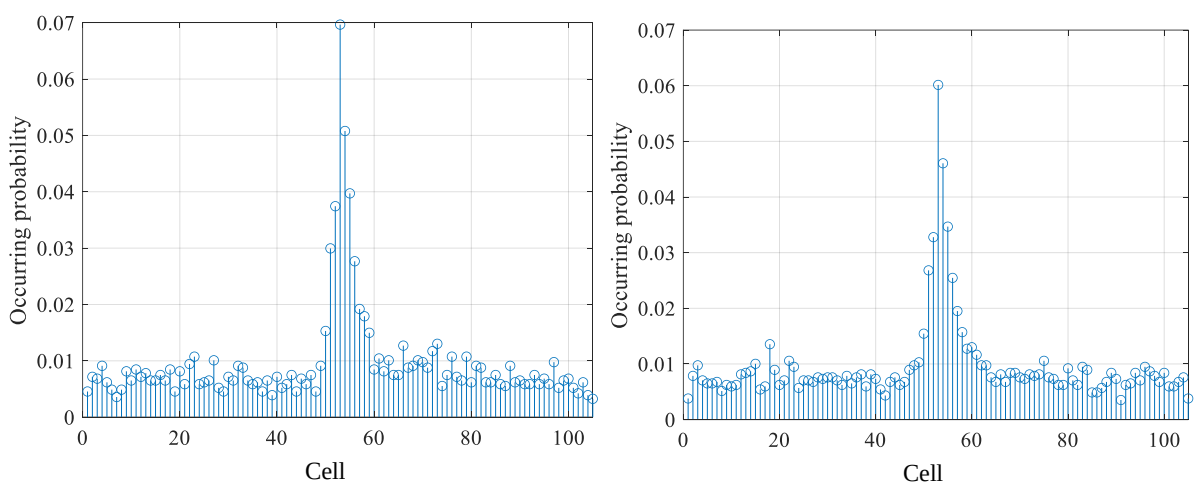

Figure 3-6 Probabilities of a cell to be occupied by a heavy vehicle in a maximum LE scenario of (a) inner lanes; (b) outer lanes (Effect 1).

3.5 Modeling of heavy vehicles weight

GVW is a critical variable to describe the characteristics of vehicle load, which has great uncertainties and must be modeled by a probabilistic approach. Gaussian, Weibull or empirical distributions are usually adopted to fit traffic random variables such as GVW, average velocity, traffic volume and small headway (Hwang et al., 2012; Kennedy et al., 1992; Kwon et al., 2011; Nowak, 1995). However, histograms of these variables with multiple peaks cannot be captured by these typical unimodal probability distribution models (Kim & Song, 2019; 2021). To accommodate the multimodal distribution of traffic parameters, GMM has been widely adopted due to its ability to accurately capture the attributes of multiple peaks (Enright & O'Brien 2013; Enright, Carey & Caprani, 2013; Kim & Song, 2019; Lu et al., 2017; Zhao et al., 2020). According to figure 3.4, in this study, the GMM is employed to represent the GVW. Meanwhile, in order to consider the correlation between vehicle weights, the Nataf transformation method is adopted.

3.5.1 GMM and determination of components number

GMM has been adopted in many fields to model uncertainties and exhibits promising performance (Yang et al. 2019). GMM comprises multiple Gaussian densities, which is suitable for modeling an arbitrary probability density function (PDF) accurately, especially for the PDF of variables with multiple peaks. For a random variable χ, the PDF of GMM can be expressed as **Equation (3-7)**:

$$p(\chi) = \sum_{k=1}^{K} \pi_k N(\chi|\mu_k, \Sigma_k) \tag{3-7}$$

where $N(\chi|\mu_k, \Sigma_k)$ is the PDF of the k-th Gaussian distribution with μ_k and Σ_k as its mean and covariance matrix, π_k represents the weight of the k-th Gaussian distribution component, which satisfies $\sum_{k=1}^{K} \pi_k = 1$ and $0 \leq \pi_k \leq 1$.

The selection of an appropriate number of components is crucial for developing a GMM model. Generally, increasing the number of components means higher accuracy of the GMM fitting, however it also leads to a decrease in efficiency (Yang et al. 2019). According to previous research, several entropy criterion methods can be used to determine the number of components, including Akaike information criterion (AIC) and Bayesian information criterion (BIC) (Li et al. 2013; Zivkovic 2004; Celeux & Soromenho 1996). In this study, the component number of the GMM is

determined using both the AIC approach and the visual judgment mixed with physical meaning method.

3.5.2 Correlation of heavy vehicles and Nataf transformation

Several consecutive trucks in one lane or side-by-side trucks in adjacent lanes are the critical scenarios causing the extreme LE, threatening the safety of bridge structures (Gil & Kang 2015; O'Brien & Enright 2013; Yuan et al. 2017; Xiong et al. 2017). The governing loading combination for long-loading length is always several groups of trucks and numerous on-bridge vehicles, not one or two sets of side-by-side trucks. Therefore, it is assumed that there is a two-by-two correlation between the GVWs of all vehicles within a certain range of the same lane for scenarios of maximum-response-per-day event, rather than simply assuming a correlation between the GVWs of two key heavy vehicles. The objective of setting this parameter is to describe the correlation between GVWs within a certain length in the same lane for the proposed scenarios, which is reflected by the correlation function. The Pearson coefficient of correlation is adopted to characterize the correlation of GVW as expressed in **Equation (3-8)**:

$$\rho_{j,k} = \frac{\alpha_{j,k}}{\lambda_j \cdot \lambda_k}, \tag{3-8}$$

where $\rho_{j,k}$ represents the coefficient of correlation between the GVW of locations l_j and l_k (i.e., the distance between *j* and *k* is short), $\alpha_{j,k}$ corresponds to the covariance between the GVWs, λ_j and λ_k indicate the standard deviations of the GVWs at l_j and l_k, respectively. It is common sense that the correlation coefficient $\rho_{j,k}$ between two GVWs becomes weaker with increasing distance lag, $|l_j - l_k|$. Referring to engineering cases in related researches, the following exponential correlation function is employed (Li, Wang & Zhang, 2016; Mahadevan & Haldar, 1991):

$$\rho_{j,k} = \exp\left(-\frac{|l_j - l_k|}{D}\right), \tag{3-9}$$

where *D* represents the scale factor reflecting the correlation length. For instance, if $|l_j - l_k|$ takes the value of one centroid interval of adjacent cells (which means $|l_j - l_k|$ = 20 m), then, $\rho_{j,k}$ = 0.3679, 0.6703, and 0.8187 when *D* is 20 m, 50 m, and 100 m respectively (i.e., $\rho_{j,k} = \exp\left(-\frac{20}{20}\right) = 0.3679$, $\rho_{j,k} = \exp\left(-\frac{20}{50}\right) = 0.6703$, $\rho_{j,k} = \exp\left(-\frac{20}{100}\right) = 0.8187$). For the

actual extreme response scenarios, the GVWs in the blank cells are not known (blank cell means an empty cell, i.e., a cell without vehicle on it). As a result, the correlation lengths cannot be calculated and, as a consequence, in the proposed model, reasonable assumptions are made regarding the correlation lengths, specifically 20 m, 50 m, and 100 m. The effects of these correlation lengths are subsequently analyzed and discussed.

Nataf transformation can be used to transfer any random variables into standard Gaussian distribution (Zhao et al. 2020; Noh, Choi & Du 2009). The marginal cumulative density functions (CDF) of an *n*-dimensional correlated random vector $\vec{\beta} = [\beta_1, \beta_2, \dots, \beta_n]$ is $F_j(\beta_j)$, and the correlation coefficient matrix $\boldsymbol{K} = [\mathrm{K}_{j,k} = \kappa_{j,k}]$. By Nataf transformation, $\vec{\beta}$ can be transferred into independent standard normal variables $\vec{\zeta} = [\zeta_j]$. The procedure of Nataf transformation is as follows (Der Kiureghian & Liu 1986; Liu & Der Kiureghian 1991; Hisada & Nakagiri 1985):

Correlated standard normal variables $\vec{\xi} = [\xi_j]$ are transferred from $\vec{\beta}$ by **Equation (3-10)**.

$$\xi_j = \Phi^{-1}\left(F_j(\beta_j)\right) \tag{3-10}$$

where $\Phi^{-1}(\cdot)$ is the inverse CDF of standard Gaussian distribution. The correlation coefficient matrix of $\vec{\xi}$ is supposed as $\boldsymbol{K}' = [\kappa'_{j,k}]$. Then the relationship between $\kappa_{j,k}$ and $\kappa'_{j,k}$ is shown as **Equation (3-11)**.

$$\kappa_{j,k} = \int_{-\infty}^{\infty}\int_{-\infty}^{\infty} \frac{F_j^{-1}\left(\Phi(\beta_j)\right) - E(\beta_j)}{SD(\beta_j)} \cdot \frac{F_k^{-1}\left(\Phi(\beta_k)\right) - E(\beta_k)}{SD(\beta_k)} \omega\left(\beta_j, \beta_k; \kappa'_{j,k}\right) d\beta_j d\beta_k \tag{3-11}$$

where $\omega\left(\beta_j, \beta_k; \kappa'_{j,k}\right)$ is given by **Equation (3-12)**, $E(\cdot)$ and $SD(\cdot)$ are the mean and standard deviation of variables, respectively.

$$\omega\left(\beta_j, \beta_k; \kappa'_{j,k}\right) = \frac{1}{2\pi\sqrt{1-\kappa'^2_{j,k}}} exp\left\{-\frac{\beta_j^2 - 2\kappa'_{j,k}\beta_j\beta_k + \beta_k^2}{2\left(1-\kappa'^2_{j,k}\right)}\right\} \tag{3-12}$$

According to **Equations (3-11)** and **(3-12)**, $\kappa'_{j,k}$ can be calculated by $\kappa_{j,k}$. The relationship between $\kappa_{j,k}$ and $\kappa'_{j,k}$ can be simplified as **Equation (3-13)**. $P_{j,k}$ can be approximately estimated by a polynomial as **Equation (3-14)**.

$$\kappa'_{j,k} = P_{j,k} \cdot \kappa_{j,k} \tag{3-13}$$

$$P_{j,k} = \frac{\kappa'_{j,k}}{\kappa_{j,k}} = p_1\kappa_{j,k}^3 + p_2\kappa_{j,k}^2 + p_3\kappa_{j,k} + p_4 \tag{3-14}$$

where the parameters p_1 to p_4 can be calculated by Monte Carlo method (Xiao 2014). Then the relationship between $\kappa_{j,k}$ and $\kappa'_{j,k}$ can be obtained by least squares fitting of polynomial as **Equation (3-15)** for outer lanes and **Equation (3-16)** for inner lanes.

$$P_{j,k} = -0.01025\kappa_{j,k}^3 + 0.01435\kappa_{j,k}^2 - 0.09334\kappa_{j,k} + 1.091p_4 \tag{3-15}$$

$$P_{j,k} = -0.01301\kappa_{j,k}^3 + 0.03364\kappa_{j,k}^2 - 0.1469\kappa_{j,k} + 1.128p_4 \tag{3-16}$$

Since the covariance matrix of $\vec{\xi}$ is positive definite, $\mathbf{K}'$ can be decomposed into a lower and an upper triangular matrix via Cholesky factorization as shown in **Equation (3-17)**:

$$\mathbf{K}' = \mathbf{A} \cdot \mathbf{A}^{\mathrm{T}} = \begin{bmatrix} a_{11} & 0 & \dots & 0 \\ a_{12} & a_{22} & \dots & 0 \\ \vdots & \vdots & & \vdots \\ a_{1n} & a_{2n} & \dots & a_{nn} \end{bmatrix} \begin{bmatrix} a_{11} & a_{12} & \dots & a_{1n} \\ 0 & a_{22} & \dots & a_{2n} \\ \vdots & \vdots & & \vdots \\ 0 & 0 & \dots & a_{nn} \end{bmatrix} = \begin{bmatrix} 1 & \kappa'_{12} & \dots & \kappa'_{1n} \\ \kappa'_{12} & 1 & \dots & \kappa'_{2n} \\ \vdots & \vdots & \ddots & \vdots \\ \kappa'_{1n} & \kappa'_{2n} & \dots & 1 \end{bmatrix} \tag{3-17}$$

where $\mathbf{A}$ is a lower triangular matrix. Therefore, the variables $\vec{\xi}$ can be expressed as the product of $\mathbf{A}$ and the independent standard normal variables $\vec{\zeta}$, as shown in **Equation (3-18)**:

$$\vec{\xi} = \mathbf{A} \cdot \vec{\zeta} \tag{3-18}$$

Then the relationship of the independent standard normal variables $\vec{\zeta}$ and the original correlated variables $\vec{\beta}$ can be established as **Equation (3-19)**:

$$\begin{aligned} \beta_1 &= F_1^{-1}\big(\Phi(a_{11}\zeta_1)\big) \\ \beta_2 &= F_2^{-1}\big(\Phi(a_{21}\zeta_1 + a_{22}\zeta_2)\big) \\ &\vdots \\ \beta_n &= F_n^{-1}\big(\Phi(a_{n1}\zeta_1 + a_{n2}\zeta_2 + \cdots + a_{nn}\zeta_n)\big) \end{aligned} \tag{3-19}$$

where $\Phi(\cdot)$ is the CDF of standard Gaussian distribution. Then, Monte Carlo method is used to analyze the scenarios of extreme LE, in which the correlated GVWs are simulated according to **Equation (3-19)**.

3.6 Extreme value theory for the return period extrapolation

Based on extreme value theory (O'Brien et al. 2015), the GEV can be employed in the study of the response value. The distribution of the maximum value for a series of independent identically distributed random variables $Z_1, Z_2, \dots, Z_\varrho$ is represented as $H(z)^\varrho$. According to **Equation (3-20)**, the normalized sample maximum $\left(max\left(Z_1, Z_2, \dots, Z_\varrho\right) - b_\varrho\right)/a_\varrho$ has a non-degenerate limiting distribution $G(z)$ that holds for all consecutive points of $G(z)$ for the asymptotic properties of the $max\left(Z_1, Z_2, \dots, Z_\varrho\right)$, providing that there is a constant sequence $a_\varrho > 0$, and $b_\varrho \in R$ ($\varrho = 1, 2, \dots$).

$$\lim_{\varrho \to \infty} H^\varrho\left(a_\varrho z + b_\varrho\right) = G(z), \quad \varrho \to \infty \tag{3-20}$$

$G(z)$ can be GEV distribution $H_{GEV}(z)$ when certain condition is satisfied (Jenkinson 1955). The distribution of $H_{GEV}(z)$ can be expressed as **Equation (3-21)**:

$$H_{GEV}(z;\ \xi, \sigma, \mu) = \begin{cases} exp\left(-\left(1 + \xi\left(\frac{z-\mu}{\sigma}\right)\right)^{-\frac{1}{\xi}}\right), & \xi \neq 0 \\ exp\left(-exp\left(-\frac{z-\mu}{\sigma}\right)\right), & \xi = 0 \end{cases} \tag{3-21}$$

where μ, σ and ξ are the location parameter, scale parameter and shape parameter of the observed data, respectively, satisfying $1 + \xi(z-\mu)/\sigma > 0$. In this thesis, the GEV distribution is used to fit the response acquired by the simulated extreme scenarios since the scenario samples are the vehicle distributions of the daily maximum effect value, which in the case of a long-span bridge can be assumed to be independent and identically distributed.

3.7 Conclusions

According to the state of the art analysis of traffic load modeling for long-span bridges in Chapter 2, the previous research simulates standard vehicle spatial distribution scenarios, paying little

attention to maximum-response-per-day events, which hold significant implications for structural performance evaluation. Thus, the simulation approach of scenarios of long-span bridges extreme LE using GMM probabilistic model under free-flow traffic based on WIM data is developed. The Monte Carlo method makes it possible to establish a probabilistic model for modeling complex spatial distributions of heavy vehicles.

CHAPTER 4 Application of extreme response scenario probabilistic model

4.1 Introduction

This chapter aims to demonstrate the practical application of the methodology proposed in Chapter 3 for a real-life long-span bridge. For the proposed probabilistic model of extreme response scenario, the distribution of vehicle locations is modeled using a Poisson process, with both stationary and non-stationary processes.

The impact of excluding light vehicles from the vehicle distribution simulation of the bridge deck is also assessed. The chapter also applies the proposed probabilistic model for extreme response scenarios to various effects of the investigated bridge. Comparison of responses are made between the proposed model and the Design Codes. In the following, without special remark the proposed model refers to the probabilistic model of extreme response scenario.

4.2 Description of the cable-stayed bridge

The proposed probabilistic model is applied to describe the vehicle location distribution associated with scenarios of extreme LE on a real typical double-tower long-span cable-stayed bridge with two-way 6 lanes (Sutong Bridge in Jiangsu Province, China). The loaded length of the investigated bridge is 2088 m, which is also the overall length of the bridge. The maximum span length is 1088m. As the loaded length increases, the number of vehicles that can be arranged in the loading area increases, and the distribution of vehicles and the average vehicle weight level become the key factors that affect the structural effect (Ruan et al. 2017). Therefore, it is necessary to consider the heavy vehicle distribution for the structural effect of long-loaded length.

According to the previous research, the average length of large vehicles is 15.13 m (Chen et al. 2019). Based on the measured WIM data, the total wheelbase (i.e., the distance from the first axle to the last axle) of the multi-axle vehicle shows a peak value of 17.5 m. Considering the influence of the front and rear overhang of the vehicle, and the distance between the vehicles while driving,

the length of the cell should be slightly longer than the wheelbase mentioned above. Therefore, for the investigated bridge, each lane is divided into 105 cells with the cell length of 20 m.

Influence lines of load effects are obtained for the research in this thesis. Figure 4-1 depicts the configuration of the bridge along with the influence line of the axial force of the longest cable (AEC). It can be seen that the selected effect has a long-loaded length which can be cooperated with the modeling of the vehicle scenarios of extreme LE.

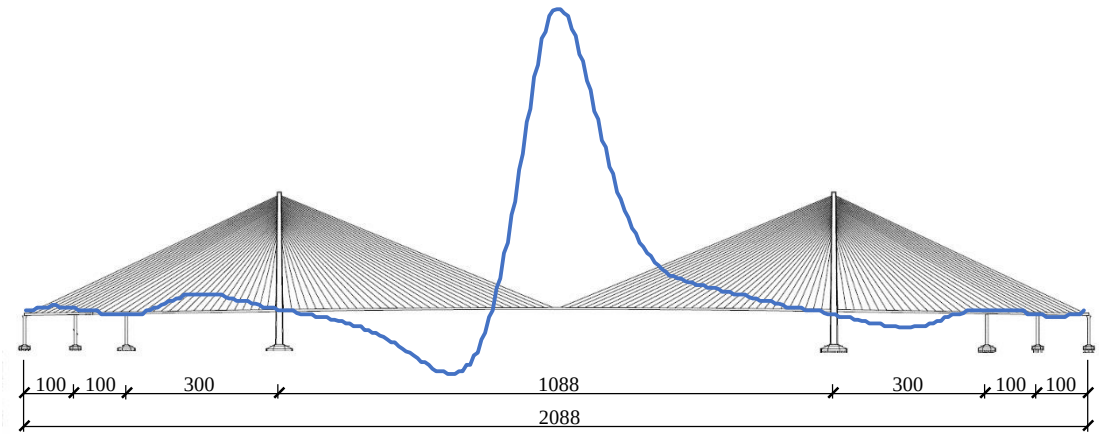

Figure 4-1 Configuration of the long-span cable-stayed bridge with the influence line of effect AFC (Unit: m).

The calculation examples in this thesis all revolve around the long-span cable-stayed bridge above, the structural effects addressed in the cases include: The axial force of the longest cable (AFC, Effect 1), the vertical deflection of main girder at mid-span of the main span (VDMS, Effect 2), the longitudinal displacement at the top of the pylon (LDTP, Effect 3), the bending moment of main girder at mid-span of the main span (BMMS, Effect 4), and the bending moment at the bottom of the pylon (BMBP, Effect 5). These LEs are of greater concern in engineering applications that have an impact on structural safety and include effects for all types of major elements of the bridge.

4.3 Scenarios of extreme LE

The developing process of the proposed model is given below through the case of Effect 1 (AFC). The following figures and tables without special remarks are the results of Effect 1, and the data of the remaining four effects are shown in the Appendix.

4.3.1 Heavy vehicle location distribution

The distribution of vehicle location for the 105 cells × 6 lanes is modeled by a Poisson process. Two cases of stationary and non-stationary processes are considered, respectively. The parameters of stationary and non-stationary Poisson processes for different lanes are listed in Table 4-1 and shown in Figure 4-2. The X-axis of Figure 4-2 represents the cell number along the whole length of the investigated bridge, totally 105 cells. The parameter λ is determined by the maximum likelihood estimation method and the average frequency of the occurrence of heavy vehicle occupancy events in each cell according to the sample data (Paszek 2007). For the case of stationary Poisson process, all cells share the same intensity level. For instance, the parameter λ of Poisson process of the total loaded length is 4.6537 vehs for outer lanes. For the case of non-stationary Poisson process, the cells along lanes are divided into three intensity levels with different λ values, which represent different heavy vehicle densities (i.e., the classification of cell intensity level is based on the probabilities of occupied cell event) depending on the cell number and the distribution parameters according to Figure 4-2.

Table 4-1 The parameters of Poisson processes for vehicle location model (veh) (Effect 1).

λ of Poisson process		Cell number				
		1-49	50-52	53	54-58	59-105
Outer lanes	Stationary			4.6537		
	Non-stationary	3.6820	13.2221	29.3900	13.2221	3.6820
Inner lanes	Stationary			1.9356		
	Non-stationary	1.4658	6.0453	14.1579	6.0453	1.4658

where outer lanes include lane 1 and 6, inner lanes include lane 2 to lane 5.

Figure 4-3 shows the cell classification according to the statistical results of sample data. The cells of intensive area have a high probability of being occupied by vehicles, which is coherent with the shape of the influence line in Figure 4-1.

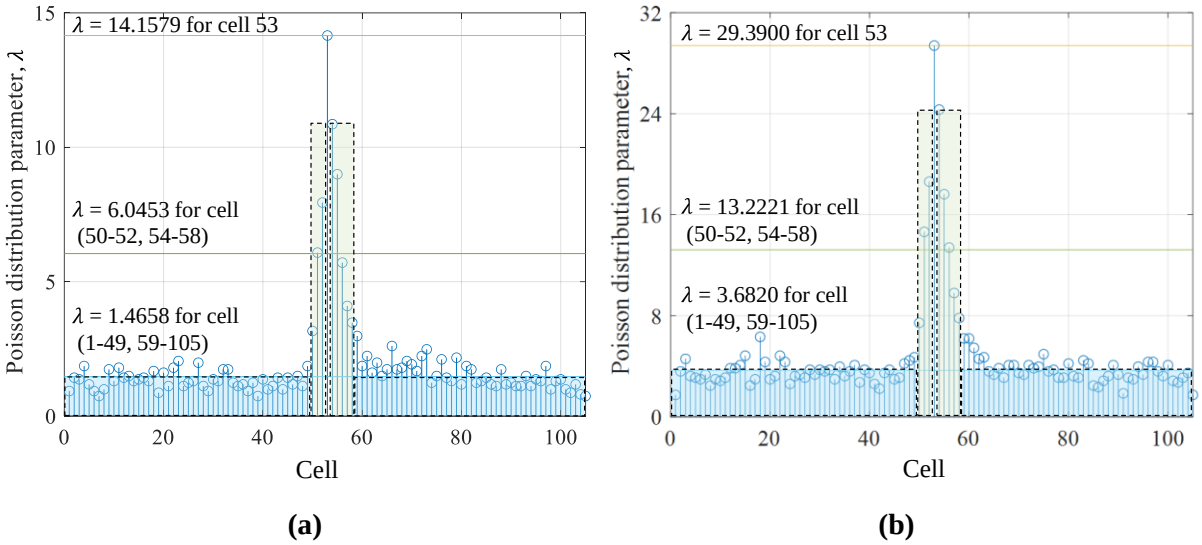

Figure 4-2 Poisson distribution parameters for each cell and the average values for different intensity level areas of (a) inner lanes; (b) outer lanes.

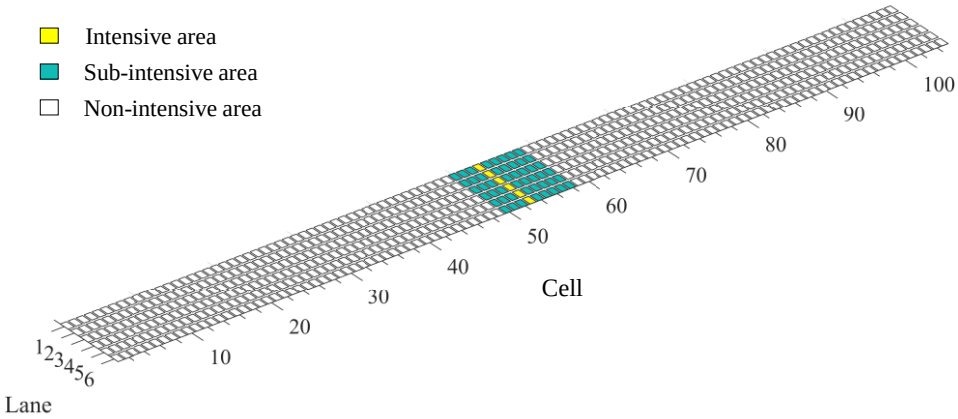

Figure 4-3 Cell classification of load intensity level according to statistics.

Six representative simulated samples for the cases of stationarity and non-stationarity are illustrated in Figure 4-4. Compared with the case of stationary process, heavy vehicles of non-stationary process are significantly more likely to be represented in intensive and sub-intensive areas near the mid-span. This result suggests that the non-stationary Poisson process has a significant effect on the spatial distribution of heavy vehicles by adjusting the weights of vehicle occupancy probabilities in different cell regions.

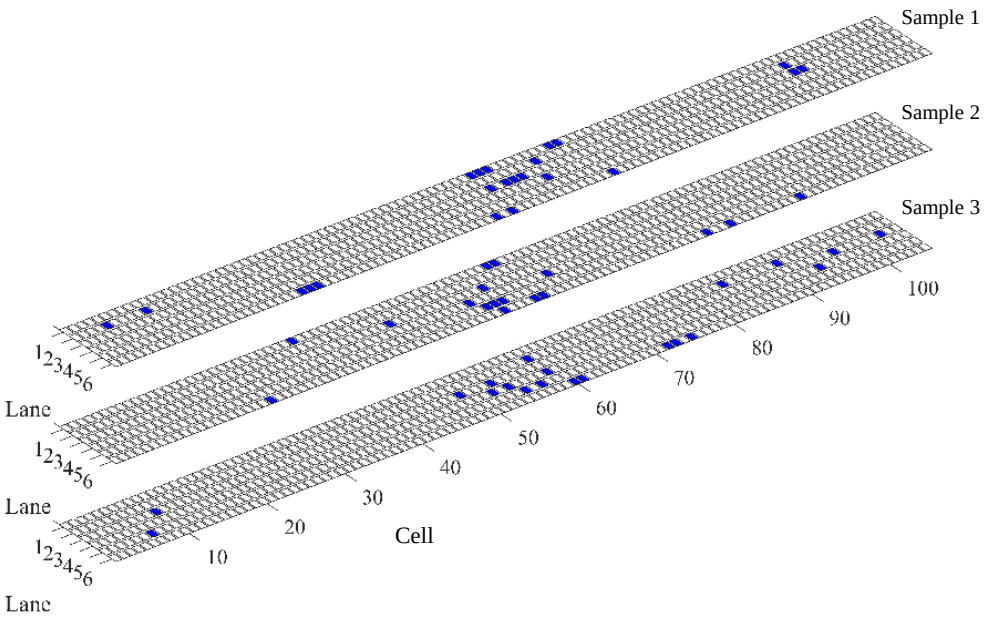

(a)

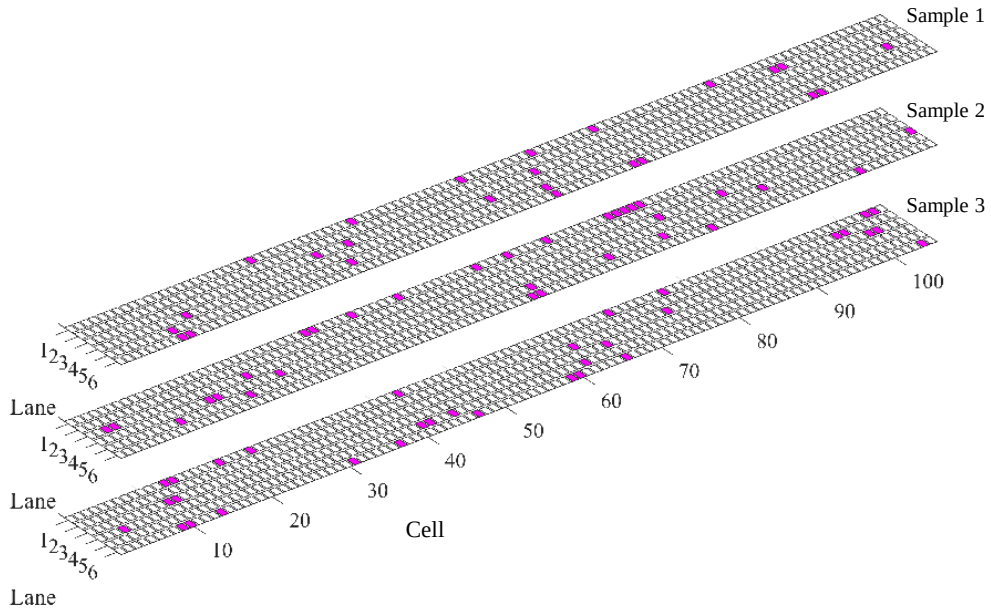

(b)

Figure 4-4 Samples of simulated heavy vehicles distribution for (a) non-stationary process; (b) stationary process.

4.3.2 Heavy vehicle weight and parameters

The samples of GVW are adopted from the heavy vehicles of the scenarios of extreme LE calculated from WIM data. The relationship between AIC of GMM and number of components for both inner lanes and outer lines are shown in Figure 4-5. The fitting effect gets better with the decrease of the AIC value, while the decreasing rate of AIC becomes slower when the number of components is large. Considering the fitting effect and the AIC values, the number of components of GMM is selected as 4. The parameters of simulated GMM are summarized in Table 4-2.

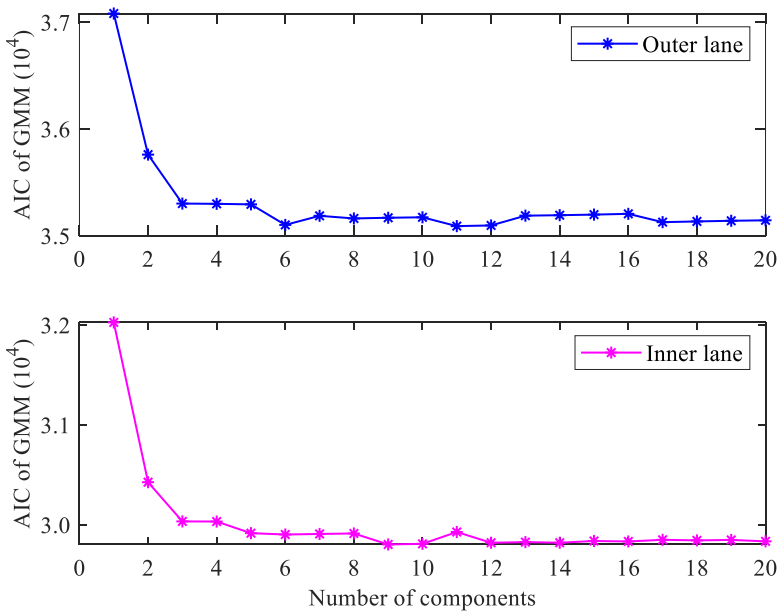

Figure 4-5 Relationship between AIC and number of components.

Table 4-2 Parameter of simulated GMM (tonnes).

GMM *i*-th component	Mean value of Outer lane	Mean value of Inner lane
1	16.98	17.02
2	29.60	29.56
3	60.80	60.66
4	99.71	101.13

4.3.3 Monte Carlo simulation of the scenarios model

In order to obtain sufficient sample data to account for the possibility of an extreme load response within the required return period, the Monte Carlo method is employed in this research. Based on

10^5 simulations, the simulated scenarios of extreme LE are generated for 8 cases, respectively. These 8 cases include stationary and non-stationary processes for location distribution, and 4 levels of correlations of GVWs between adjacent cells in the scenarios of extreme LE are considered (i.e., *D* equals to 20 m, 50 m, 100 m, and uncorrelated). Figure 4-6 illustrates the effect of GVWs simulation with different correlation lengths.

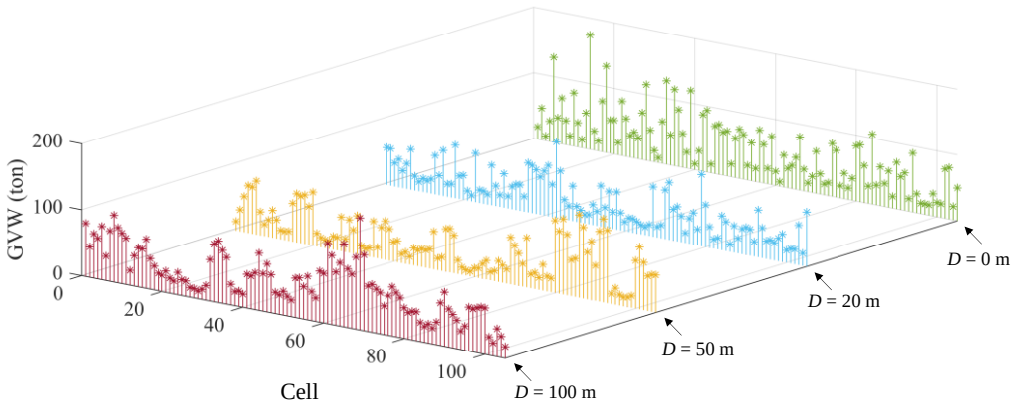

Figure 4-6 Simulation samples of GVWs from different correlation length *D* for outer lane.

Several representative simulated samples on the bridge deck are depicted in Figure 4-7. The cases of stationary process and non-stationary process location distribution are illustrated in Figure 4-7 **(a)** and **(b)**, respectively. The difference between stationary and non-stationary process methods can be clearly observed in the figure. In Figure 4-7 (a), the heavy vehicles in the extreme response scenario are more evenly dispersed on the bridge deck. In contrast, in Figure 4-7 (b), the heavy vehicles in the extreme response scenario tend to be concentrated in the mid-span region of the bridge deck, indicating that the complicated spatial distribution of heavy vehicles on the bridge deck can be effectively characterized by this model. Meanwhile, the simulation of non-stationary process is more accurate than the stationary process and is recommended for use in subsequent studies.

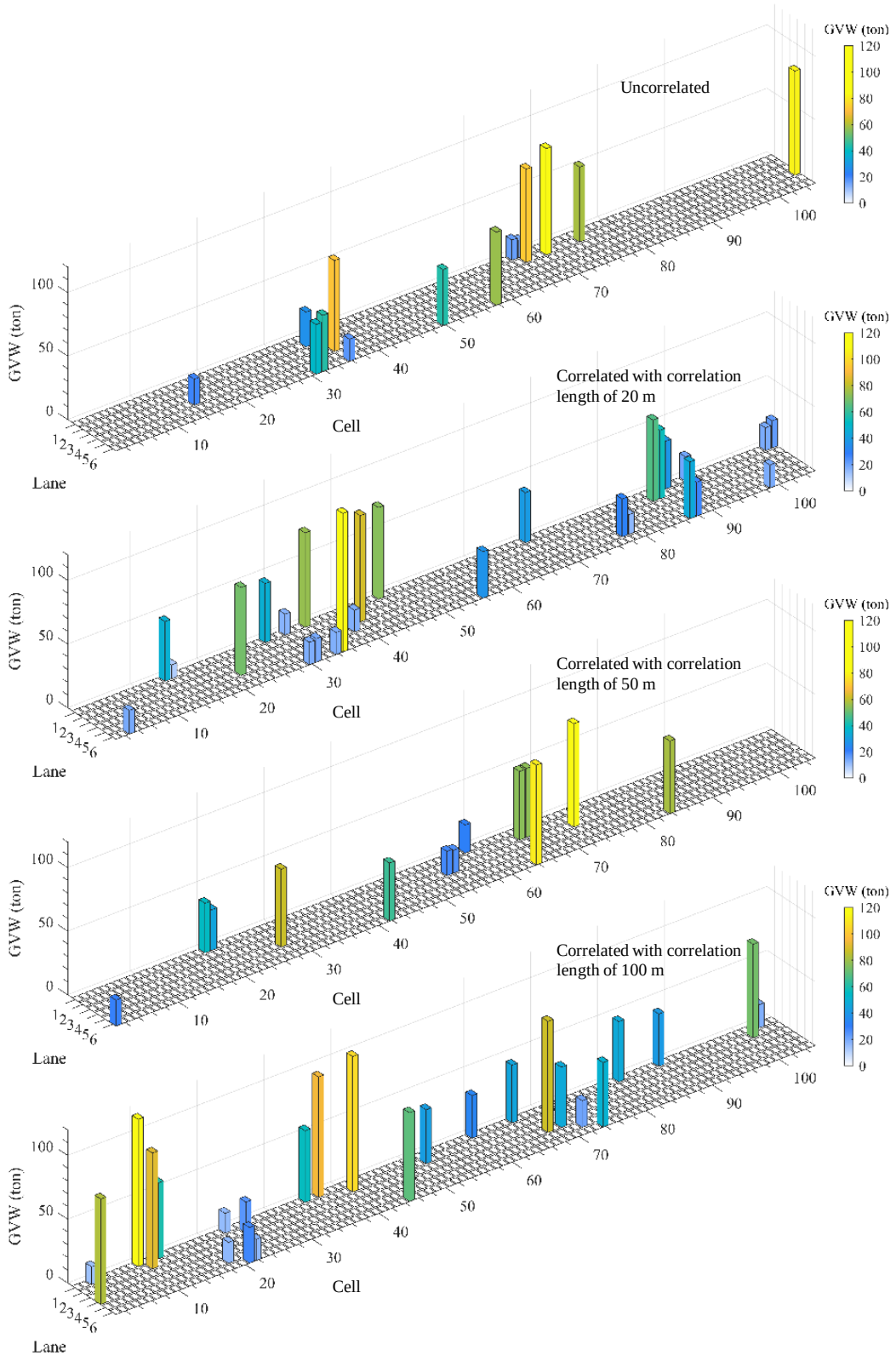
Uncorrelated
Correlated with correlation length of 20 m
Correlated with correlation length of 50 m
Correlated with correlation length of 100 m
GVW (ton)
Cell
Lane

(a)

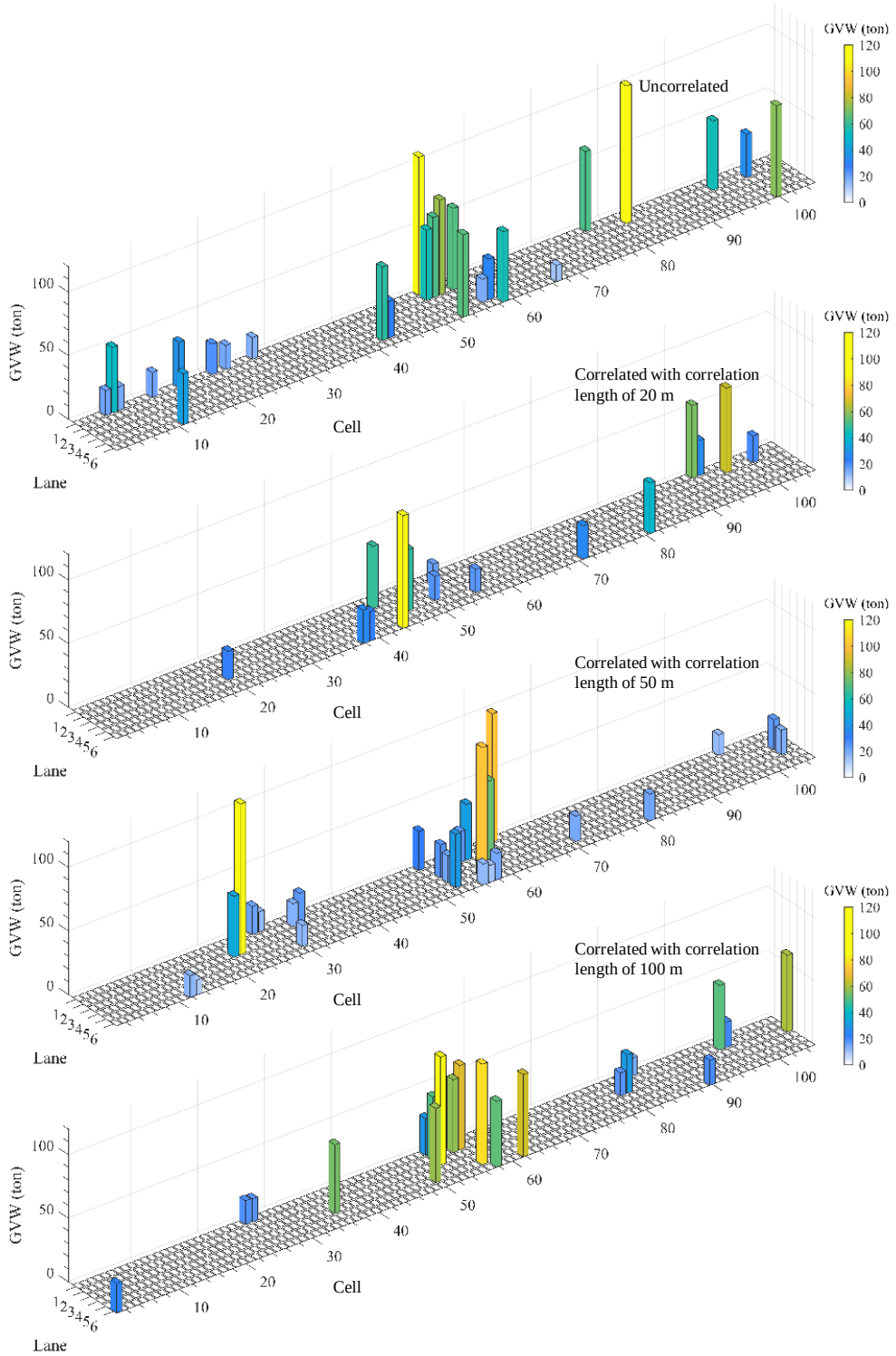

(b)

Figure 4-7 Simulated samples of scenarios for (a) stationary process location distribution; (b) non-stationary process location distribution

4.4 Impacts of ignoring light vehicles and moving vehicle-centroid into cell on LE

Ignoring the light vehicles in the modeling of vehicle distribution on bridge deck can bring convenience to computation, while its impact still needs to be evaluated. Due to the small GVWs of these vehicles, the structural effect is slightly affected by ignoring them. Commonly, vehicles with gross weight larger than 10 tonnes can be treated as heavy vehicles (Chen et al. 2019; Ruan et al. 2017). Therefore, vehicles with GVW smaller than 10 tonnes are removed in a second analysis. Figure 4-8 presents the influence of ignoring light vehicles in the simulation process. The abscissa of the figure shows 423 samples. For each sample, the top subfigure gives the ratio of response calculated by ignoring light vehicles to response calculated by considering all vehicles in the scenario, which is displayed in percentage. The bottom subfigure shows the ratio of number of light vehicles to total number of vehicles. It can be seen that the vast majority of response is generated by heavy vehicles. For 423 samples, the effect losses induced by ignoring light vehicles are almost less than 5%. However, by this kind of simplification, the corresponding total number of vehicles on bridge deck that need to be considered in the modeling is significantly reduced. More importantly, in the process of vehicle spatial distribution modeling, this approach can eliminate the interference of lighter vehicles and accurately establish the probabilistic model for heavy vehicles which contributes significantly to the LE.

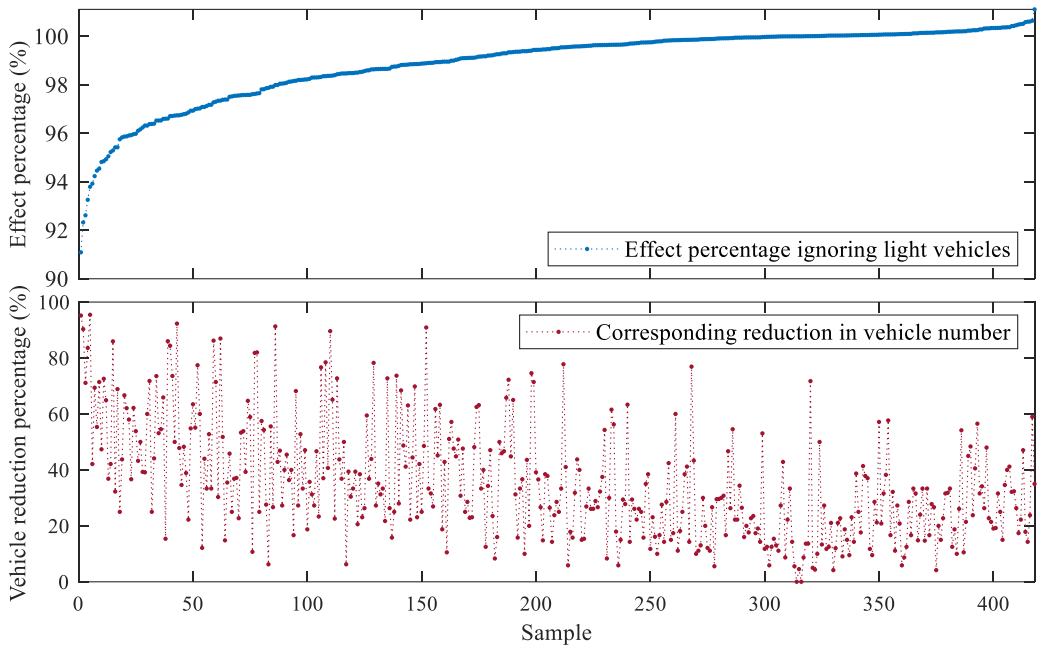

Figure 4-8 Impact on LE by ignoring light vehicles.

Meanwhile, the influence of moving the centroid of heavy vehicles into the cell on obtaining LEs is also presented. The relative error of LE caused by moving vehicles into cell is displayed on the normal probability paper as shown in Figure 4-9 **(a)**. The relative error histogram of LE is presented in Figure 4-9 **(b)**. The relative error is centered between 0 and 2%. As observed, shifting the loading location of heavy vehicles from their actual position to the nearest cell center is acceptable in terms of maintaining the required level of accuracy.

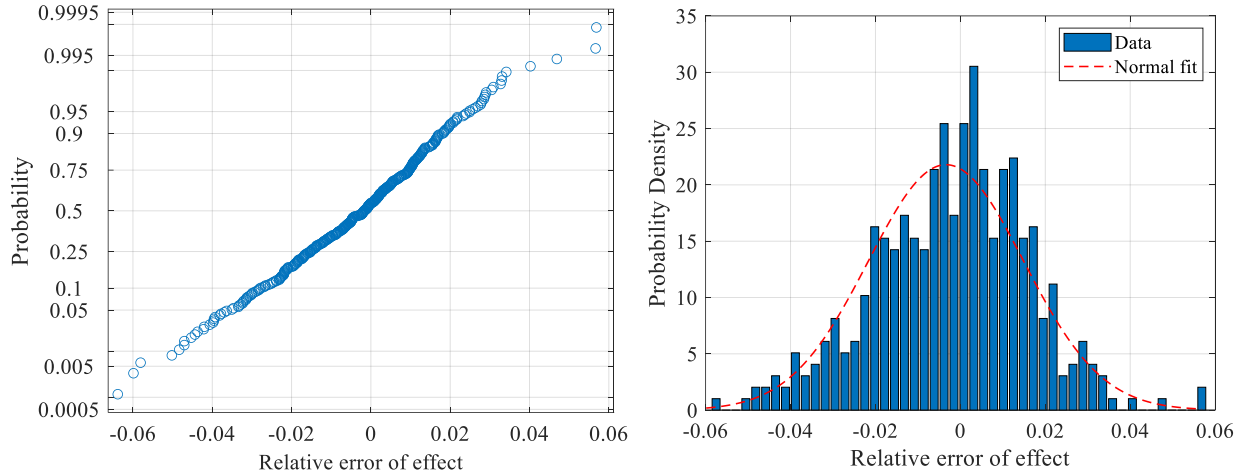

(a) **(b)**

Figure 4-9 Relative error of LE caused by moving vehicles into cell: (a) normal probability paper; (b) Histogram.

For different types of effects, the size of cell results in different levels of error in the response values. Figure 4-10 shows the error of moving heavy vehicles into cells for different effects when the cell length is 20m. Figure 4-11 shows the error when the cell length is 10m. Note that the error here refers to the relative error (the ratio of the response difference to the original response value). It can be seen that the error level related to the cell length and the shape of the ILs. For some highly peaked ILs (such as Effect 4), smaller cell sizes (such as 10 m) should be selected to ensure that errors are within acceptable limits. Therefore, for effects with a small effective area of influence, a suitable cell length should be selected to ensure accuracy. The cell length itself is a flexible parameter that can be adjusted. For example, in this thesis a cell length of 10m is used for congested traffic modeling. At the same time, this thesis focuses on the global effects (when a vehicle is applied anywhere on the whole loading length, a significant response can be created) of long-span bridges. Only effects with a long effective influence range are discussed in relation to the extreme response scenario; effects with a short effective influence range are similar to the extreme value acquisition mechanism for small and medium-span bridges, which is determined by three or less heavy vehicles, and therefore are not the focus of this study. If the method proposed in this thesis is subsequently applied to the research of partial effects, the cell lengths can be flexibly selected to achieve accuracy guarantees.

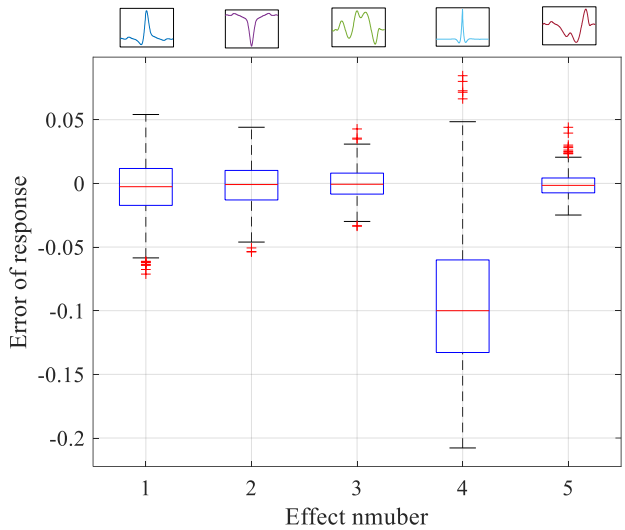

Figure 4-10 Error boxplot of moving heavy vehicles into cells (cell length = 20 m).

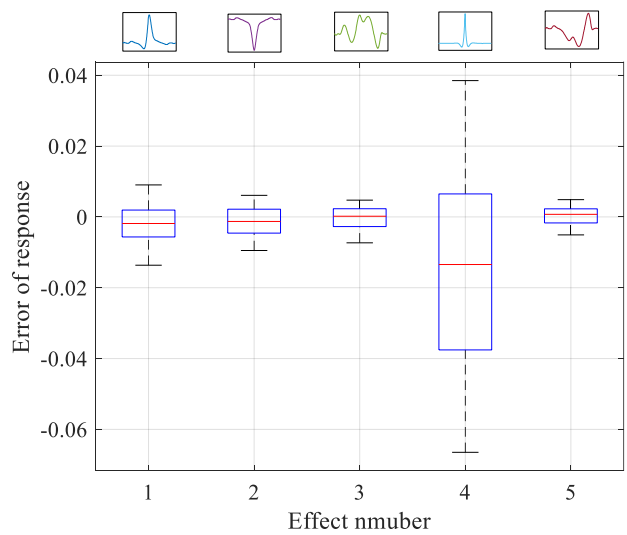

Figure 4-11 Error boxplot of moving heavy vehicles into cells (cell length = 10 m).

Extreme response scenarios with a high number of vehicles on the bridge deck were selected as showcase examples, as shown in Figure 4-12. According to this sensitivity study, a cell length of 10m was selected for Effect 4 and 20m for the other effects.

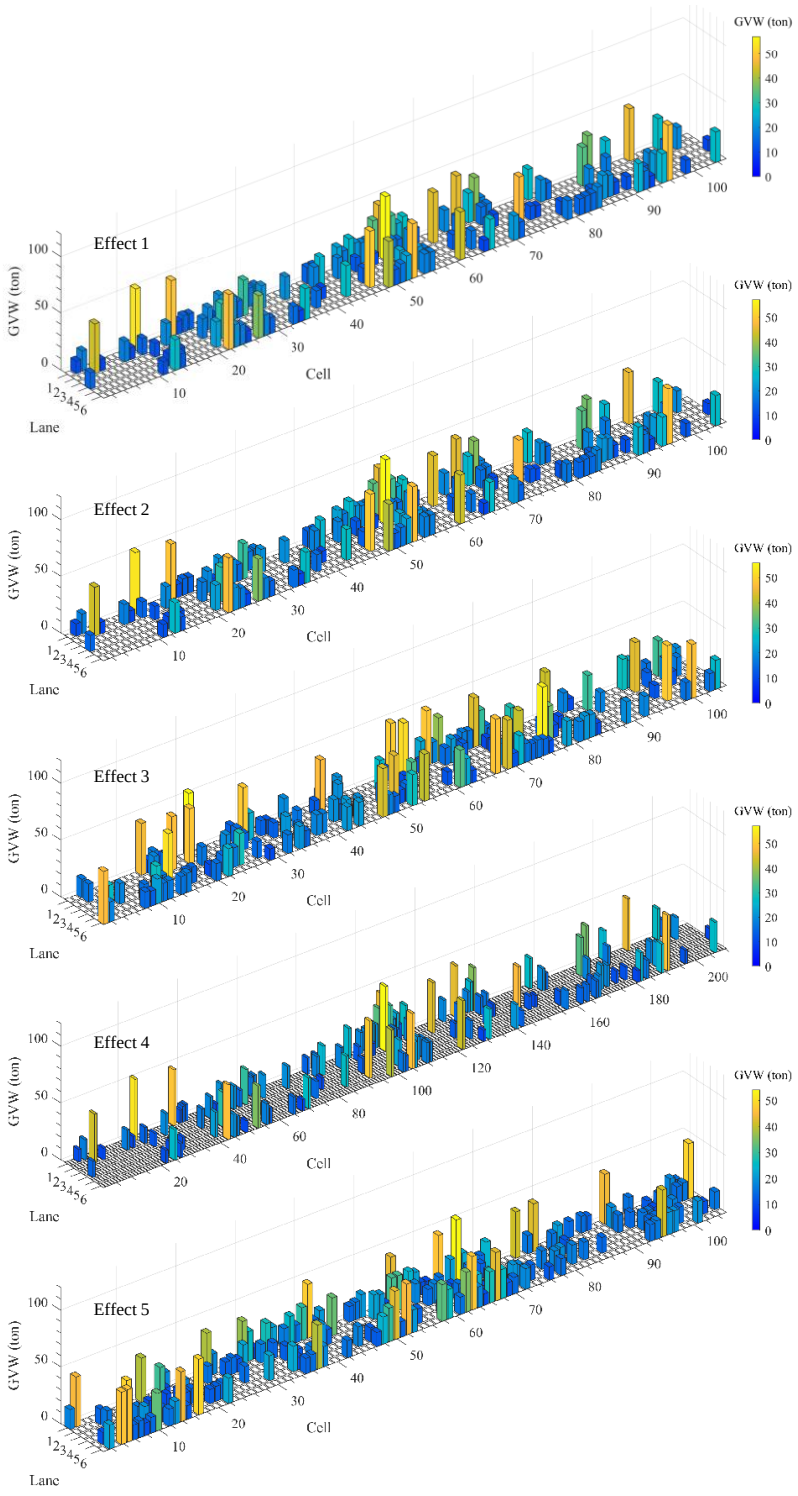

Figure 4-12 Extreme response scenarios for different effects with different cell lengths.

4.5 Impacts of stationarity and correlation in vehicle weight on extreme LE

This section examines the effects of stationarity and correlation in GVWs on the extreme value LE. Due to the lack of statistical data associated with the correlation of GVWs of adjacent heavy vehicles, four cases of correlation are considered in aforementioned analysis, ρ = 0.3679, 0.6703 and 0.8187 (i.e., D is 20 m, 50 m, and 100 m), and no correlation, respectively. Performing 105 simulations, the sensitivity of maximum axial force of cable to the stationarity and correlation in GVWs is analyzed.

Since the vehicle scenario samples are vehicle distributions of the maximum daily effect value, the GEV distribution can be applied to fit the response obtained by the simulated scenarios. Figure 4-13 **(a)** displays the differences between the distribution functions in stationary and non-stationary conditions of the simulation results on the Gumbel probability paper. Figure 4-13 **(b)** shows the histogram and the fitted curves of the simulation results for stationary and non-stationary processes. It can be seen that the GEV distribution shows a good fitting effect on the tail tendency of the data. The upper tail of response is long which is consistent with the characteristics of GEV.

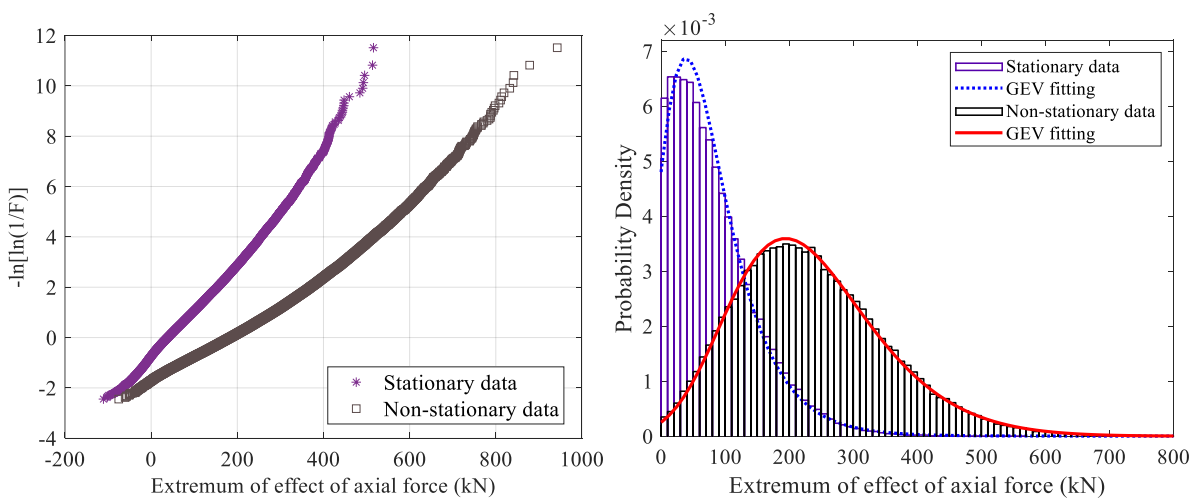

(a) **(b)**

Figure 4-13 Probability density and fitting of the simulation results for non-stationary and stationary processes when the GVWs are uncorrelated: (a) Gumbel probability paper; (b) Histogram.

In order to compare the effects of stationarity of vehicle location on the simulation results, the GVWs with uncorrelated state is considered. The effect extremum of the simulated scenarios of extreme LE for non-stationary process is significantly larger than that of stationary process. For the extreme values of these two processes, the 0.9999 times quantile of response is 800 kN for non-stationary process, and 450 kN for stationary process. The non-stationary process simulation method for the location of vehicles contributes more to the extreme values. Meanwhile, because the design live load for long-span bridges should include multiple trucks (Wang & Xu 2019), and the impossibility of calculating the frequency for each possible spatial distribution pattern (Chen et al. 2019), then, the probability of the on-bridge vehicle distribution pattern for a certain effect is an important factor. The arrangement of vehicle distribution has an obvious relationship with the effect type, and the statistical results of the sensitive areas of the bridge deck are different for different load effects. According to the classification research of the effect depending on the effective influenced region (Ruan et al. 2017), the vehicle scenarios of extreme LE should be modeled separately for different types of effects. Although building the model separately for different effects may bring a large computational cost, it cannot be avoided in the process of loading the simulated traffic on the influence line and finding the maximum response value per day for the bridge assessment. Meanwhile, the non-stationary process method can better simulate the pattern of the vehicle distribution, thereby improving the response calculation accuracy by the simulated scenarios.

Figure 4-14 (a) displays the differences between the distribution functions of cable axial force for non-stationary process and different correlation levels on the Gumbel probability paper. Figure 4-14 **(b)** and **(c)** show the CDFs of extremum of axial force for non-stationary process. Theses CDFs corresponding to different correlation level of GVWs intersect in the region with CDF values between 0.7 and 0.8. When CDF value is more than 0.8, the exceeding probability is larger for the extreme effect simulated with higher correlation. The extreme value increases with the increase of the correlation in the GVWs. This is due to the fact that the distribution of the effect extremum of simulated scenarios has longer tail behavior for larger correlation. At a high percentile level as shown in Figure 4-14 **(c)**, the effect extremum increases significantly with increasing correlation coefficient of GVWs. This is in accordance with the physical meaning that a larger probability of heavy vehicle queuing will lead to a larger probability of occurrence of extreme response values. An obvious fact is that the correlation coefficient of GVWs has a direct relationship with the

probability of heavy vehicle queuing. It can also be seen that, with a sufficient number of Monte Carlo simulations, statistical differences in the simulation results under different correlations can be manifested.

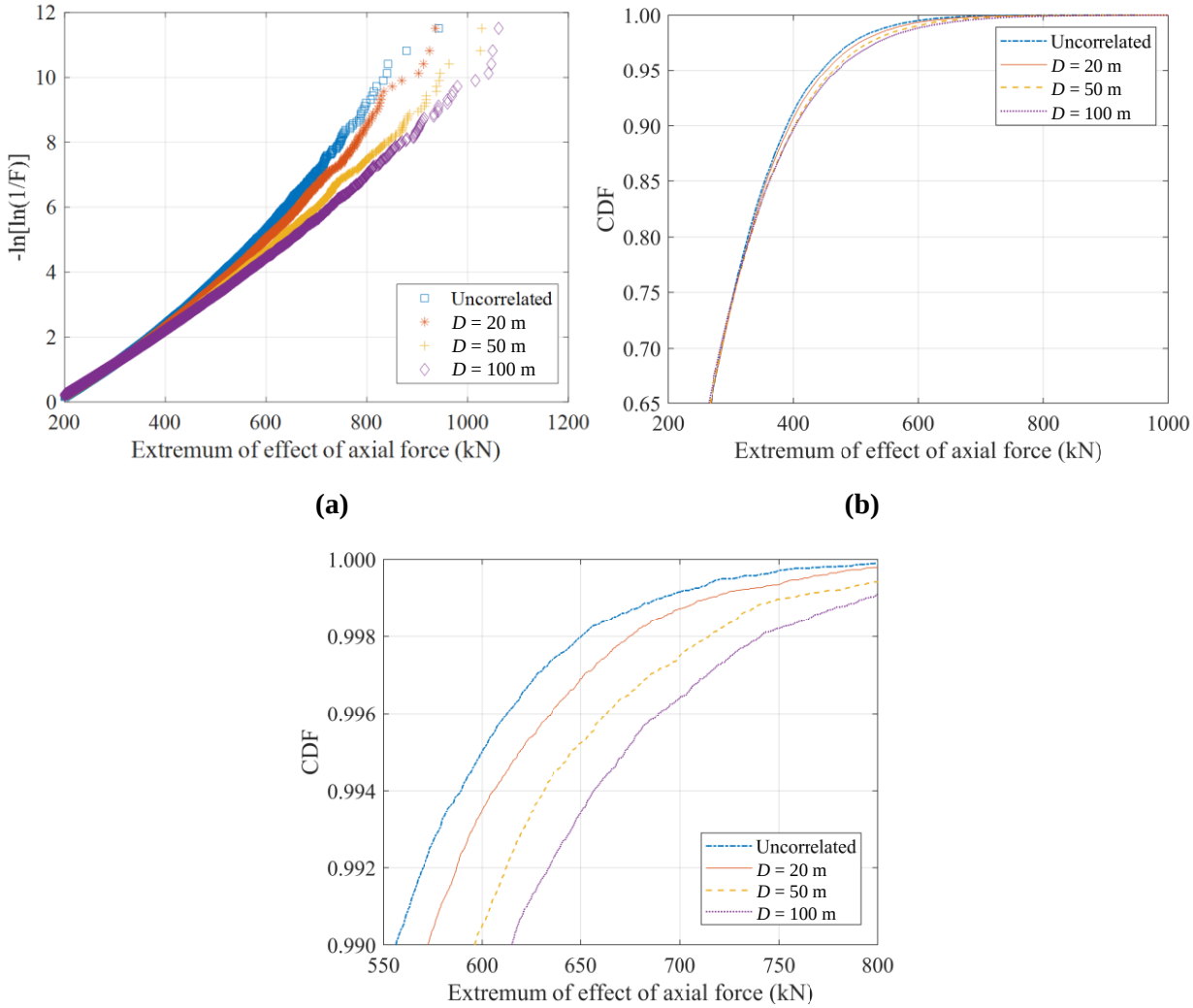

Figure 4-14 Simulated CDFs of extremum of axial force for non-stationary process (a) Gumbel probability paper; (b) overall CDF; (c) tail behavior.

Figure 4-15 shows different quantile values of maximum effect of simulated data. With the increase of correlation coefficient, the quantile value of extreme effect of simulated data becomes higher, as it is expected. For the case of non-stationary process, the 0.9999 quantile value of simulated data increases from 802.9 (i.e., uncorrelated) to 826.5 (i.e., D = 20 m; ρ = 0.3679), 917.6 (i.e., D = 50 m; ρ = 0.6703) and 960.1 (i.e., D = 100 m; ρ = 0.8187). In addition, the obvious

difference between stationary and non-stationary processes assumption can be observed in Figure 4-15 **(a)** and **(b)**. In summary, the most unfavorable effect is obtained by considering non-stationarity of the vehicle location and correlation between the GVWs.

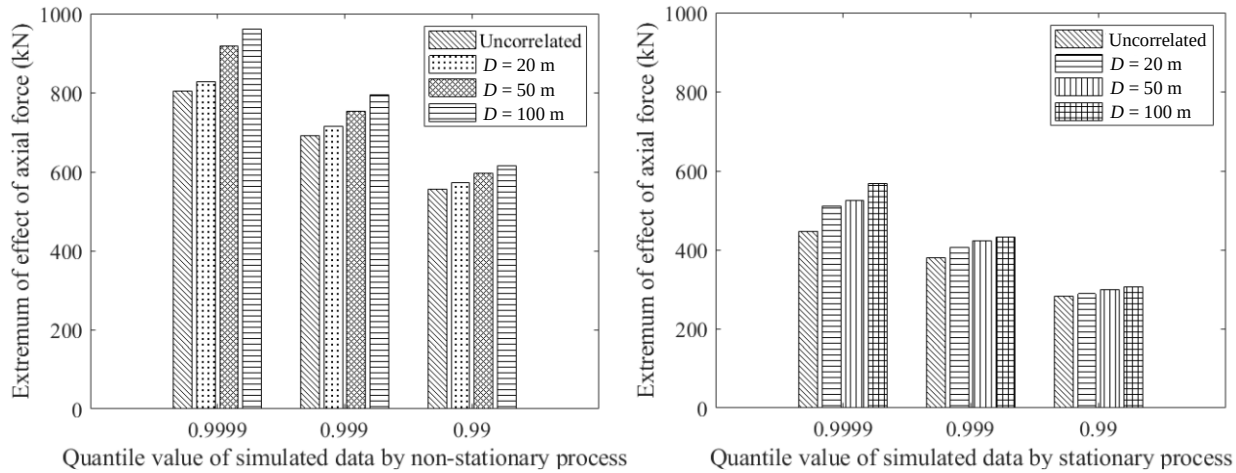

(a) **(b)**

Figure 4-15 Quantile value of effect extremum of simulated data by (a) non-stationary process; (b) stationary process.

4.6 Comparison of load model effect with Design Codes

The proposed probabilistic model of vehicle scenarios of extreme LE is applied to the five effects of the investigated bridge. For comparison with the responses derived from the Chinese code D60 (Ministry of Communications and Transportation, 2015), the responses calculated by the simulated scenarios are all extrapolated to the expected response results that will not be overpassed 95% of the cases in a design period of 100-year. The D60 specifies a characteristic traffic LEs as that value which has a 5% probability of being exceeded in 100 years, which is comparable to a value with a return period of around $1/\left(1-0.95^{1/100}\right) = 1950$ years (Ruan et al. 2017). The effects calculated by simulated data and their extrapolation curves are plotted on Gumbel probability paper as shown in Figure 4-16. The GEV based extrapolation method is employed to fit the simulated samples and 10^5 simulated samples are used. Based on extreme value theory (O'Brien et al. 2015), various methods are used to predict extremes based on limited data; among these

methods, the block maxima approach using GEV has been widely adopted (Zhou, Caprani & Zhang 2021).

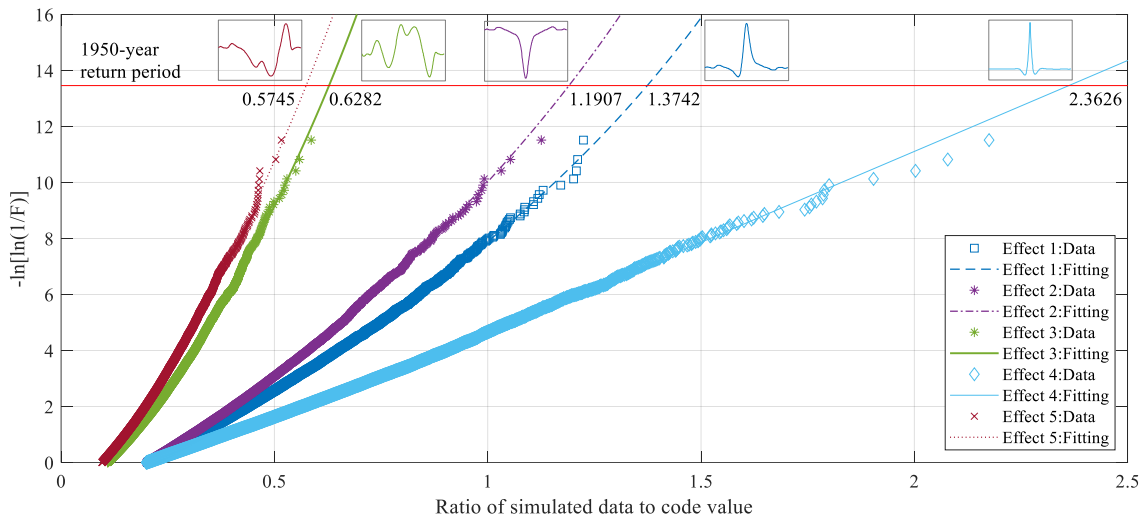

Figure 4-16 Ratio of simulated extreme response to Chinese code value for different effects with D = 100 m and non-stationary process.

In Figure 4-16, the abscissa represents the ratio of responses of several effects to corresponding code value of D60, and the 1950-year return period value is calculated by $-log\left(-log\left(1-1/(1950\times 365)\right)\right) = 13.48$. The considered effects are the axial force of the longest cable (AFC, Effect 1), the vertical deflection at mid-span of the main span (VDMS, Effect 2), the longitudinal displacement at the top of the pylon (LDTP, Effect 3), the bending moment at mid-span of the main span (BMMS, Effect 4), and the bending moment at the bottom of the pylon (BMBP, Effect 5). The shape of the influence line for each effect is also plotted in Figure 4-16. It can be seen that in the unfavorable extreme state of the simulated data of D = 100 m and non-stationary process, the responses ratio of the LDTP and the BMBP are 0.628 and 0.575, which means the effects derived from proposed model are much lower than the code value. The response ratio of the BMMS is 2.363, which means the effect derived from proposed model is much higher than the code value. It should be noted that larger moments result in increased stresses at the upper or lower edges of the bridge deck slab. In the provisions of the code, the checking of stresses is within the scope of ultimate limit states. Excessive response values of bending moments, while reflecting some traffic load problems laterally, cannot be used as direct evidence to question the code.

Therefore, the longer the effective loading range of the effect, the more conservative the code's loading result. Based on the comparison among the responses results, different effects show varying degrees of adaptability to the code load model, which suggest that it becomes critical to develop the load model for different effects separately according to the actual vehicle scenarios of extreme response event.

Several codes are chosen to compare with the simulated load responses, including D60, Eurocode, AASHTO, and BS5400 (AASHTO 2004; BS EN 1991-2 2003; BS 5400-2 2006; Ministry of Communications and Transportation, 2015). In terms of bridge loaded length, these codes have certain rules that must be followed when they are used. The load model is only suitable for highway bridges with spans less than 200 m according to Eurocode. Until the 7th (2014) edition, when the HL-93 load model was introduced for long-span bridges, AASHTO expected bridge spans to be lower than 500 feet (152.4 m). In JTG D60-2015, a longitudinal reduction factor of 0.93 is used for bridges over 1000 m. In BS5400, the HAUDL decreases as the length increases, that can be thought as a longitudinal reduction factor.

Table 4-3 compares the LEs calculated by the modeled vehicle scenarios and the codes. The effects of simulated data are calculated with non-stationary process and D = 100 m (maximum correlation between GVWs) which could be a possible traffic state for the investigated bridge giving the most unfavorable results. By placing the load models on the influence line with the same sign of influence value, the effects of the codes are obtained. The simulation extrapolated effects corresponding to the return period specified by codes are given in Table 5-7. The return period of each code is calculated according to the given service life. The return period of Chinese D60 is 1950 years (5% probability of exceedance in a reference period of 100 years); Eurocode is 1000 years (5% in a period of 50 years); BS 5400 is 2400 years (5% in a period of 120 years) and AASHTO is 75 years (based on the mean 75-year maximum LEs) (Cooper 2011; Micu et al. 2019; Nowak 1993; Nowak 1994; Ghosn, Moses & Wang 2003). The extrapolated value is related to the return period considered in the respective Code. Some partial extrapolated structural effects loaded by the simulated scenarios are lower than those derived from the codes, while others are higher. Specifically, for Effect 4 (BMMS), the extrapolated value is more than twice of the D60 value. The Eurocode provides the highest results, whereas the other codes are typically on the same level. This is due to the fact that the load model of the Eurocode is only applicable to bridges with spans

less than 200 m. Meanwhile, a site-specific traffic scenarios modeling approach should take into account the extreme effect value that the bridge will experience during the reference period, with acceptable reliability. By comparing the simulation results with the code value, it can be seen that the method proposed in this thesis provides an effective way for addressing this problem. Furthermore, since traffic characteristics are site-specific (Getachew & O'Brien 2007; O'Brien 2015; Ruan et al. 2017; Lipari, Caprani & O'Brien 2017), the simulation process and results in this case are strongly dependent on the site-specific data. For this reason, in the next chapter the Bayesian up-dating of the model is carried out to take into account different traffic conditions.

Table 4-3 Comparison of the responses derived from simulation load and codes for different effects of the investigated bridge.

Traffic load response	Max Simulated value	CV and ESV for the corresponding return periods							
		ChinaD60		AASHTO		Eurocode		BS5400	
		CV	ESV	CV	ESV	CV	ESV	CV	ESV
AFC ($\times 10^3$)/kN	1.08	0.87	1.19	0.98	1.02	2.07	1.16	1.78	1.20
VDMS/m	-1.45	-1.17	-1.40	-1.31	-1.18	-2.85	-1.35	-2.49	-1.41
LDTP/m	0.22	0.37	0.23	0.41	0.20	0.95	0.23	0.82	0.24
BMMS ($\times 10^5$)/kN·m	1.75	0.79	1.86	0.93	1.46	1.59	1.78	1.34	1.88
BMBP ($\times 10^5$)/kN·m	-1.91	-3.66	-2.10	-4.02	-1.77	-9.27	-2.04	-7.99	-2.12

CV: code value; ESV: extrapolated simulated value.

4.7 Conclusions

In this chapter, a typical double-tower cable-stayed bridge is introduced as a case study to demonstrate the extreme response scenario simulation of spatial vehicle distribution. Generally, the feasibility and advantages of the proposed probabilistic model for long-loaded length vehicle extreme response scenarios are demonstrated. The simulation method and process depend strongly on the site-specific data, which should be used to calibrate the site-specific bridge performance. And by comparison different responses of simulated data, it can be illustrated that different effects show various levels of sensitivity to the code value, which prove it is essential to build the load model for different effect separately according to the actual extreme response scenarios.

CHAPTER 5 Validation and extended applications of the scenario probabilistic model

5.1 Introduction

A new proposed traffic load model always needs to be validated. The validation strategies are different depending on the objectives of the proposed model and the real data available to carry out the validation. Therefore, an improved CA traffic model (Ruan et al., 2017) is selected as a simulation model for alternative traffic flows in this chapter for extreme scenario model validation. This CA traffic simulation method has been carefully calibrated by comparing data such as traffic parameters and load effects between simulation results and WIM data. The application of this CA method allows for rigorous acquisition of traffic flow with high simulation accuracy that are consistent with the original WIM data. The accuracy and reasonableness of the proposed model in simulating extreme response scenarios is discussed by comparing the simulation results between the model of extreme response scenarios and the introduced CA model which represents the original WIM data.

In addition to accuracy verification of the load model, whether the model has wider applicability is also an element of the model performance to be examined. The load model should have a flexible scope of application and wide applicability to meet the modelling requirements of different types and spans of bridges with different assessment objectives. In this chapter, the proposed extreme response scenario model is constructed for the type of traffic that inevitably needs to be discussed for long-span bridges: congested traffic. As congested traffic differs from free flow in many aspects such as vehicle composition, vehicle density, and traffic speed, there are many differences in model assumptions and parameter selection for the construction of the extreme response scenario model, reflecting the flexibility of the application of the proposed extreme response scenario model. At the same time, the analysis of long-term measured WIM data shows that free flow is also important in the daily structural assessment of long-span bridges. The extreme response scenarios of free flow are no less threatening to the safety of structures than congested flow.

5.2 Validation of the proposed model

In order to validate the proposed model of scenario of maximum-per-day event, an improved CA for microscopic traffic simulation is introduced to generate artificial WIM data to extend the amount of the original WIM data. In the proposed extreme response scenario model, there are two unknown parameters, the distribution of GVW and the Poisson parameter related to vehicle location. They can be acquired by the extreme response scenario samples derived from WIM data. In this way, the proposed model can be validated through the comparison of LEs obtained with the proposed model and the original and artificial WIM data. The time period used in both models for validation is 730 days. The validations are based on comparing the results of the proposed scenario model with those of simulated WIM data (artificial WIM data by CA method) and original WIM data. The distributions of GVWs and the Poisson parameters from the proposed model and WIM data are compared. Meanwhile, a comparison is conducted between the maximum-per-day LEs and the total load on the bridge deck obtained from the proposed model and those obtained from simulated WIM data (artificial WIM data by CA method).

5.2.1 Validation of loading scenarios

Table 5-1 displays the specified CA parameters based on the original WIM data. The bridge loading length of the simulation is selected as 3000 m. Traffic flows in two directions are simulated separately because the maximum number of lanes that can be simulated at the same time is four. The total time length of simulated traffic flows is two years, and the daily traffic volume ranges from 16,500 to 50,000, which is randomly selected according to the original WIM data. One second is selected as the time step due to the fact that it is accurate enough for traffic loading.

It should be ensured that the simulated WIM data could well reflects the statistical parameters (i.e., vehicle headways, GVWs, traffic velocity, traffic composition, and traffic volume) of traffic loads and flow of the original WIM data. The statistical information of the scenario of maximum-per-day event used for validation is obtained by loading the vehicle sequences of simulated WIM data on influence lines.

Table 5-1 Accuracy and filtration criteria of WIM data.

Parameter	Value	Definition
Simulation length	3000 m	The length of investigated bridge is 2088 m.
Lane number	3 * 2 = 6	The maximum number of lanes that can be simulated at the same time is 4 (only a limit of the software).
Daily traffic volume	From 16500 to 50000	
Number of days	730	
Time step	1 s	

The GVWs from both the proposed scenario model and the scenario obtained with the original WIM data are compared in Table 5-2. The relative errors are all lower than ± 1.3%. The highest relative errors appear at the second and fourth component of GMM for GVWs of the outer lane. The distribution of GVWs from the proposed scenario model is quite similar to the original WIM data, ensuring that the generated LEs are equivalent.

Table 5-2 Parameter comparison of simulated and original GMM (tonnes).

GMM *i*-th component	Mean value of Outer lane			Mean value of Inner lane		
	Original data/tonnes	Simulated data/tonnes	Relative error	Original data/tonnes	Simulated data/tonnes	Relative error
1	16.98	16.97	-0.1%	17.02	17.06	0.21%
2	29.60	29.22	-1.3%	29.56	29.77	0.71%
3	60.80	60.44	-0.6%	60.66	60.64	-0.04%
4	99.71	100.76	1.1%	101.13	100.35	-0.77%

Table 5-3 gives the comparison of Poisson parameters (stationary Poisson process). The Poisson parameters of the proposed model exhibit uniform variation similar to those of WIM data, and the relative errors are less than 20% for all LEs, but always biased towards safety.

Table 5-3 Comparison of Poisson parameters from the proposed model and simulated WIM data (artificial WIM data by CA method) (all lanes) (veh).

Effect number	Outer lane			Inner lane		
	Scenario model	Original WIM	Relative errors	Scenario model	Original WIM	Relative errors
AFC	5.27	4.65	18.9%	2.30	1.94	13.2%
VDMS	5.45	4.86	18.9%	2.44	2.05	12.2%
LDTP	5.88	5.21	20.3%	2.68	2.23	12.7%
BMMS	4.80	4.22	20.4%	2.07	1.72	13.9%
BMBP	5.91	5.25	20.1%	2.71	2.26	12.7%

5.2.2 Validation of LEs

It is required that the simulation of LEs by the proposed scenario model should be commensurate as those obtained by real measurements in the bridge or by simulated traffic loads derived from reliable and already verified traffic models. As no real measurements of the interested LEs are available for this bridge, LEs from the proposed scenario model and simulated WIM data by CA are compared in detail. The simulation loading length is 3000 m (the length of the investigated bridge is 2088 m), and the bridge entrance is located 500 m away from one side of the bridge.

In general, the LEs in the upper tail are the most important in the evaluation of bridge traffic loads. Thus, the obtained LEs from the proposed scenario model and simulated WIM data are derived from the maximum value of each day. The number of samples of proposed extreme response scenario model is 100000, the number of samples of simulated WIM data is 780. Figure 5-1 to Figure 5-5 show the comparison of the upper tail of five effects from proposed model and simulated WIM data (artificial WIM data by CA method). It can be seen that the proposed model shows higher response values in the upper tail, which is related to the larger number of Monte Carlo simulations of the proposed extreme response scenarios model, but also proves that the model is able to simulate the distribution of heavy vehicles on the bridge deck that can produce extreme response values. At the same time, it can be seen that the proposed model shows a large number of lower response values in the lower tail. This is due to the fact that the proposed model is a probabilistic model and its unscreened simulation results will inevitably contain a large number of samples with low response values. However, as structural safety is primarily concerned with the extreme value portion of the effect, the proposed model is able to produce extreme response scenarios that are comparable to the WIM data and in the safe side for the present case study.

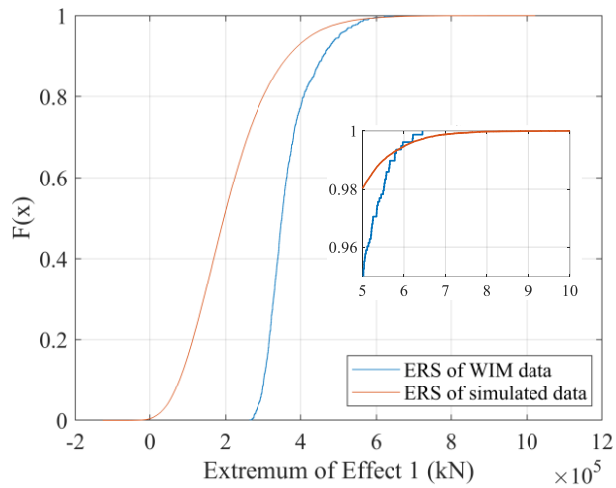

Figure 5-1 Comparison of the upper tail of Effect 1 from proposed model and simulated WIM data (artificial WIM data by CA method).

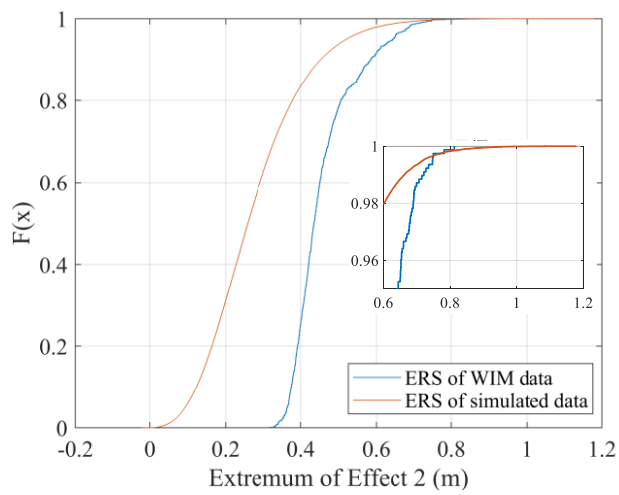

Figure 5-2 Comparison of the upper tail of Effect 2 from proposed model and simulated WIM data (artificial WIM data by CA method).

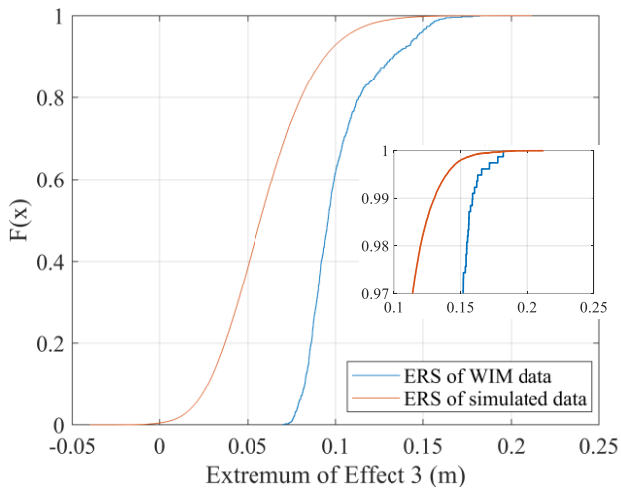

Figure 5-3 Comparison of the upper tail of Effect 3 from proposed model and simulated WIM data (artificial WIM data by CA method).

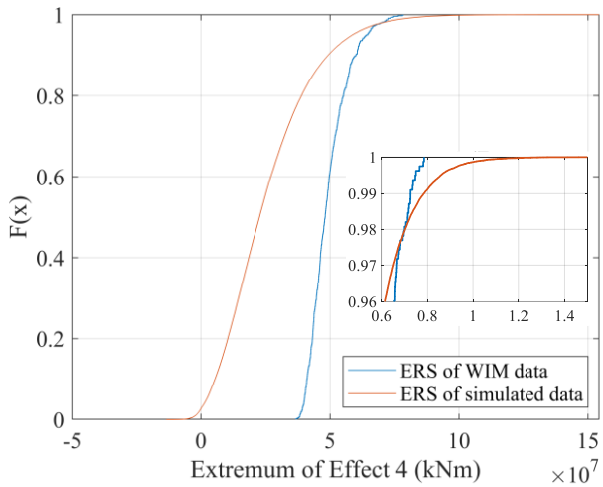

Figure 5-4 Comparison of the upper tail of Effect 4 from proposed model and simulated WIM data (artificial WIM data by CA method).

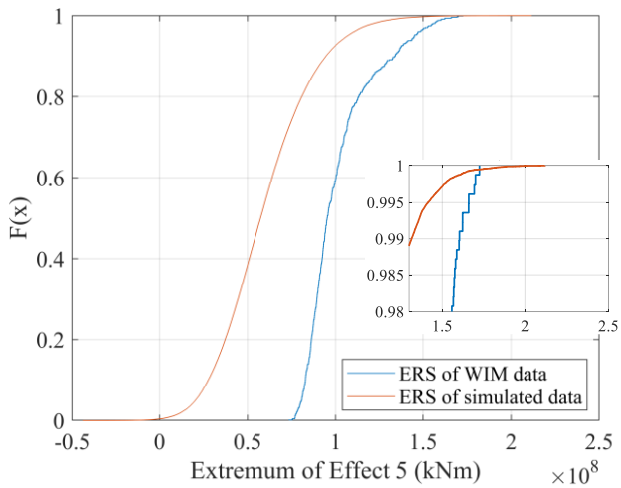

Figure 5-5 Comparison of the upper tail of Effect 5 from proposed model and simulated WIM data (artificial WIM data by CA method).

The total weight of vehicles on the deck corresponding to a scenario of a maximum-per-day event is also a relevant parameter to demonstrate the validity of the proposed model when compared to the WIM data, as shown in Figure 5-6. There are some outliers in the upper part, indicating some extremely maximum gross weights induced by the heavy GVWs. In comparison, the outliers are rare in the lower part. The minimum values are significantly different between the scenario model and the WIM data, but they are not of concern to the objectives of this work, which focus on the maximum effects. The maximum values are very close and always slightly higher than that of simulated WIM data, which indicates that the simulation number of the proposed model is sufficiently high and the proposed model is able to produce extreme response scenarios that are comparable to the WIM data and in the safe side for the case study presented in this thesis.

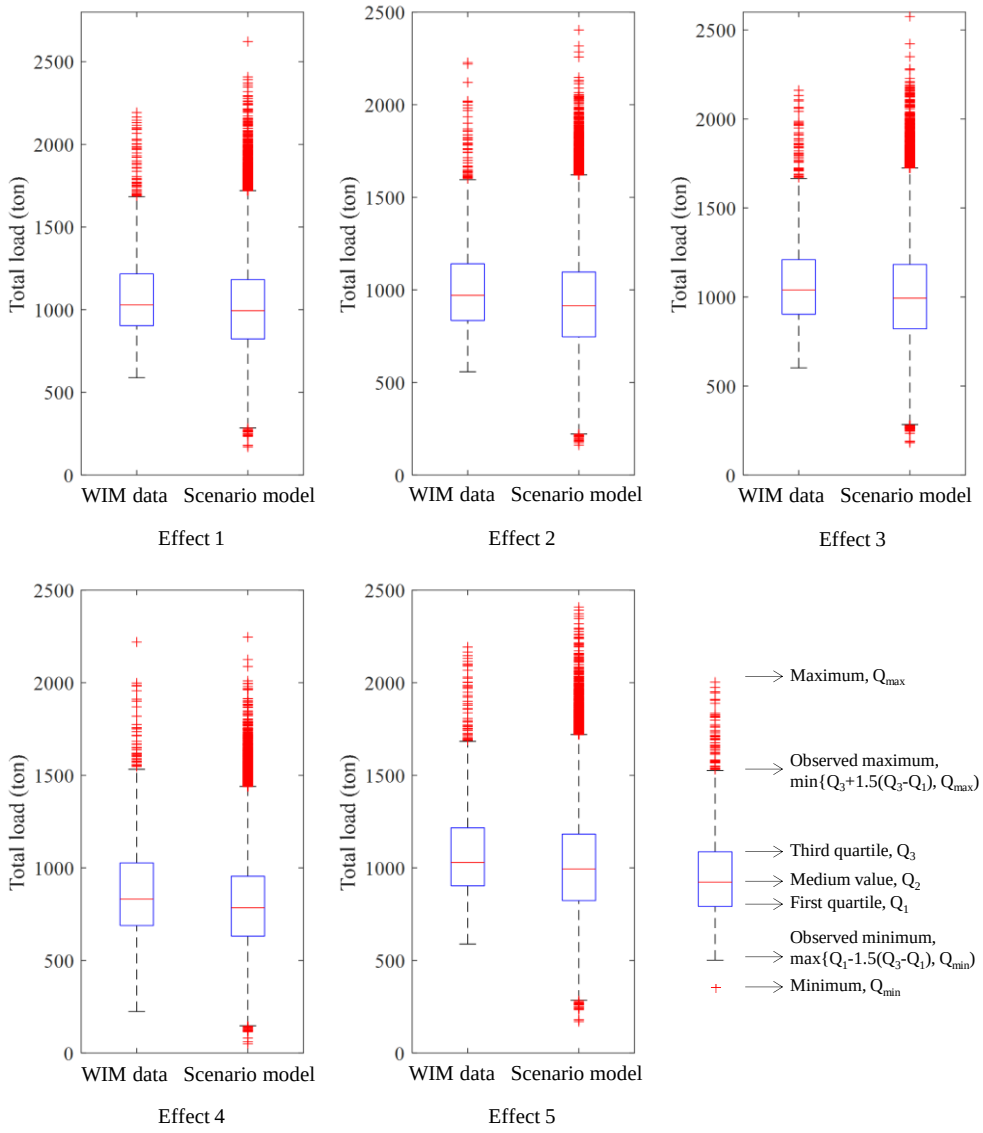

Figure 5-6 Box plot of gross weight on bridge deck of scenario of maximum-per-day event from proposed model and simulated WIM data.

Overall, the validation items of the proposed model show good agreement with those by simulated WIM data and original WIM data. The simulated WIM data is obtained by using a previously validated traffic simulation model (Ruan et al. 2017). The maximum-per-day total load and load effects are very close to and always slightly higher than that of simulated WIM data, which indicates that the proposed model is biased towards the safety side. These results confirm the

validity of the probabilistic scenario model developed in this paper for estimating the maximum LEs on a long-span bridge.

5.3 Congestion scenario simulation by the proposed model

Although mainly developed for the simulation in flow traffic conditions, the model is also applicable to the simulation of congestion scenarios. In this section, a simulation of congested traffic by the proposed model is here presented and, consequently, the loading effects of congested and free flow are compared. The results illustrate that the extreme scenario of free flow traffic is equally important for the safety of long-span bridges.

In the study, 423 daily extreme scenarios (i.e., maximum-per-day event of the effect of cable force, Effect 1) of free-flow were obtained from WIM data as the sample for the developed model. The times at which these 423 samples achieved the extremes (i.e., the response extremes achieved at the points of the day, on a 24-hour basis) were further counted, as shown in Figure 5-7. It can be seen that most of the extreme scenarios occur between 20:00 pm and 7:00 am the next day, and only a small number of extreme scenarios (86 in total) occur during the daytime hours. Common sense dictates that trucks tend to travel at night. At the same time, almost all large cities in the vicinity of the WIM-site are closed to truck traffic during daytime hours, even though there are no restrictions on truck travel times on highways where the WIM station is located. For example, in Shanghai, trucks are banned from the roads in the city area from 07:00 am to 20:00 pm daily. It can be seen that for the daily state free traffic flow, the daily extremes tend to occur more often at night (i.e., with a higher proportion of heavy vehicles and lower traffic flow characteristics), when traffic is less likely to be congested.

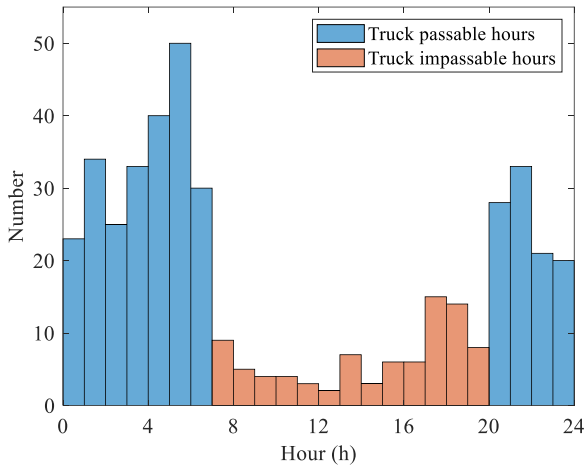

Figure 5-7 Histogram of occurrence time of the extreme scenarios.

The 86 extreme scenarios samples that achieved extreme response values during the daytime mentioned above were further analyzed. For these samples, the ratio of extreme response to Chinese D60 code were calculated, and simultaneous hourly traffic volumes were counted, and plotted in Figure 5-8. The attributes of each scenario sample are identified by a marked shape. For example, circle represents that the sample belongs to holidays and weekends. The results reveal that extreme scenarios with high hourly traffic flow typically have low response values. The sample with the highest hourly traffic flow has an hourly traffic flow of 4083 veh/h, while the ratio of the response value to the Chinese code D60 is only 0.165. Nonetheless, higher hourly traffic volumes pose a potential risk for congestion in free traffic flow.

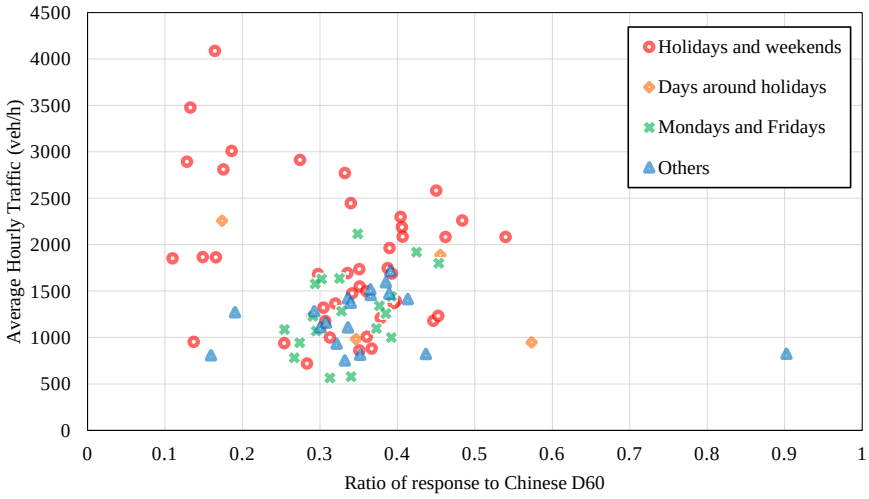

Figure 5-8 The average hourly traffic and ratio of response to D60 for extreme scenarios during daytime.

To examine the traffic components in the case of higher hourly traffic volumes, the GVW (gross vehicle weight) information associated with the scenarios of hourly traffic volumes above 3000 veh/h is obtained. For each high-traffic volume scenario, the GVW information within one hour before and after the extreme values is collected. Figure 5-9 depicts the GVW distribution of the high-traffic volume scenarios. It can be seen that GVW tends to concentrate in vehicles weighing less than 4 tonnes for high-traffic volume scenarios. Meanwhile, the number of vehicles weighing between 4 to 66 tonnes are relatively rare.

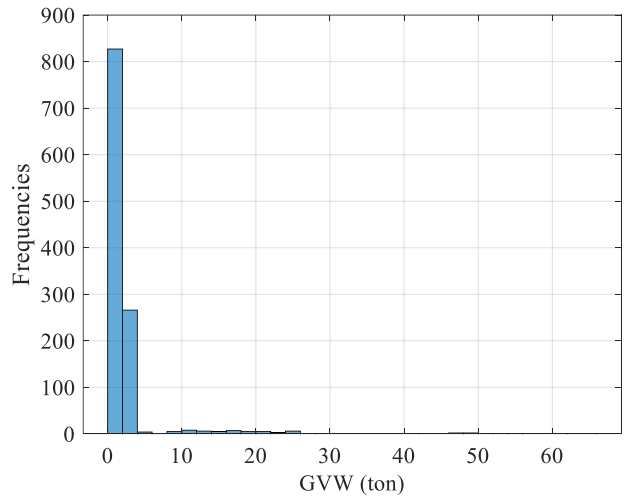

Figure 5-9 The GVW distribution of high hourly traffic volume scenarios.

In order to obtain enough congestion scenarios as objects for the proposed model to simulate congestion scenarios, the micro-simulation model can be used to produce the congested traffic suitable for critical long-span bridge-loading scenarios, as presented in Enright et al. (2013). The cellular automata (CA) has been used in several fields. With the aid of CA method, complex movements of vehicles, such as speed changes, lane changes, etc. (Chen & Wu, 2011; O'Brien et al., 2012) can be simulated successfully and the generated long-term traffic flow maximum effects can be obtained. Traffic micro-simulation based on CA is applied to obtain the detailed information associated with vehicle load, vehicle velocity, headway distance, and lane position (Ruan et al., 2017). After a vehicle is produced, its movement is controlled by the local rules that determine the driving modes (i.e., acceleration, cruising, coasting, and braking). The CA method has been verified, as presented in Tian et al. (2016). Thus, the congestion traffic data used in this study are obtained by using CA model.

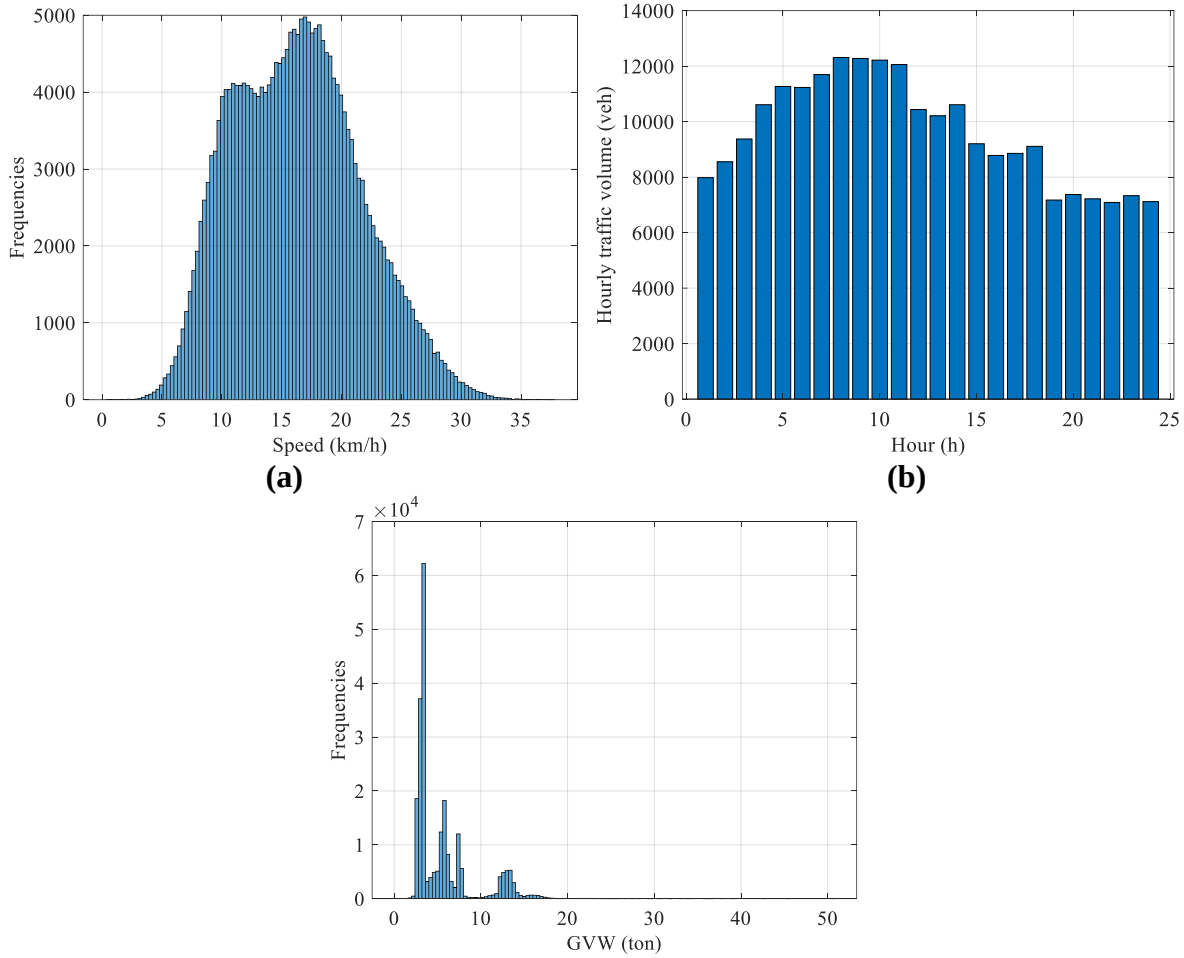

Figure 5-10 The (a) average speed histogram; (b) traffic flow histogram for each hour; (c) GVW distribution histogram of the generated congested traffic.

An input flow rate of 12,000 vehicles per hour is used for the six lanes. A total of 24 h of congested traffic is generated. To implement the bottleneck, each vehicle's desired velocity is changed to 15-20 km/h. This arrangement induces homogeneous congested traffic, which is characterized by a low average velocity but, in contrast to fully jammed traffic, has relatively high traffic flow (Kennedy et al. 1992). The average speed histogram, traffic flow histogram for each hour, and GVW distribution histogram of the generated congested traffic are shown in Figure 5-10. It can be seen that the level of vehicles with GVW from 4 tonnes to 60 tonnes is magnified in the simulated congested flow.

The extreme scenarios of congestion flow are calculated for the five effects mentioned in the paper:

--the axial force of the longest cable (AFC, Effect 1);

--the vertical deflection at mid-span of the main span (VDMS, Effect 2);

--the longitudinal displacement at the top of the pylon (LDTP, Effect 3);

--the bending moment at mid-span of the main span (BMMS, Effect 4);

--the bending moment at the bottom of the pylon (BMBP, Effect 5).

For each effect, the extreme response scenario is calculated every second, and the top 100 extreme value scenarios with the largest response are selected as simulation samples for further simulation based on the proposed model.

For the extreme response scenarios of the congestion flow, the probability of occurrence of vehicles in each cell on the outer lanes is counted as shown in Figure 5-11. It can be seen that in the extreme scenarios of congestion, there is still a tendency for the distribution of vehicles along the longitudinal direction of the bridge, which varies according to the type of effect. Therefore, the simulation of the location of vehicles on the bridge deck can still be performed using a non-stationary Poisson distribution as proposed in this thesis.

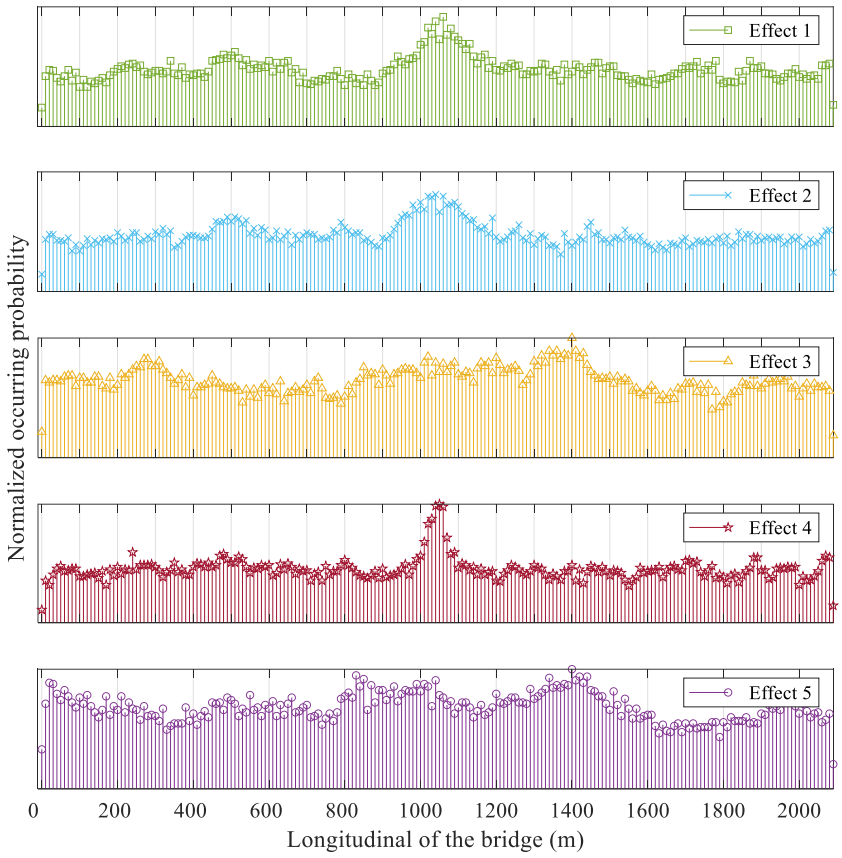

Figure 5-11 The probability of occurrence of vehicles in each cell on the outer lanes.

In the following, the proposed model is applied to simulate the extreme response scenarios of congestion flow with Effect 1 as an example. Figure 5-12 depicts the probabilities of a cell being occupied by a vehicle in extreme response scenario for the congestion flow. The non-stationary characteristics of the outer lane is more pronounced than that of the inner lane. This may be due to the fact that for traffic scenarios when heavier vehicles are concentrated in a specific location, it tends to lead to response extremes. For congested traffic, the proportion of heavier vehicles is not high. Their tendency to drive in the outer lane is more pronounced. Also, the data and GMM fitting of GVWs for the congestion extreme response scenarios are given in Figure 5-13, which is the basic information for simulating GVW.

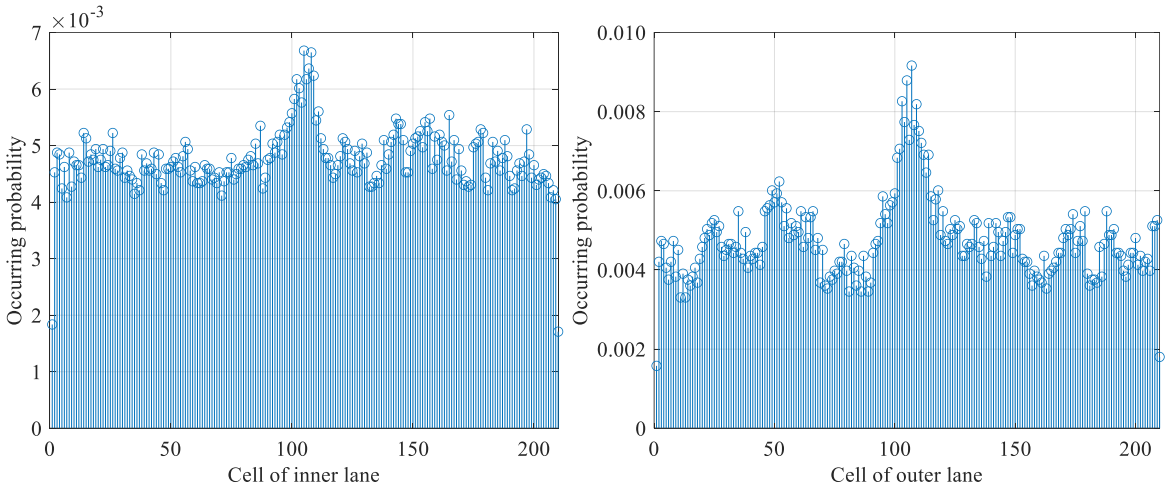

Figure 5-12 Probabilities of a cell to be occupied by a vehicle in an extreme response scenario and congested flow.

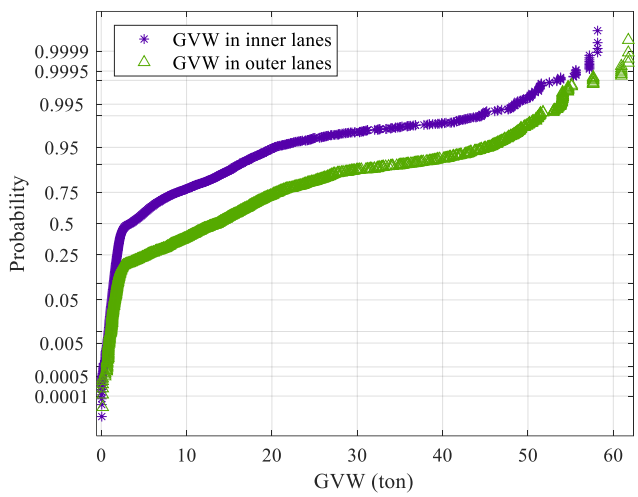

(a)

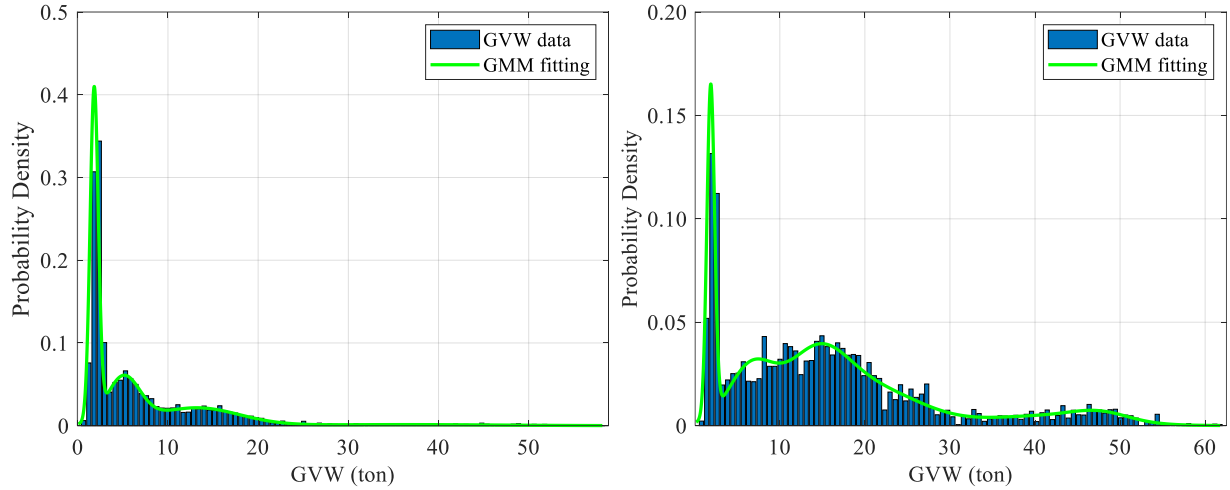

(b) **(c)**

Figure 5-13 Data and fitting of GVW in (a) normal probability paper; (b) inner lanes; (c) outer lanes.

In the simulation of the congestion scenario, other issues that need to be discussed are (1) whether light vehicles need to be ignored and (2) the selection of cell scale. Figure 5-14 depicts several extreme response scenarios of Effect 1 of the congested traffic flow.

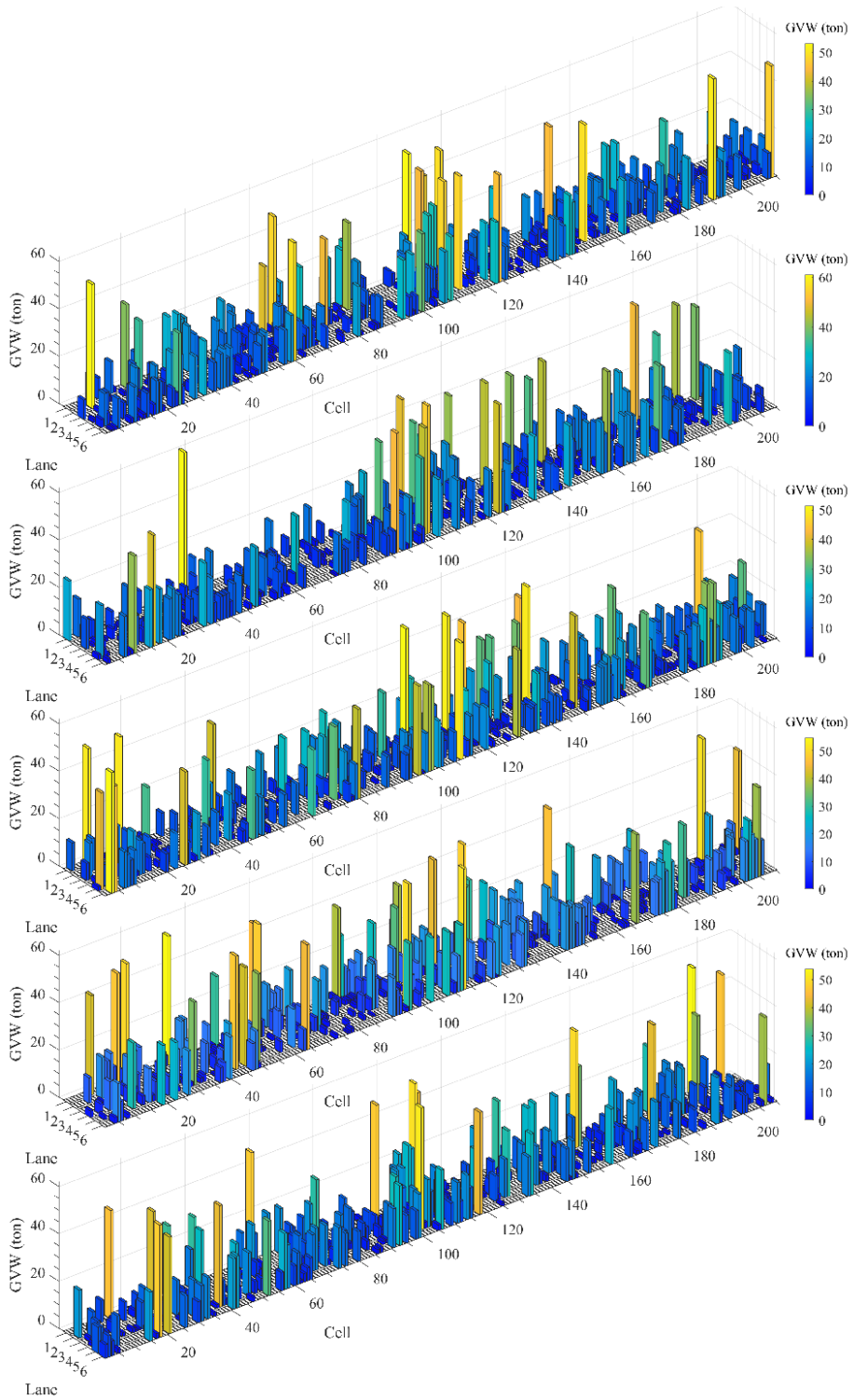

Figure 5-14 Samples of extreme response scenarios of congestion flow (load effect 1).

A comparison of ignoring or considering light vehicles in the congestion scenario is presented in Figure 5-15**.** If the lighter vehicles are ignored, the effect loss is in the range of 8% to 24% with a median of 15%. During congestion, the proportion of light vehicles is higher and the GVWs of heavy vehicles is lower compared to the level of normal traffic scenarios. Therefore, the effect of light vehicles should not be ignored when performing simulations of congestion extremes scenarios.

On the basis of considering the light vehicles, the length of the cell should be adjusted. The length of small vehicles for domestic use is generally greater than 4.5 meters, and the relevant Chinese regulations recommend a safe following distance of 10 m when the speed is below 20km/h (The State Council of the People's Republic of China, 2004). Therefore, the cell length is chosen as 10 meters when simulating congestion scenarios. Then, the extreme response scenarios were simulated 10^4 times by the proposed model. Several samples of simulations for Effect 1 are shown in Figure 5-16.

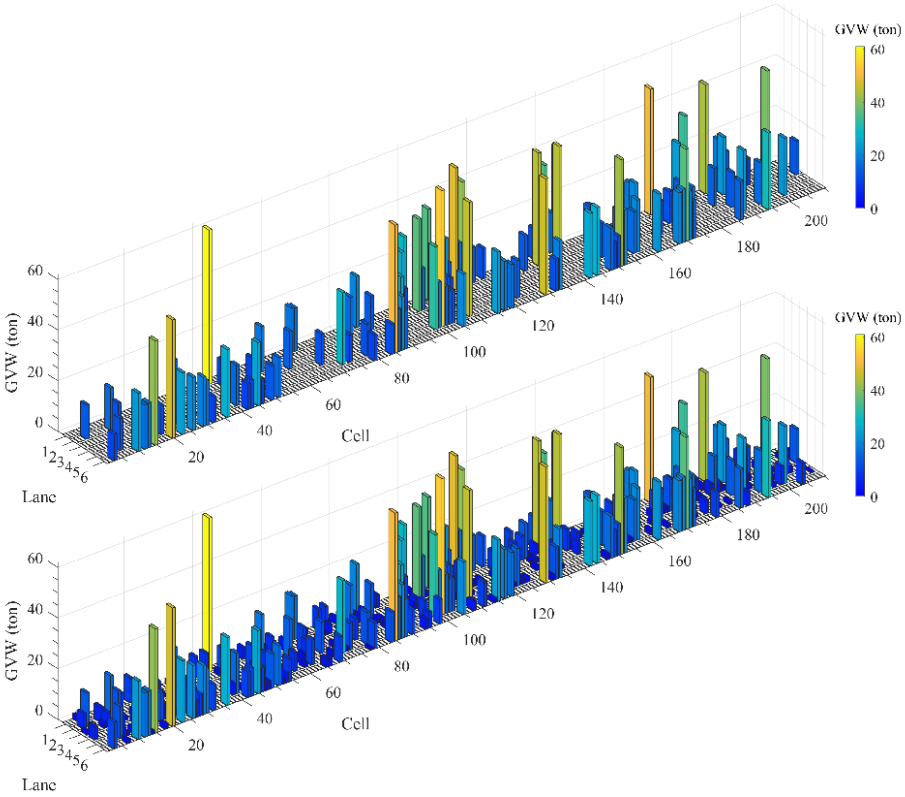

Figure 5-15 Comparison of ignoring light vehicles and not ignoring light vehicles of a congestion scenario.

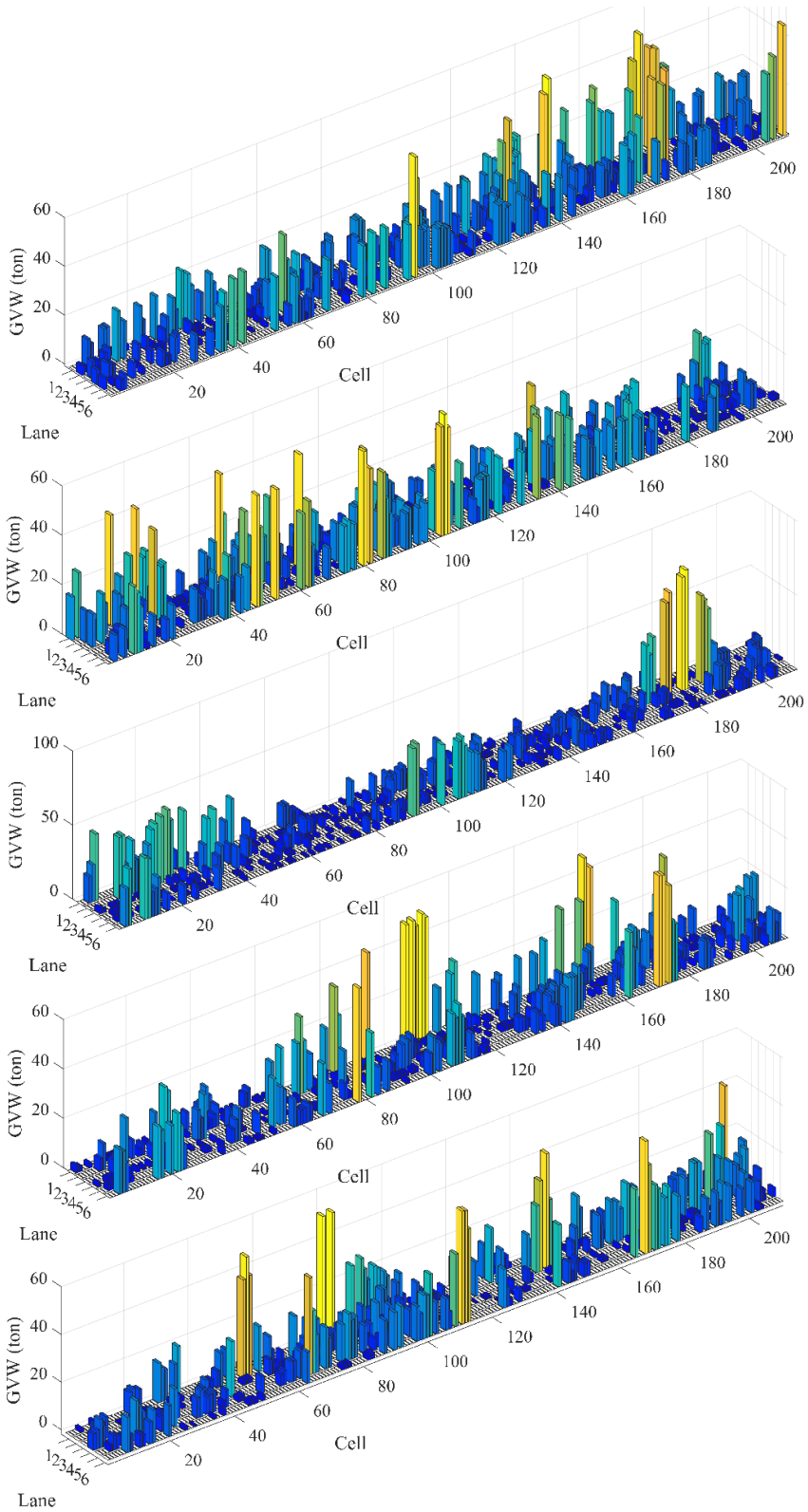

Figure 5-16 Samples of simulated congestion scenarios by the proposed model.

Figure 5-17 shows the probability density plot of the ratio of LE from the simulated congestion scenarios to Chinese code value. The extreme response of the 10,000 simulated congestion scenarios is up to 1.4 times the code value. Meanwhile, the extreme response of the selected congestion scenarios samples generated by the CA method are distributed between 0.6 to 0.85, therefore the simulated results can better cover the results of the CA samples, and extending the simulation including many congestion extreme scenarios that are not included in the CA samples.

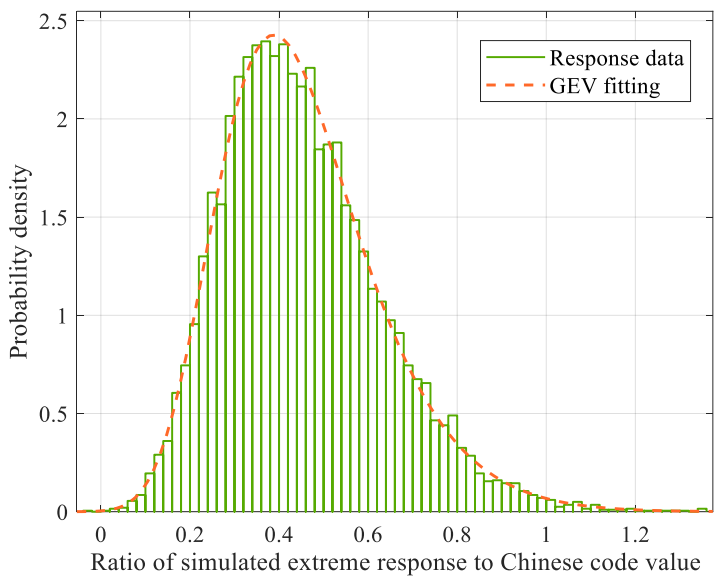

Figure 5-17 Probability density of the ratio of LE from simulated congestion scenarios to Chinese code value.

As 10,000 simulations is a good representative value of the number of congestion scenarios during a period of 100 years, the response extremes generated by congestion are less than 1.4 times of the Chinese code value during the 100-year design period. At the same time, the extreme response generated by free traffic is extrapolated to 1.3742 times the code value during the 100-year design period. Therefore, similar extreme values are obtained under congested and free flow traffic conditions depending on the traffic situations along the day.

Since long-span bridges are managed with appropriate traffic restrictions, it is believed that congestion will gradually become less in the future. In summary, congestion is usually caused by morning peak, evening peak or abnormal conditions such as holidays and extreme weather, and the vehicle composition is generally lighter than normal traffic. Therefore, as shown in the

previous example, the extreme response level of free flow may be of the same order than that of congested flow. Meanwhile, with the increasing demand for site-specific traffic flow modeling of long-span bridges, it is necessary to study the extreme response scenarios for free flow. The research of free-flow extremum scenarios can also provide a powerful tool for real-time correspondence between response values and traffic scenarios (i.e., real-time damage warning). Furthermore, congested traffic flow is simulated by calibrated CA in this study, as no real congestion data is available for the bridge. With the improvement of detection technology different from WIM, more accurate model parameters can be obtained based on the acquisition of real congestion data. This issue will be addressed in future research.

5.4 Conclusions

This chapter presents a detailed validation of the extreme response scenario model proposed in the thesis and discusses the accuracy of the simulated extreme response scenarios compared to the corresponding parameters of the original measured data from WIM information. Based on this, the proposed model is applied to construct an extreme response scenario for congested traffic, whereby the significance of the free-flow and congested-flow states for the structural safety assessment of long-span bridges is discussed, and the wide range of applications and flexibility of the proposed extreme response scenario model for different application scenarios is demonstrated.

CHAPTER 6 Site-specific traffic load model of long-span bridges via Bayesian updating

6.1 Introduction

This chapter proposes a site-specific traffic load model to derive the maximum LEs within a reference period for long-span bridges and develops a Bayesian inference-based approach for its updating according to the actual traffic conditions (annual average daily traffic volume (AADT) and distribution of GVW). The model is better suited for free-flow traffic conditions, which are also critical to long-span bridge assessment, and not congested situations. The process of building the site-specific traffic load model and the updating methodology is illustrated in Figure 6-1. As can be seen in the figure, this thesis revolves around the construction of a site-specific traffic load model. The probabilistic model of extreme scenario section proposes a method that can simulate the distribution of heavy vehicle locations on bridge decks for extreme response scenarios and can describe the uneven distribution of bridge load levels (corresponding to the uniformly distributed line load of Load form 4). The application of this method together with the Monte Carlo method allows a large number of simulated extreme response scenarios to be generated, providing the basis for the construction of a site-specific traffic load model. The site-specific load model updating section provides a method for updating the site-specific traffic load model based on newly observed traffic data. Case studies of all the proposed methods and models are also presented. A probabilistic model for heavy vehicle location scenarios on the deck leading to extreme LEs is developed in Chapter 3. The definition of these vehicle scenarios is the vehicle spatial distribution when the maximum effect is obtained. To this end, the bridge deck is divided into cells to simulate the vehicles distributions deriving on extreme scenarios. Once the load model based on extreme scenario is built as presented in chapter 3, a Bayesian inference based on PF (Maruyama & Hoshiya 2008; Li, Fang & Shi 2021; Lin & Jiao 2021) is developed for the model updating according to the traffic status.

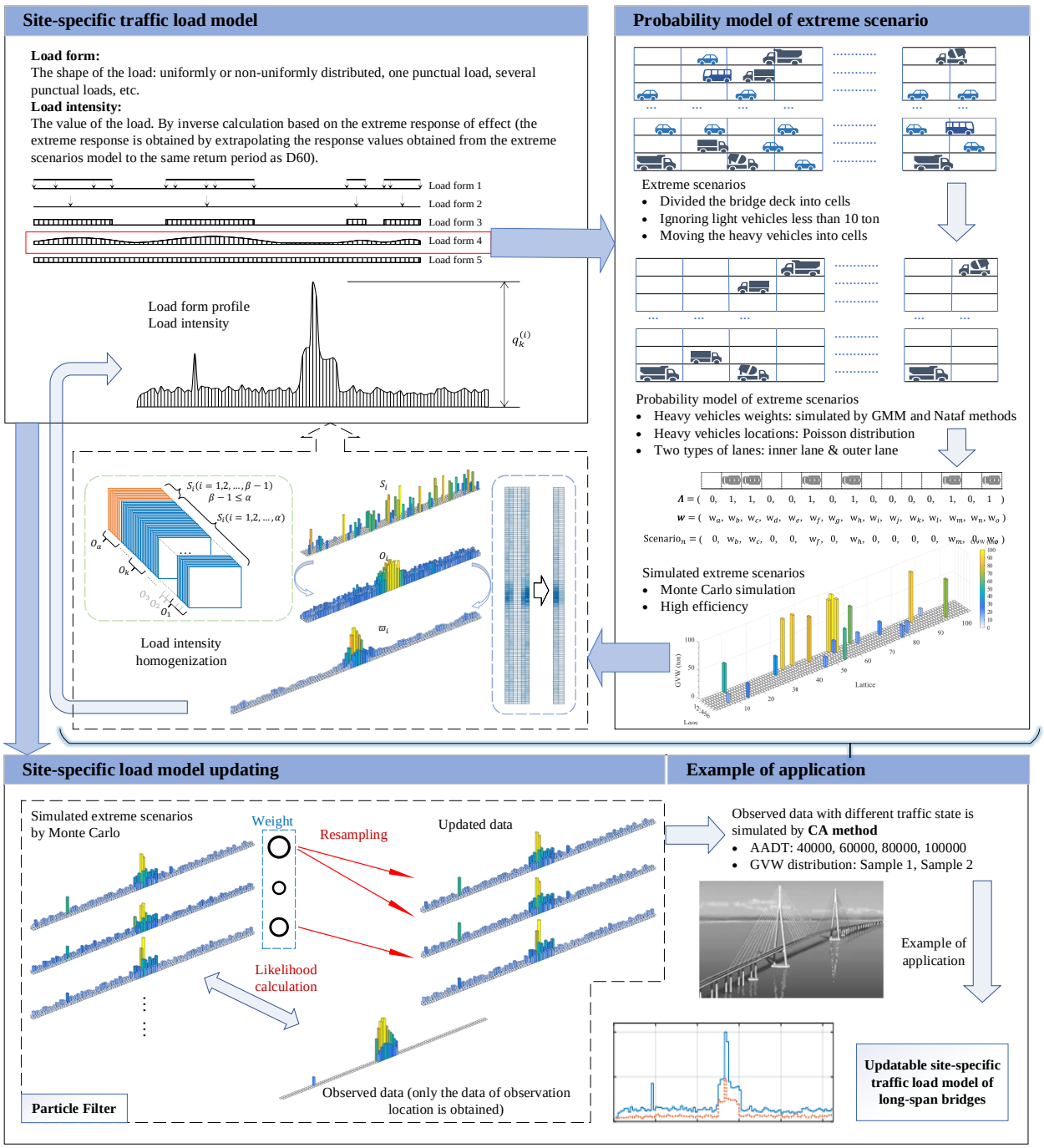

Figure 6-1 Flowchart of the modeling procedure of site-specific traffic load model.

6.2 Definition of the site-specific traffic load model

When defining a site-specific traffic load model, to obtain the extreme LEs is an important issue (Ruan et al. 2017). The focus of this chapter is also to obtain a model for maximum LEs in long-

span bridges and to compare it with the traffic load models available in some bridge codes. The extreme LE is the one that the bridge will never see within a reference period with an acceptable probability. Based on the defined probability of occurrence and the corresponding reference period, these extreme responses can be associated to a certain return period. According to Zhou's (2018) study, the daily extreme response scenario is obtained to carry out subsequent research. For the site-specific traffic load model proposed in this thesis, daily extreme responses for specific effects were simulated and chosen as samples of the maximum daily effect. With the extrapolation method, the simulated daily extreme responses can be extrapolated to obtain the effect for a certain return period, making possible the comparison with the traffic model in relevant codes where the associated return period is given.

A traffic load model is a simplified tool to obtain relevant traffic LEs in the design and assessment of bridges. When proposing a traffic load model, the following requirements should be considered:

1) The extreme load responses due to traffic for each effect in the reference period should be modelled with a certain reliability level.

2) Allowing to engineering application, the traffic load model must be as simple as possible but still leading to accurate results always in the safe side.

The primary concern is how to strike a balance between these factors (Ruan et al. 2017). The balance in the traditional load models is typically achieved taken into account the following important variables: 1) load form (the shape of the load: uniformly or non-uniformly distributed, one punctual load, several punctual loads, etc.), 2) loading pattern (how the load should be placed in the bridge to get the maximum/minimum effects), 3) load intensity (the value of the load). The definition of these variables for the load model proposed here is justified in the following sections.

6.3 Effect of the shape of influence line of long-span bridges in the load model

As a numerical representation of the structural responses to vehicle loads, influence line has been widely used in the study of vehicle LEs on long-span bridges. By analyzing the shape of the influence line (i.e., positive and negative influence value, positive and negative influence area,

trend, distribution complexity, and effective influence area, etc.), the structural effect of the vehicular load can be well studied.

As a complex structural system, long-span bridges have various types of effects. For traffic load assessment, some effects only show a noticeable response when the location of the vehicle is within a limited region in the longitudinal direction. However, other effects have significant responses for the total available length of the loading area. As an example, Figure 6-2 shows the influence lines of three typical effects of a cable-stayed bridge with a main span of 1088 m, and the maximum absolute value of each influence line is used to normalize the influence values. It can be seen that the influence value of the longitudinal displacement at the top of the pylon (LDTP) varies significantly along the longitudinal axis of the bridge. For instance, the lengths of the negative part and positive part of influence line are on a similar level, and the same situation appears in the maximum absolute values of these two parts. This implies that a large response can be produced when a vehicle is applied anywhere along the whole loaded length.

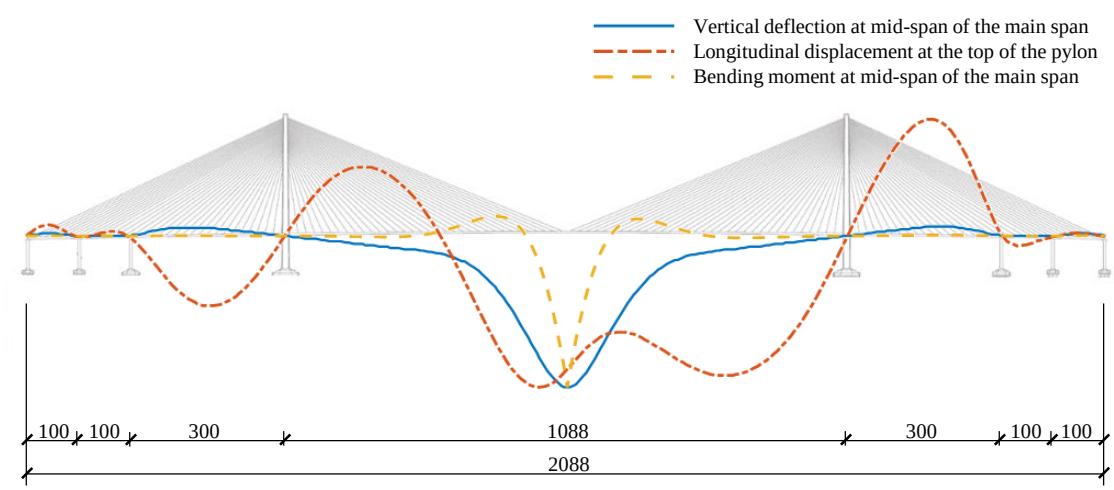

Figure 6-2 Configuration of the Sutong bridge with the influence lines of three effects (Unit: m).

On the contrary, the effective loading region for the effect of bending moment at the mid-span of the main span is only around the middle of the main span, as the influence values in other regions are negligible. In addition, there are significant differences in the extrema and loading regions of the positive and negative portions of the influence value for this effect. This implies that a large response can only be produced when positioning a vehicle in the effective region of the loaded length, which is considerably less than the total length. Based on the shape characteristics of

influence lines, the effects of long-span bridges can be classified as global effects, partial effects, etc., for more efficient and refined structural assessments (Ruan et al. 2017).

Furthermore, Zhou et al. (2019) proposed an efficient approach for modeling the traffic load of long-span bridges according to the characteristics of the effects. In the approach, macro- and micro-simulation method of traffic load were used in different regions of the influence line effect to get high calculation efficiency without sacrificing accuracy. The mathematical criteria and classification method for different regions of influence lines were proposed and validated. For sensitive regions, the value of the influence line is high, and a loss of accuracy would result if using a simplified macro-simulation method. In insensitive regions, where the value of influence line is small, it is unnecessary to use a complex and ineffective micro-simulation method for traffic simulation. Therefore, focusing on sensitive areas of the influence lines becomes a feasible and efficient method for traffic load modeling.

As for the loading pattern, in the present traffic load models, e.g., D60 (General code for design of highway bridges and culverts. JTG D60-2015, Beijing), BS5400, AASHTO, ASCE loading, Eurocode, etc., the load forms are supposed to be placed on the influence regions with the same sign of influence value, in order to produce the most unfavourable load response (EN 1991-2 2010; AASHTO 2002; BS 5400-2 2006; Buckland 1981; Ministry of Communications and Transportation 2015). However, this arrangement commonly presents a low occurrence probability in real situations. To illustrate this, Figure 6-3 depicts the occurring probability of heavy vehicles over 10 tonnes appearing in the real extreme scenarios on the outer lane for different effects of a long-span cable-stayed bridge with a main span of 1088 m (the Sutong bridge, presented as example in Chapter 5) based on the data gathered by WIM data along 423 days. As seen in the figure, the distribution law of the vehicle load under the real extreme effect scenarios is substantially different from those setting in the bridge codes. In fact, the vehicle distribution pattern that causes extreme response for certain effects is strongly related to the shape of the influence lines. The occurring probability of heavy vehicles in Figure 6-3 demonstrates that the influence line will lead to different distribution of vehicle densities along the bridge in extreme scenarios. Therefore, it is feasible and necessary to determine the appearance of the traffic load form for different effects according to the different shape of influence lines.

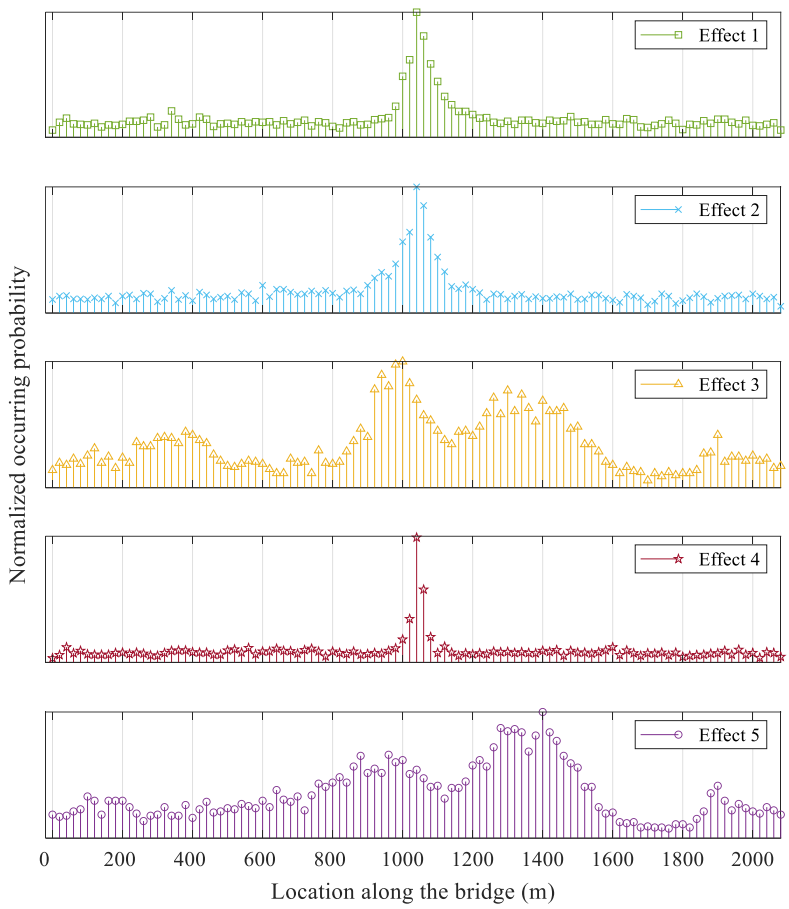

Figure 6-3 Occurring probability of heavy vehicle in the extreme scenarios on the outer lane for different effects of a long-span cable-stayed bridge with a main span of 1088 m.

6.4 Selection of the form of the site-specific load model

According to Zhou's (2018) research, **Table 6-1** lists the load form in various design codes. In general, for overall effects, three kinds of common load forms are frequently used: 1) uniformly distributed line load with concentrated load, 2) uniformly distributed line load, and 3) uniformly distributed surface load with concentrated load. The concentrated load typically simulates a heavy vehicle that can produce a significant response if placed in a zone with a high influence line value. The uniformly distributed loads are widely advised in designing bridges with long loaded lengths as they represent the essential average load level for response calculation.

Table 6-1 Load forms for the overall design in different codes.

Design codes	Load form
D60	Uniformly distributed line load with concentrated load
Eurocode	Uniformly distributed surface load with concentrated loads
BS5400	Uniformly distributed line load with concentrated load
ASSHTO	Uniformly distributed line load or uniformly distributed line load with concentrated loads
ASCE loading	Uniformly distributed line load with concentrated load

Figure 6-4 illustrates various possible load forms for vehicle sequence with decreasing fidelity/accuracy. The vehicle sequence is an arrangement of several vehicles with headways or gaps in a queue, which is commonly considered for global structural effects. Load form 1 is composed of several sets of axle weight loads. Load form 2 comprises several sets of GVW loading, and load form 3 is a uniformly line distributed GVW loading. Furthermore, the vehicle sequence loading can be modeled by a distributed line load with variable intensity (load form 4). A traffic load model with a uniformly distributed line load (load form 5) can be utilized when this simplification is at an acceptable level. In this case, the variability associated with weight density is disregarded. Instead, the total weight of the vehicle sequence is reflected by an average line load.

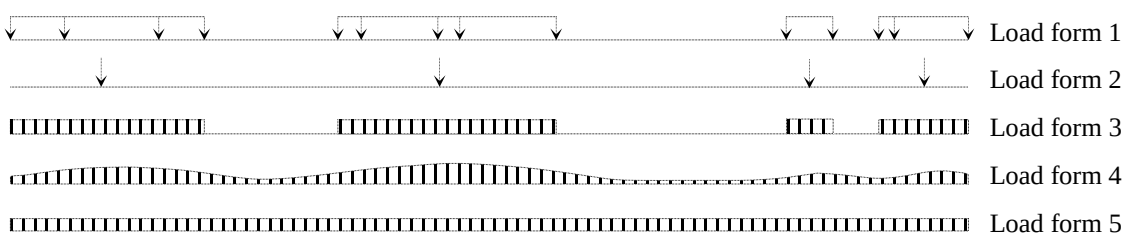

Figure 6-4 Different vehicle sequence load forms.

Because a probabilistic approach is followed to derive the maximum LEs, when choosing the load form, the accuracy and the computational cost of a simulation process should be considered. To deduce the characteristic values of LEs for the assessment of the bridge over their lifetime, a huge amount of traffic loading scenarios must be simulated to consider the high randomness of traffic load in both spatial and temporal domains.

In the modeling of a vehicle sequence for overall bridge effects, a relatively accurate loading can be achieved by load forms 1 to 3, while load form 5 exhibits high simplicity and efficiency but

low accuracy as well. Theoretically, load form 5 provides a highly efficient simulation due to the fact that only load intensities are sampled other than generating individual vehicles and pass them through the bridge. The LEs can be calculated directly by multiplying the load intensity and the area of the influence line. However, owing to the low loading precision of this type of load form, it is rarely used in research. Nevertheless, in most design codes (e.g., D60 and AASHTO), load form 5 is adopted due to its simplicity as a crude illustration of traffic loading.

Generating vehicle sequences similar to load forms 1 to 3 by micro-simulation method, will result in a high computational cost. In fact, these load forms were utilized as the current traffic simulation criterion for long-span bridges by some authors at a high computational cost (O'Brien, Lipari & Caprani 2015; Caprani, O'Brien & Lipari 2016; Carey, Caprani & Enright 2018). In conclusion, to achieve a balance between computational speed and accuracy, in the present research load form 4 is selected to develop the traffic load model for the design and assessment of long-span bridges based on the vehicle extreme scenario probabilistic model. (Declaration: Much of the content in this section is drawn from Zhou's (2018) research, which the author introduces as the basis for subsequent research in this thesis).

6.5 Selection of load intensity

Load intensity of the site-specific traffic load model is calibrated based on the extreme value of the response effect, aforementioned load forms, and loading patterns (Zhou et al. 2019). Since the bridge responses show a strong correlation with traffic parameters and on-bridge traffic conditions, and different types of LEs have different influence line shapes, the load intensity should be able to express the change of the traffic flow condition over time. In addition, the value should be updated, and quantified separately for different effects.

The response to traffic of a long-span bridge is directly related to the basic parameters of traffic flow, such as the AADT, distribution of GVW, etc. Considering the convenience of engineering applications, the influence parameters should be as simple as possible. For this reason, for the proposed site-specific load model, the above-mentioned influencing parameters are expressed in the form of correction factors, as shown in **Equation (6-1)**.

$$R_k^{(i)} = \eta_1^{(i)} r_k^{(i)} \; or \; R_k^{(i)} = \eta_2^{(i)} r_k^{(i)} \tag{6-1}$$

where $R_k^{(i)}$ denotes the ratio of the actual traffic load response to code D60 for the *i*-th effect. Taking into account the traffic characteristics (AADT, GVW); $r_k^{(i)}$ is the ratio of the traffic load response for *i*-th effect corresponding to the original extreme scenario model to code D60. The original extreme scenario is defined based on the WIM data available, representative of a specific traffic condition (AADT and GVW distribution). As the characteristic value in the code D60 corresponds to a return period of 1950 years, the defined ratios only make sense if the traffic load response also corresponds to the same return period. Therefore, by Monte Carlo simulation (MCS), 10^5 daily extreme responses for a certain effect are obtained. Then, by a generalized extreme value (GEV) based extrapolation method, the extreme response with the same return period as D60 can be extrapolated; $\eta_1^{(i)}$ denotes the correction factor for the traffic parameters associated with AADT (different from original scenario) for *i*-th effect; $\eta_2^{(i)}$ represents the correction factor for the *i*-th effect associated to the distribution of GVW (different from original scenario) in the traffic flow. In Chapter 5, the above parameters will be calculated as shown in Table 6-2 for the example bridge.

Table 6-2 Correction factors for different LEs and traffic conditions.

The *i*-th effect		AFC	VDMS	LDTP	BMMS	BMBP
Standard ratio value $r_k^{(i)}$		1.374	1.191	0.628	2.363	0.575
Response value $r_k^{(i)}$		1191 kN	-1.40 m	0.234 m	185801 kNm	-210542 kNm
AADT $\eta_1^{(i)}$	40000	1.015	0.999	1.005	1.039	1.000
	60000	1.269	1.257	1.216	1.221	1.185
	80000	1.449	1.437	1.507	1.340	1.375
	100000	1.599	1.601	1.811	1.414	1.821
GVW distribution $\eta_2^{(i)}$	Sample 1	1.568	1.421	1.444	1.434	1.403
	Sample 2	0.999	0.991	0.991	0.926	0.932

*Note: The axial force of the longest cable (AFC, Effect 1), the vertical deflection of main girder at mid-span of the main span (VDMS, Effect 2), the longitudinal displacement at the top of the pylon (LDTP, Effect 3), the bending moment of main girder at mid-span of the main span (BMMS, Effect 4), and the bending moment at the bottom of the pylon (BMBP, Effect 5).

6.6 Bayesian approach for updating traffic scenarios

The traffic flow parameters evolve over time. Therefore, the modeling of vehicle load scenarios leading to extreme effects scenarios needs to consider such evolution, as for instance, the growth of AADT. Therefore, a particle filter (PF) method was utilized to conduct the updating and optimization of the model of vehicle scenarios when new observed information is obtained. The

traffic flow with different AADTs and GVW distributions, used as new observed information, were simulated by employing the CA method. CA has been used in several fields. In the traffic domain it was used to analyze the vulnerability of road networks for dangerous goods transportation (RNDGT) under cascading failure considering intentional attack (Huang et al. 2021). In order to simulate the traffic flow based on measured WIM data, the CA method was introduced and developed rapidly in terms of theory and tools (Ruan et al. 2017; Tian et al. 2016). With the aid of CA method, complex movements of vehicles, such as speed changes, lane changes, etc. can be simulated successfully and the generated long-term traffic flow maximum effects can be obtained (Chen & Wu 2011; Ruan et al. 2017). In the thesis, the CA method was introduced to generate new traffic flows as observation information for use in the update. The description and details of the method can be found in the research of Ruan et al. (2017).

The response of LEs are highly correlated with the location of heavy vehicles on the bridge deck, especially for long-span bridges (Caprani, O'Brien & McLachlan 2008; Caprani 2013; Chen & Wu 2011; O'Brien, Hayrapetova & Walsh 2012; Xu, Chen & Xia 2012). Therefore, the load distribution changes with time due to changes in the traffic composition should also be considered. As a result, modifications to the traffic environment must be regularly observed and considered when predicting traffic loads (Kim & Song 2021). Based on new observations and data gathered from ongoing monitoring of the traffic environment of the bridge, many updating and optimization approaches for the traffic load model were proposed to predict the extremes of traffic LEs (O'Brien et al. 2015; Yu & Cai 2019). However, the distribution of heavy vehicles on the bridge deck when the extreme response is obtained is not explicitly considered in these methods. For the probabilistic model of extreme scenarios, a new updating method for the spatial distribution of vehicle load is required. Many surrounding conditions, such as the construction of new bridges or factories in the vicinity or the temporary closing of alternative routes, can affect the vehicle composition within the traffic flow and the parameters causing extreme scenarios. Therefore, the traffic load scenario of extreme LEs corresponds to a spatial random variable which parameters change over time.

Given that $\boldsymbol{X} = [\boldsymbol{x_1}, \boldsymbol{x_2}, \dots, \boldsymbol{x_m}, \dots, \boldsymbol{x_\vartheta}]$ is a set of random fields, where $\boldsymbol{x_m}$ is a random variable simulated by the probabilistic model presented in Chapter 3 ($\boldsymbol{x_m}$ represents one extreme scenario under stationary traffic conditions), and $\boldsymbol{\vartheta}$ is the total number of MCS for extreme scenarios (in this paper, 10^5 MCS is taken). Then, $\boldsymbol{X}$ is a spatial stochastic process that varies with time and

describes the vehicle load distribution on the bridge deck for extreme scenarios for similar traffic conditions. However, the characteristics of $\boldsymbol{X}$ along time can be highly affected by the evolution of the traffic flow and configuration of the heavy vehicles and, therefore, deriving in non-stationary traffic conditions and in a non-stationary stochastic process. Many efforts have been devoted to investigate the non-stationary nature of traffic varying with time. Many prediction methods and derivation functions were developed to study the impacts of the constant growth of truck weight and the growing traffic volume on structural performance (Yu et al. 2019; Leahy, O'Brien & O Connor 2016; O'Brien, Bordallo-Ruiz & Enright 2014). Accordingly, the extreme scenarios prediction can be expressed by a function $f(\cdot)$ as **Equation (6-2)**:

$$\boldsymbol{X}^{(t)} = f\left(\boldsymbol{X}^{(t-1)}, \boldsymbol{\psi}^{(t)}\right) \tag{6-2}$$

where $\boldsymbol{\psi}^{(t)}$ represents the system error generated during the prediction process, t is the time state. Considering a time period where traffic flow and composition can be considered as constant, $\boldsymbol{X}$ is assumed to be stationary, that is, $f(\cdot)$ represents a linear equality relationship. Subsequently, with PF method, the spatial load model for extreme scenarios can be updated using new-observed data.

Actually, if the relationship between the random variables in the prediction model and the observed data is nonlinear or the random variables distributions are non-Gaussian, it is typically unfeasible to use a rigorous theoretical method to update the prediction model. In these conditions, PF is a flexible technique for updating random variables that can be applied without any restrictions for systems and noise types (Fisher & Tippett 1928; Kitagawa 1996; Chen et al. 2021; Zang et al. 2021). The updating method of PF for the random fields was proposed and applied by several researchers (Maruyama & Hoshiya 2008; Liu et al. 2019; Tulsyan, Bhushan Gopaluni & Khare 2016).

According to the state space model (SSM) method (Tulsyan, Bhushan Gopaluni & Khare 2016), the observation $\boldsymbol{Y}^{(t)}$ is assumed to be conditionally independent of each other given latent state $\boldsymbol{X}^{(t)}$. The dimension of $\boldsymbol{Y}^{(t)}$ is u, which represents the number of cells observed on the bridge deck. The dimension of $\boldsymbol{X}^{(t)}$ is $x_a \times x_b = \iota$, where x_a and x_b are the number of cells in the transverse and longitudinal direction, respectively. For the spatially observed data $\boldsymbol{Y}^{(t)}$, the interrelationship with $\boldsymbol{X}^{(t)}$ can be expressed as **Equation (6-3)**:

$$\boldsymbol{Y}^{(t)} = \Lambda \cdot \boldsymbol{X}^{(t)} + \boldsymbol{e}^{(t)} \tag{6-3}$$

where Λ is a function matrix providing measurement locations information with dimensions of $u \times \iota$. and $\boldsymbol{e}^{(t)}$ is the observation error. The dimension of $\boldsymbol{e}^{(t)}$ is also u. The detail of the dimension of each parameter is discussed in the section Application of Bayesian inference for updating the vehicle spatial distribution of extreme scenarios.

State estimation for SSMs in the Bayesian framework is solved by recursively calculating the state posterior density as **Equation (6-4)**:

$$\mathbb{X}^{(t)} | \left(\mathbb{Y}^{(1:t)} = \mathbb{y}^{1:t}\right) \sim p\left(\mathbb{X}^{(t)} \middle| \mathbb{Y}^{(1:t)}\right) \tag{6-4}$$

where $p\left(\mathbb{X}^{(t)} \middle| \mathbb{Y}^{(1:t)}\right)$ is the posterior or filtering density and $\mathbb{X}^{(t)}$ is assumed herein to be a Markov process, and 1: *t* means time 1 to time *t* (Tulsyan, Bhushan Gopaluni & Khare 2016). Based on Bayesian theory and the Markov property, the filtering density can be written as **Equation (6-5)**:

$$p\left(\mathbb{X}^{(t)} \middle| \mathbb{Y}^{(1:t)}\right) = \frac{p\left(\mathbb{Y}^{(t)} \middle| \mathbb{X}^{(t)}\right) p\left(\mathbb{X}^{(t)} \middle| \mathbb{Y}^{(1:t-1)}\right)}{p\left(\mathbb{Y}^{(t)} \middle| \mathbb{Y}^{(1:t-1)}\right)} \tag{6-5}$$

where $p\left(\mathbb{Y}^{(t)} \middle| \mathbb{X}^{(t)}\right)$ and $p\left(\mathbb{X}^{(t)} \middle| \mathbb{Y}^{(1:t-1)}\right)$are the likelihood and the state prior, and $p\left(\mathbb{Y}^{(t)} \middle| \mathbb{Y}^{(1:t-1)}\right)$ is a normalizing constant, which is often not explicitly known in state estimation. Therefore, the constant can be ignored as **Equation (6-6)**:

$$p\left(\mathbb{X}^{(t)} \middle| \mathbb{Y}^{(1:t)}\right) \propto p\left(\mathbb{Y}^{(t)} \middle| \mathbb{X}^{(t)}\right) p\left(\mathbb{X}^{(t)} \middle| \mathbb{Y}^{(1:t-1)}\right) \tag{6-6}$$

Then, using marginalization, $p\left(\mathbb{X}^{(t)} \middle| \mathbb{Y}^{(1:t-1)}\right)$ can be expressed as **Equation (6-7)**:

$$p\left(\mathbb{X}^{(t)} \middle| \mathbb{Y}^{(1:t-1)}\right) = \int p\left(\mathbb{X}^{(t)} \middle| \mathbb{X}^{(t-1)}\right) p\left(\mathbb{X}^{(t-1)} \middle| \mathbb{Y}^{(1:t-1)}\right) d\mathbb{x}_{t-1} \tag{6-7}$$

Meanwhile, for an already generated random field, if the observation is carried out at the site, then the newly obtained data can be used to update the above model (Maruyama & Hoshiya 2008). In order to get the optimal estimation of random field $\boldsymbol{X}^{(t)}$ utilizing the spatially observation data $\boldsymbol{Y}^{(t)}$, combined with **Equation (6-2)** the discrete version of the fundamental updating formula for the conditional probability $p\left(\boldsymbol{X}^{(t)} = \boldsymbol{x}_m^{(t)} \middle| \boldsymbol{Y}^{(t)}\right)$ can be written as **Equation (6-8)**:

$$p\left(\boldsymbol{X}^{(t)}=\boldsymbol{x}_m^{(t)}\middle|\boldsymbol{Y}^{(t)}\right)=\frac{p\left(\boldsymbol{Y}^{(t)}\middle|\boldsymbol{X}^{(t)}=\boldsymbol{x}_m^{(t)}\right)p\left(\boldsymbol{X}^{(t)}=\boldsymbol{x}_m^{(t)}\right)}{\sum_{h=1}^{\vartheta}p\left(\boldsymbol{X}^{(t)}=\boldsymbol{x}_h^{(t)}\right)p\left(\boldsymbol{Y}^{(t)}\middle|\boldsymbol{X}^{(t)}=\boldsymbol{x}_h^{(t)}\right)} \tag{6-8}$$

where $\boldsymbol{x}_h^{(t)}$ is sampled with equal probability. If the total number of sample realizations is α, $p\left(\boldsymbol{X}^{(t)}=\boldsymbol{x}_h^{(t)}\right)$ can be written as **Equation (6-9)**:

$$p\left(\boldsymbol{X}^{(t)}=\boldsymbol{x}_h^{(t)}\right)=\frac{1}{\alpha} \tag{6-9}$$

and $p\left(\boldsymbol{Y}^{(t)}\middle|\boldsymbol{X}^{(t)}=\boldsymbol{x}_m^{(t)}\right)$ is the conditional PDF, which is the weight of the observation $\boldsymbol{Y}^{(t)}$. Consequently, according to **Equation (6-9)**, the weight ratio can be derived from **Equation (6-8)**, expressed as **Equation (6-10)**:

$$p\left(\boldsymbol{X}^{(t)}=\boldsymbol{x}_m^{(t)}\middle|\boldsymbol{Y}^{(t)}\right)=\frac{\omega_m^{(t)}}{\sum_{h=1}^{\vartheta}\omega_h^{(t)}} \tag{6-10}$$

where:

$$\omega_m^{(t)}=p\left(\boldsymbol{Y}^{(t)}-\Lambda\cdot\boldsymbol{x}_m^{(t)}\right) \tag{6-11}$$

$\omega_m^{(t)}$ denotes the weight for each $\boldsymbol{X}^{(t)}$ based on $\boldsymbol{Y}^{(t)}$. Since $\boldsymbol{Y}^{(t)}$ and $\Lambda\cdot\boldsymbol{x}_m^{(t)}$ in **Equation (6-11)** are vectors, $p\left(\boldsymbol{Y}^{(t)}-\Lambda\cdot\boldsymbol{x}_m^{(t)}\right)$ is computed according to multivariate Gaussian PDF of the observation error $\boldsymbol{e}^{(t)}$.

The updating process is shown in Figure 6-5, the spatial observed data is $\boldsymbol{Y}^{(t)}$, the spatial load distribution is $\boldsymbol{X}^{(t)}=\left[\boldsymbol{x}_1^{(t)},\boldsymbol{x}_2^{(t)},\dots,\boldsymbol{x}_m^{(t)},\dots,\boldsymbol{x}_\vartheta^{(t)}\right]$ and the smoothed samples mean the smoothing process to pass from the original extreme scenario to the spatial load distribution $\boldsymbol{X}^{(t)}$ as shown in Figure 6-6. The process can be summarized as follows: firstly, the observed spatial data $\boldsymbol{Y}^{(t)}$ is used in the calculation of weight ratios for each $\boldsymbol{x}_m^{(t)}$ according to **Equations (6-10)** and **(6-11)**. Secondly, the updated random fields, $\boldsymbol{X}^{(t)}$ are then obtained by a resampling process using the weight ratios. The resampling process is depicted in Figure 6-5. The random fields with small weights are eliminated. It should be noted that the random field updating here is only for the load form. The extreme value is determined by the extreme scenario model, MCS method and the

extrapolation method. Therefore, eliminating the fields with small weights does not result in loss of accuracy in the calculation of the extreme value. The resampled index is the serial number of the random field samples. Each index corresponds to a certain weight. Figure 6-7 shows a schematic explanation of the resampling process. The horizontal arrows represent the equal divisions to determine which particles are sampled. For instance, the weight of the sample with index 6 is ω_m, which is one of the largest. Therefore, the sample with index 6 is selected 3 times as instructed by the purple arrows, similar to sample 9 as shown by the red arrows. Samples 1, 3 and 8 will be sampled once, while samples with index 2, 4, 5 and 7 are not selected because of the lower weight.

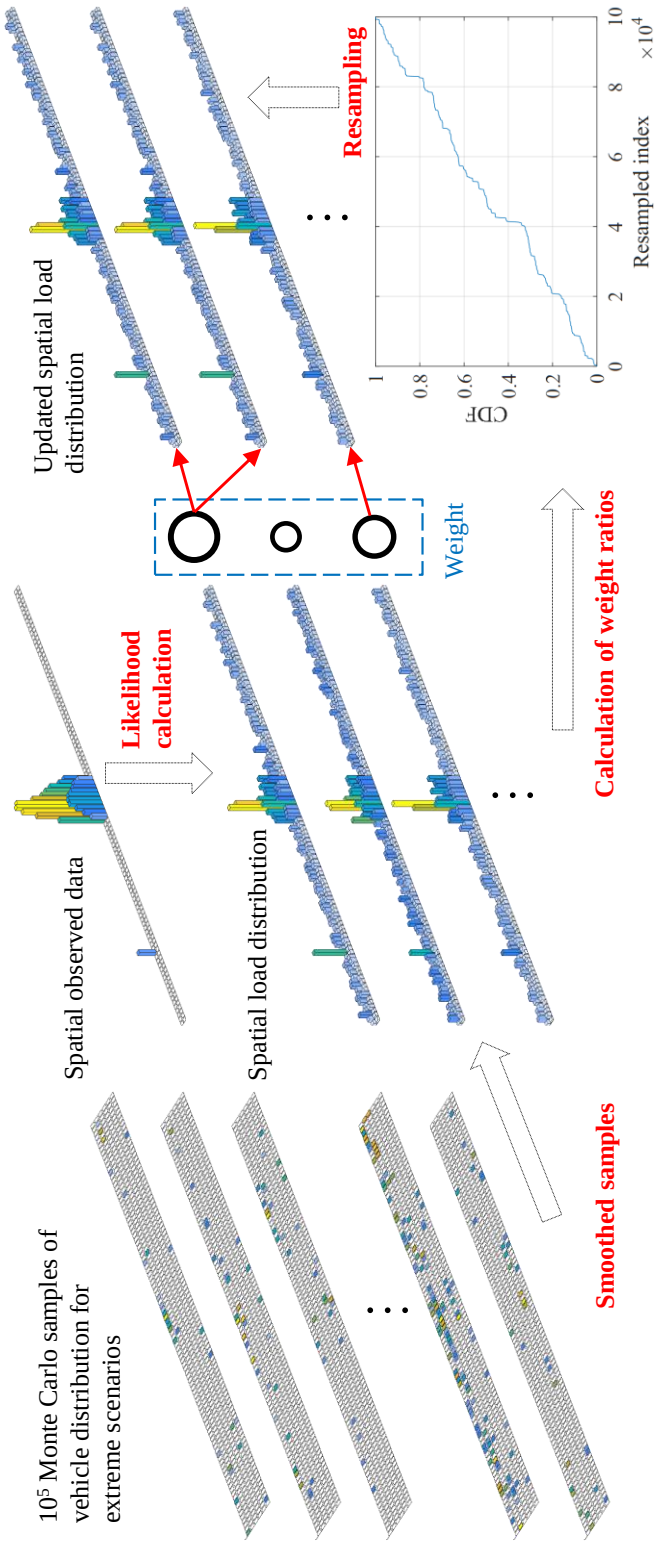

Figure 6-5 Procedure of PF for updating spatial random fields based on observed data.

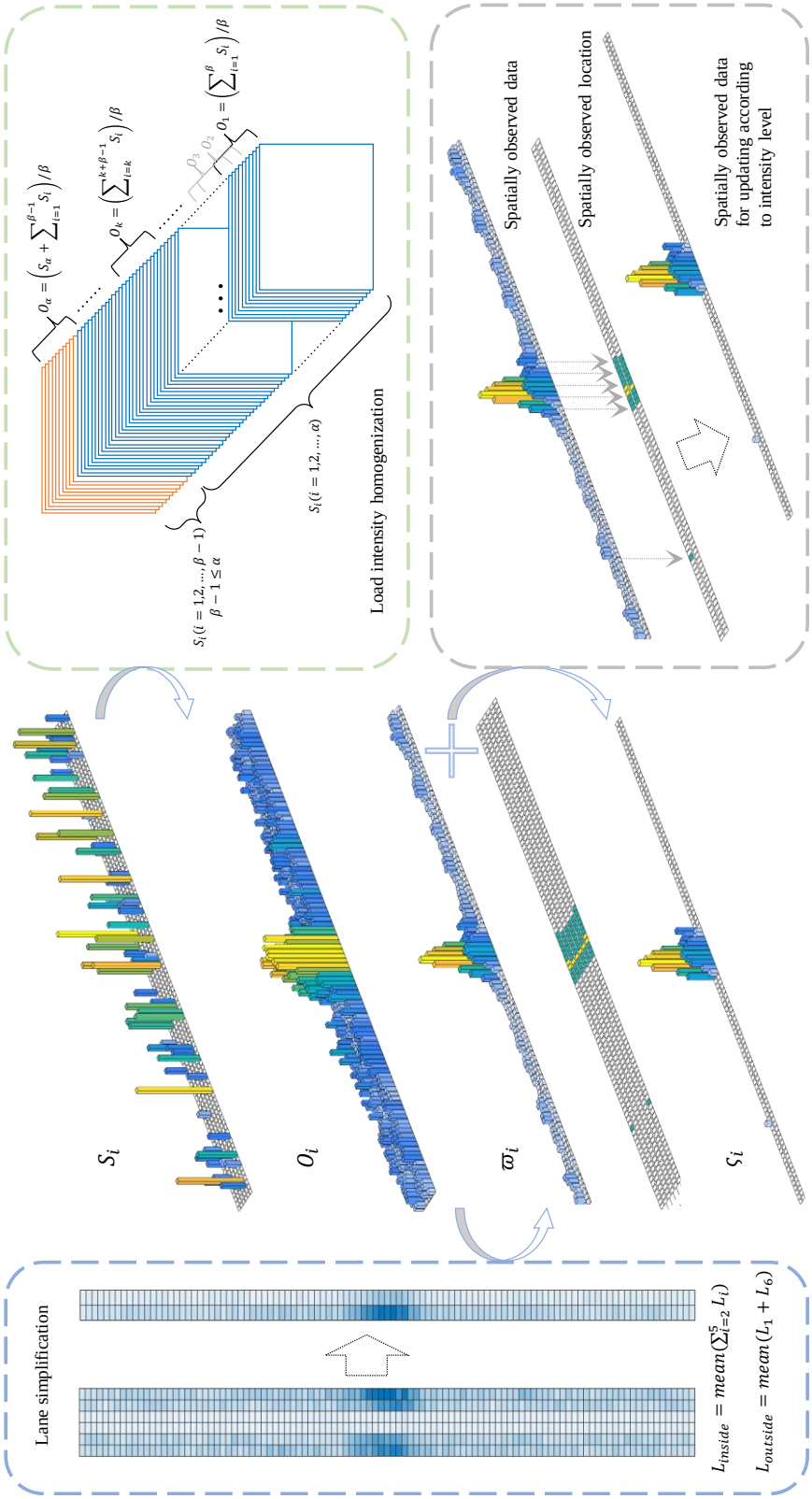

Figure 6-6 Smoothing process of samples for spatial updating.

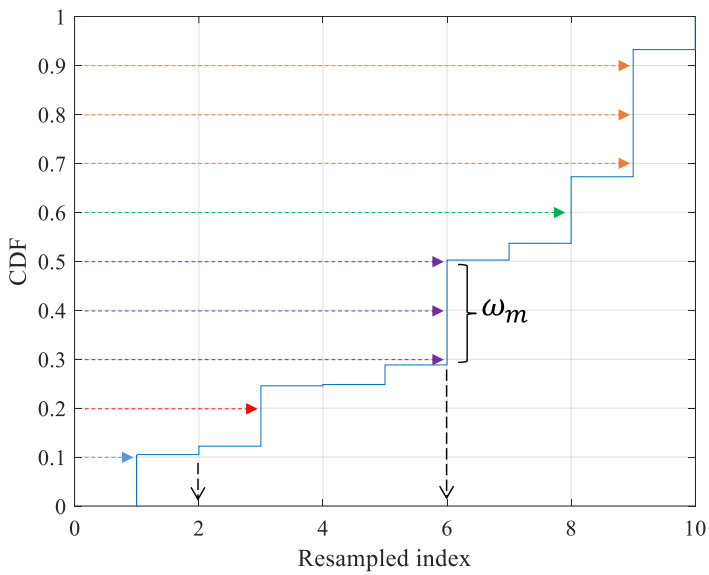

Figure 6-7 Schematic plot of the resampling process.

6.7 Conclusions

In this Chapter, a prior site-specific traffic load spatial distribution model and its updated posterior version considering actual traffic conditions via Bayesian inference were proposed. MCS is adopted to generate the vehicle scenarios that can cause extreme effects. Then, Bayesian inference approach is developed for the updating of spatial load distribution in the above scenarios utilizing the PF method. The proposed method is able to address complex spatial distribution updating problems for traffic load modeling.

CHAPTER 7 Application of the site-specific traffic model and its Bayesian updating

7.1 Application of Bayesian inference for updating the vehicle spatial distribution of extreme scenarios

The considered effects AFC (Effect 1), VDMS (Effect 2), LDTP (Effect 3), BMMS (Effect 4), BMBP (Effect 5) are the same as defined in the previous chapters. The shape of the influence line for each effect is plotted in Figure 7-1. According to the occurring probability of heavy vehicles in the extreme scenarios for different effects, the cells in the bridge deck are grouped into several areas, as illustrated in Figure 7-1. There are three categories, namely, intensive area, sub-intensive area, and non-intensive area. The intensive area and sub-intensive area represent the highest intensity level, and they will be used in the updating process as the observed locations. The division is based on the occurring probability of a heavy vehicle in the cell in the extreme scenarios. When the occurring probability of a heavy vehicle is between 0.9 to 1 times of the maximum value (the maxima of occurring probability of all the cells), the cell belongs to the intensive area. If the occurring probability is between 0.5 to 0.9 times of the maximum value, the cell belongs to the sub-intensive area. Other cells belong to the non-intensive area. This division method greatly reduces the number of observation points for the posterior up-dating and allows to focus on the areas where heavy vehicles appear with higher probability and producing the higher effects, thereby improving the computational efficiency.

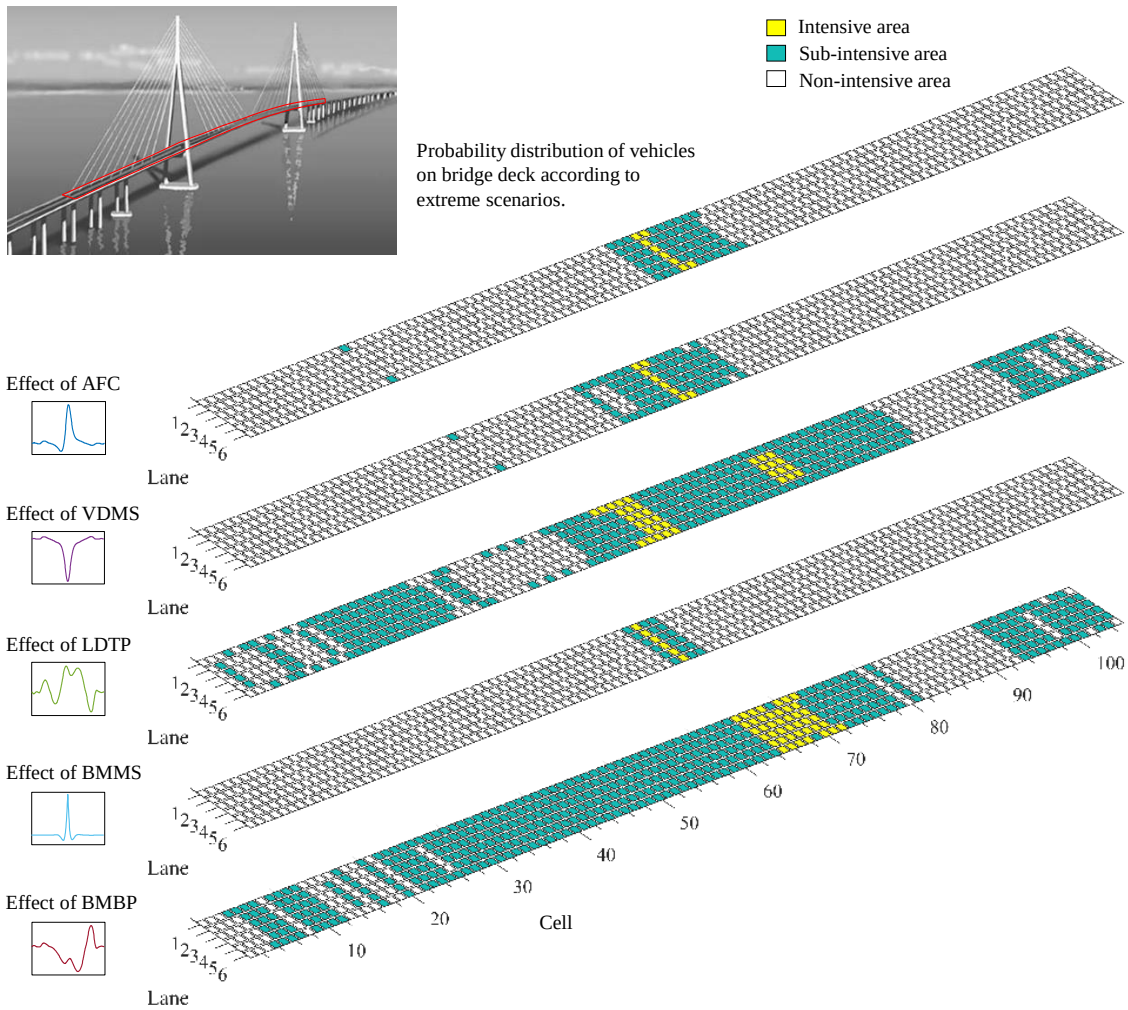

Figure 7-1 Configuration of the long-span cable-stayed bridge with the influence lines of five effects and definition of the 3 different intensity areas (Unit: m).

Meanwhile, to simulate the changes in traffic flow or traffic composition, the micro-simulation method is used. With this tool, it is convenient to use the control variate method to study the load model optimization according to different traffic parameters (Hull & White 1988). Traffic micro-simulation based on CA is applied to obtain the detailed information associated with vehicle load, vehicle velocity, headway distance, and lane position (Ruan et al. 2017). The simulation is formulated in two steps according to Tian et al. (2016): (1) generate the vehicle sequences at the entrance of the simulation section; (2) run the vehicles over the bridge based on the specified rules of movement. Traffic volume, traffic composition, lane choice, speed, and weight should be modeled probabilistically to perform the vehicle generation. After a vehicle is produced, its

movement is controlled by the local rules that determine the driving modes (i.e., acceleration, cruising, coasting, and braking). With the vehicle positions available at each point in-time, the targeted LE can be calculated by imposing the position of the vehicles on the corresponding influence line. The CA method has been verified, as presented in Tian et al. (2016).

The observed information (i.e., different scenarios generated by CA method) is integrated probabilistically with the prior information (i.e., the probabilistic model for the extreme effect scenarios) to derive the posterior distribution of the extreme scenarios under the Bayesian framework.

The bridge has six lanes and the deck is divided into 105 longitudinal cells of 20 m length, what is determined according to the length statistics of heavy vehicles (105 * 20 = 2100 m, which is slightly longer than the total length of the Sutong Bridge). The six lanes are grouped into two: outer lanes and inner lanes. Lane 1 and 6 are outer lanes and lanes 2 to 5 are inner lanes, as shown in Figure 7-1.

For each effect, the extreme scenarios were simulated to get 10^5 samples by the probabilistic traffic model and MCS, hereafter referred to as the prior scenario. Then, several extreme scenarios calculated from traffic data (generated by CA method) with different AADT (in the present case 40000, 60000, 80000, 100000) are obtained for the updating process, hereafter referred to as the observed scenario. Let us define S_i as one sample of these scenarios, either prior or observed. Either obtained by the prior traffic scenario model or by CA using measured data, the sample generated or calculated represents one possible realization of a vehicle distribution scenario producing a maximum LE. This single sample is completely random and therefore is not appropriate as a component for a random field updating. It is necessary to perform a certain data processing of these original samples so that the obtained random field O_i can effectively express the evolution of the distribution of vehicles in each cell. Each adjacent 200 samples were gathered to have a uniformized process, and the processes are nested with each other. It means that each original sample S_i has been applied 10^5 times for the prior scenario, thus 10^5 new samples O_i are obtained. The expression of this process is shown as **Equation (7-1)**:

$$O_1 = \left(\sum_{i=1}^{\beta} S_i\right)/\beta$$

$$\cdots\cdots$$

$$O_k = \left(\sum_{i=k}^{k+\beta-1} S_i\right)/\beta \tag{7-1}$$

$$\cdots\cdots$$

$$O_\alpha = \left(S_\alpha + \sum_{i=1}^{\beta-1} S_i\right)/\beta$$

where S_i $(i = 1,2,\dots,\alpha)$ represents the original samples and O_i $(i = 1,2,\dots,\alpha)$ represents the newly obtained samples. The total amount of samples is 10^5, that is $\alpha = 10^5$. β represents the number of averaged original elements S_i contained in the new element O_i (β = 200 in the present case) for both prior and observed scenarios.

Taking into account the requirement of simplicity for the load model, the two outer lanes are averaged and participate in the updating process as one column, and the same is done for the four inner lanes. So, the total number of sampling cells is 105 × 2 = 210 cells. This process of transforming from 6 lanes field O_i to 2 columns field ϖ_i are expressed as **Equation (7-2)**:

$$L_{inside} = mean\left(\sum_{i=2}^{5} L_i\right)$$

$$L_{outside} = mean(L_1 + L_6) \tag{7-2}$$

The intensive and sub-intensive area represents the area with the highest probability of vehicles appearing in extreme scenarios. Therefore, these two areas are selected as the observed locations for updating. The location of these two areas in the random field ϖ_i is selected as the observed spatial data ς_i.

After the above smoothing process of the samples for spatial updating, the PF can be carried out. Effect 4 (Effect of BMMS in Figure 7-1) is selected to illustrate this procedure. The intensive and sub-intensive areas of Effect 4 are concentrated in the mid-span region of the bridge deck. There are four cells in these areas for both the outer and inner lanes, as shown in the green and yellow

color blocks for the effect of BMMS in Figure 7-1. With the assumption that the vehicle load distribution intensity is acquired at these locations along the lanes, the vector $\boldsymbol{Y}^{(t)}$ in Figure 7-2 contains eight rows indicating the eight observed values of vehicle load intensity on the bridge deck. The matrix Λ illustrated in Figure 7-2 indicates the observed locations on the bridge deck corresponding to the observed vehicle load intensity. According to the results obtained in the calibration of WIM systems, one can model the observation error $\boldsymbol{e}^{(t)}$ for the vehicle load measurement as a Gaussian distribution with a zero mean and standard deviation of 3 tonnes. Given the Λ, $\boldsymbol{Y}^{(t)}$, and $\boldsymbol{e}^{(t)}$, the $\omega_m^{(t)}$ of a random field $\boldsymbol{x}_m^{(t)}$ can be computed as expressed by **Equation (7-3)** according to the multivariate Gaussian PDF (Gonçalves et al. 2022):

$$\omega_m^{(t)} = (2\pi)^{-u/2} \cdot |\Gamma|^{-1/2} \cdot exp\left[-\frac{1}{2}\left(\boldsymbol{Y}^{(t)} - \Lambda \cdot \boldsymbol{x}_m^{(t)}\right)^T \Gamma^{-1}\left(\boldsymbol{Y}^{(t)} - \Lambda \cdot \boldsymbol{x}_m^{(t)}\right)\right] \tag{7-3}$$

where Γ is the covariance matrix of the observation error with dimensions of $u \times u$ (i.e. u = 8). With the calculated weight for each random field, the resampling is carried out.

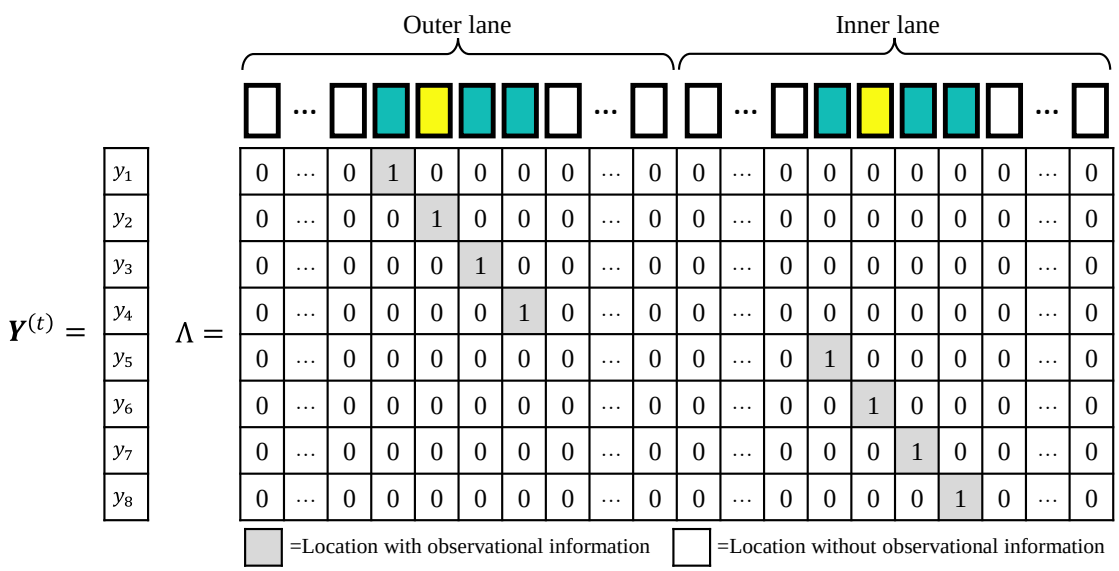

Figure 7-2 Observation vector on the bridge deck and matrix Λ representing the observed locations on the lanes.

The observed data can be obtained under different traffic volumes (i.e., different AADT of 40000, 60000, 80000, 100000 for example). According to the load form 4, Figure 7-3 shows the spatial random field results of outer lane vehicle load intensity updated by four traffic volumes. It can be

seen that, when the AADT increases, the updated vehicle load intensity also increases in the intensive and sub-intensive areas for Effect 4 (BMMS). Therefore, the updating method can effectively describe the load intensity change corresponding to the traffic volume evolution. It should be noted that the spatial updating method is only used to update the profile of the load form, the updating of load intensity is done. So, the vehicle load distribution intensity shown in Figure 7-3 is an intermediate result, not the final load intensity value of the updated model.

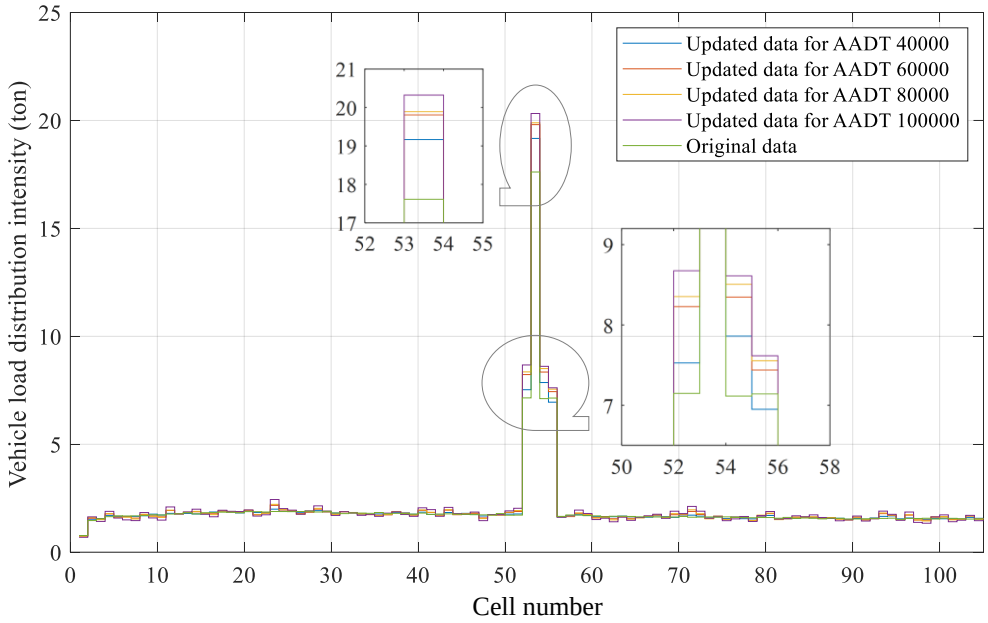

Figure 7-3 Distribution of vehicle load intensity for outer lane before and after updating using four traffic states.

7.2 Traffic load model updated for different traffic states

The observed data used in the updating process explained above could be obtained by WIM under different traffic volumes. However, owing to the WIM data with significant uncertainty, it is difficult to obtain the observation data under a specific traffic condition, so that the control variate method cannot be well applied. To solve this problem, the CA method was used to generate the different traffic data as observed data for the updating (artificial WIM data). Several traffic states (i.e., AADT of 40000, 60000, 80000, and 100000, and two GVWs distribution samples, namely, sample 1 and sample 2) were simulated as the observation data. For each simulated traffic state, the simulation time is 15 days. Figure 7-4 shows the probabilistic distribution of the ratio of actual

response to code D60 (η_1) of the four simulated traffic states with different AADT for the five effects. It can be observed that the response value increases as the AADT grows. Figure 7-5 depicts the PDFs of GVWs from observed data with different GVWs distributions generated by the CA method. These two GVWs probability densities are significantly different from each other. The GVWs of sample 1 are significantly larger than those of sample 2.

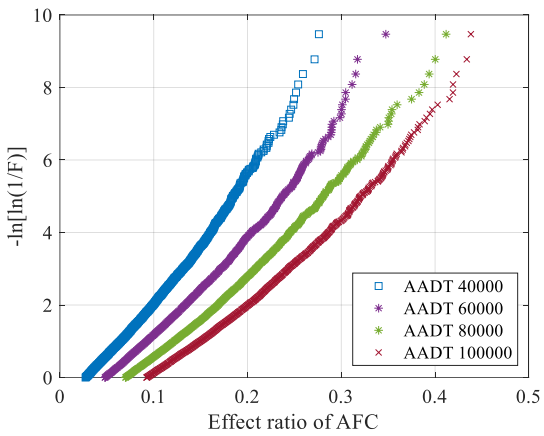

(a)

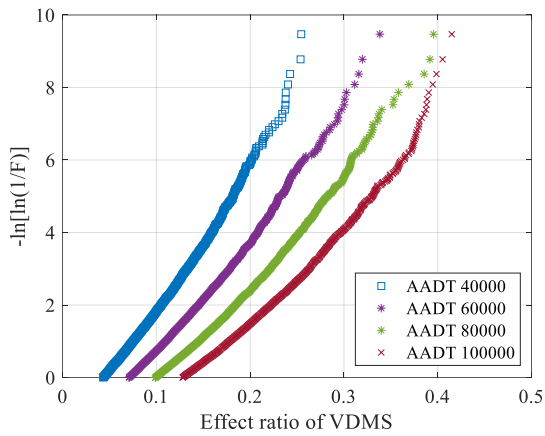

(b)

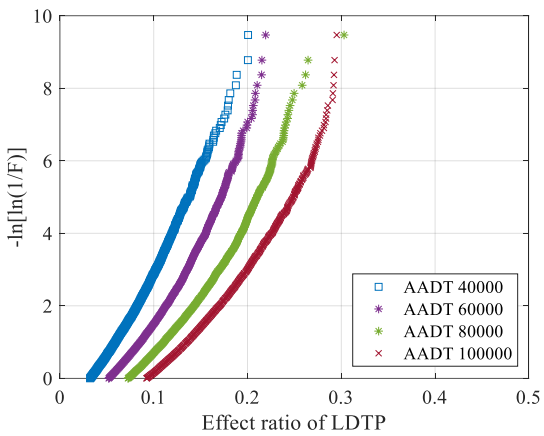

(c)

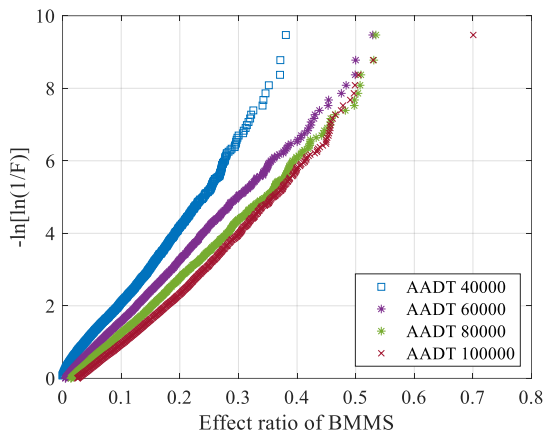

(d)

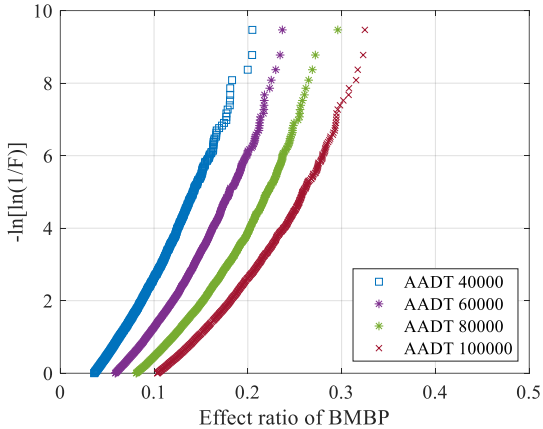

(e)

Figure 7-4 Effect ratio to D60 from observed data with different AADT generated by CA method.

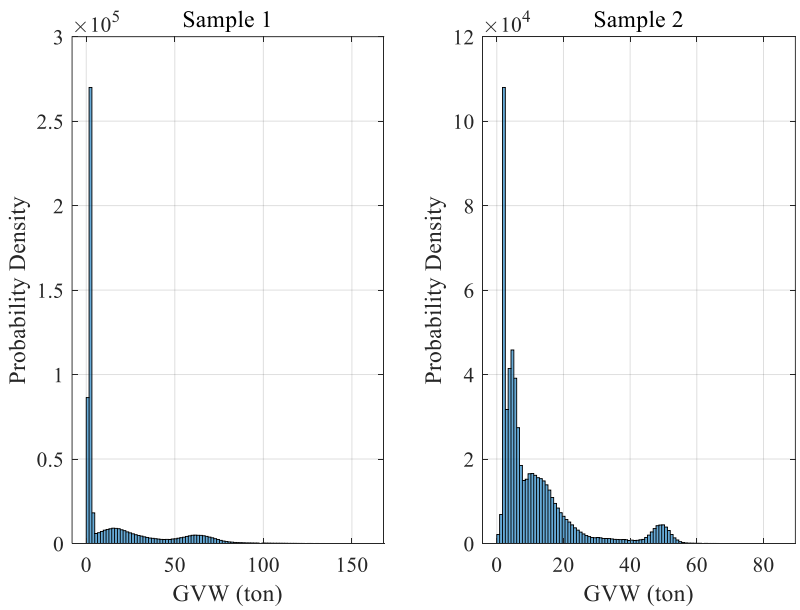

Figure 7-5 PDF of GVWs from observed data with different GVWs distribution generated by CA method.

Figure 7-6 shows the load profiles of the traffic model for both outer lane and inner lane for the five effects. The load intensity of the inner lane is significantly lower than that of the outer lane. Therefore, for the application of the traffic model, the profiles are normalized by assigning a value 1 to the maximum value of the outer lane. It can be seen that the profiles are quite different. This is due to the difference in the distribution of intensive area for each effect.

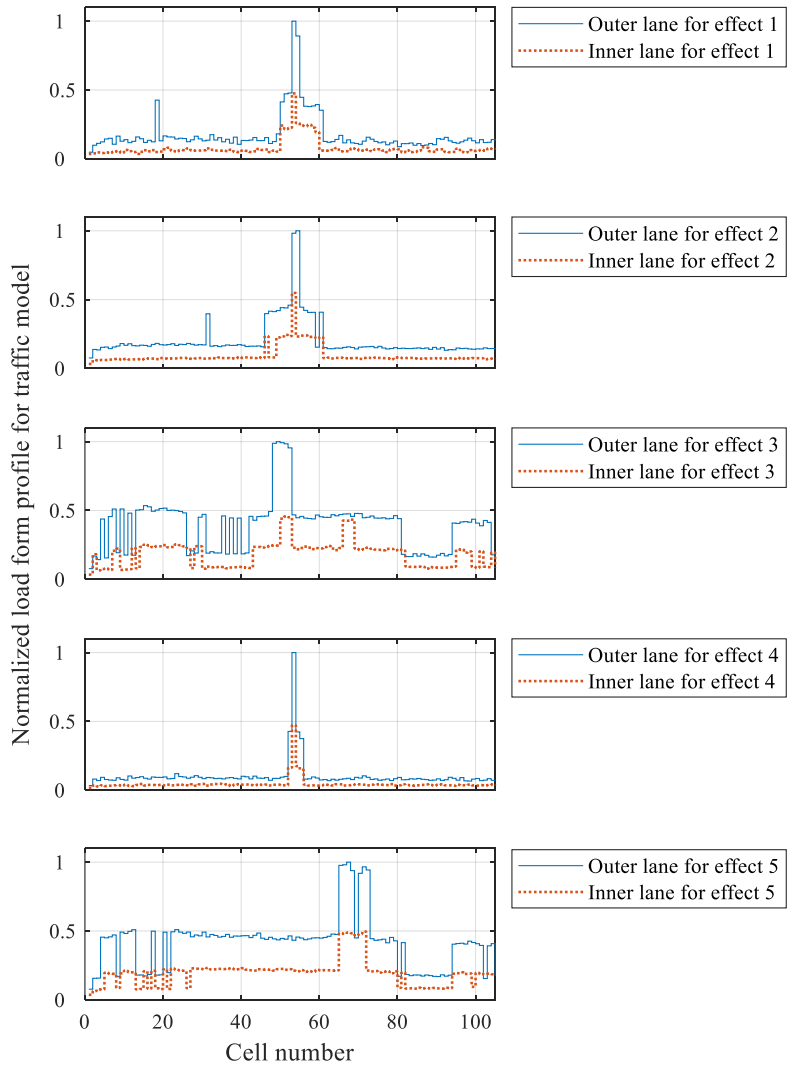

Figure 7-6 Updated load form profile of traffic model for five effects and AADT equal to 100000.

For the load intensity of the traffic model, the responses of observed traffic data should be calculated to determine the updated load value under different traffic states. This is because the updated random field of heavy vehicles on the bridge deck was implemented by comparing the similarity of the random field generated by prior distribution and observed spatial data and by redistribution of weights associated with the original random field. Therefore, the shape of the updated random fields is consistent with the selected original ones. However, the real scenarios of the heavy vehicle distribution under the new traffic conditions are not integrated into the updated fields. The essence of the updating process is to filter out the field clusters from the original

database that are more in line with the new traffic state under a certain error control. Thus, the updated results can represent well the scenario of the new traffic state on the load profile, but not the load intensity. Therefore, to assign intensity values to the updated profiles under different traffic states, it is necessary to analyze the effects of the observed data and the original data.

The response ratio of updated results of different AADT to original data are shown in Figure 7-7. The GVW distribution used in Figure 7-7 is the same as the one of the original probability vehicle scenario models. The correction factor in Figure 7-7 refers to the factor $\eta_1^{(i)}$ in **Equation (6-1)**. The updated responses increase as the AADT grows for all five effects. Figure 7-8 presents the response ratio of updated results of different GVWs samples to original data. It can be seen that the response of sample 1 is much higher than that of sample 2 for all five effects. For the lighter traffic (sample 2), the ratio is close or less than 1. The correction factor in Figure 7-8 refers to the factor $\eta_2^{(i)}$ in **Equation (6-1)**.

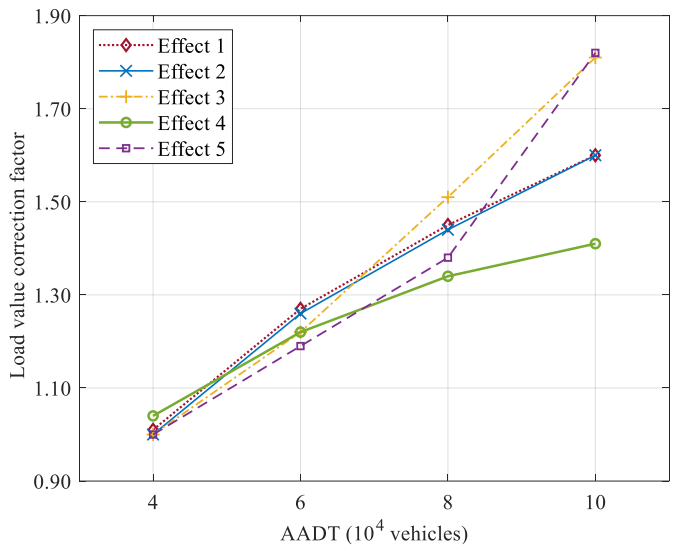

Figure 7-7 Response ratio of updated results to original scenario for different traffic states.

Using the observed data under different traffic states, the spatial distribution of traffic load intensity can be updated by the Bayesian inference method. The response ratio of updated results to original data can be obtained. As outlined in Chapter 2, they are all given as the ratio of response to code D60 and in the format of a correction factor.

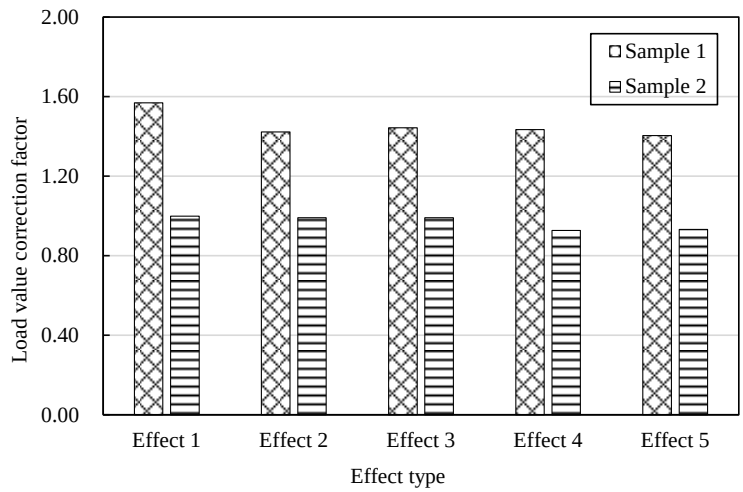

Figure 7-8 Influence of GVW statistical distribution on the response ratio of updated results to original scenario.

Table 7-1 depicts the load model response correction factors for different traffic states as well as the standard ratio values $r_k^{(i)}$. The standard ratio value $r_k^{(i)}$ is the ratio of the response of the original probabilistic model of traffic scenarios to the D60 load value. The response ratio $r_k^{(i)}$ has already been extrapolated with a return period of 1950 years. It can be seen that the correction factors for different traffic states vary greatly depending on the LEs. For instance, for the case of AADT 100,000, the correction factors for effects 3 and 5 are 1.811 and 1.821, respectively, while the correction factor for Effect 4 (BMMS) is 1.414. At the same time, it can be observed that effects with similar effective loaded lengths have similar trends in the values of the correction factor.

Table 7-1 Correction factors for different LEs and traffic conditions.

The *i*-th effect		AFC	VDMS	LDTP	BMMS	BMBP
Standard ratio value $r_k^{(i)}$		1.374	1.191	0.628	2.363	0.575
AADT $\eta_1^{(i)}$	40000	1.015	0.999	1.005	1.039	1.000
	60000	1.269	1.257	1.216	1.221	1.185
	80000	1.449	1.437	1.507	1.340	1.375
	100000	1.599	1.601	1.811	1.414	1.821
GVW distribution	Sample 1	1.568	1.421	1.444	1.434	1.403
$\eta_2^{(i)}$	Sample 2	0.999	0.991	0.991	0.926	0.932

For the most unfavourable conditions with 100000 AADT, the response value ratio for Effect 4 (BMMS) is 2.363 × 1.414 = 3.341, indicating that the maximum load effect by the proposed model is more than 3 times higher than the load effect predicted by code D60. However, the response values for Effect 3 (LDTP) and 5 (BMBP) are almost in the same level as D60 (0.628 × 1.811 = 1.137 and 0.575 × 1.821 = 1.047). In this case, the code D60 provides quite accurate results, but still on the unsafe zone. Taking into account these results, it seems rational to develop a site-specific traffic load model for different effects as done in this research.

According to the above results and the load profile for each effect, the load intensity can be calibrated as shown in Table 7-2. $q_k^{(i)}$ represents the maximum load intensity for the outer lane for each effect. The intensity value for other location on the outer lane and for all the location on the inner lane are taken according to the shape scale shown in Figure 7-6. The load form profile in Table 7-2 is a schematic diagram. It means that for different effect of the investigated bridge, the shape of load form profile is different. It is un-uniformly distributed as corresponds to the load form 4 adopted. Based on the traffic model given in Table 7-2, the total load on the six lanes due to the traffic model for each case was calculated as shown in Table 7-3 and Figure 7-9. The total load corresponding to Effect 3 (LDTP) and 5 (BMBP) are much higher than that of code D60, while the extrapolated response ratio of these two effects to code D60 under AADT of 100000 are only 1.137 and 1.047, which are at the same response level as code D60. The total load corresponding to Effect 4 (BMMS) is slightly lower than that of code D60 while the extrapolated response ratio of this effect to code D60 is 3.341. Again, this result indicates that the load model of code D60 cannot account for the vehicle load spatial distribution on the bridge deck. A similar conclusion is of application to other codes that adopt similar load model profiles as AAHSTO, BS and Eurocode. The proposed model addressed this shortcoming and can build targeted load models for different effects.

Table 7-2 Load intensity and load form schematic diagram of traffic model for different structural effects.

The *i*-th effect		AFC	VDMS	LDTP	BMMS	BMBP
Load intensity $q_k^{(i)}$ (Unit: kN/m)		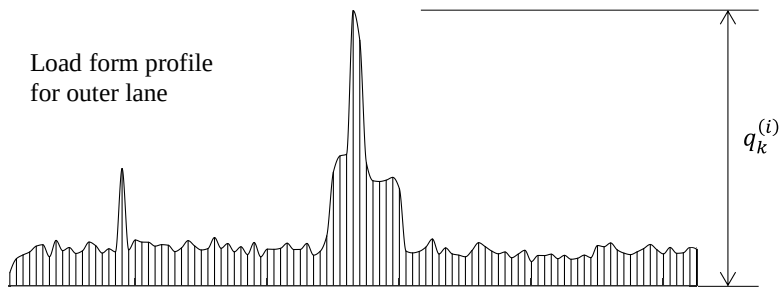				
AADT	40000	24.07	22.89	18.85	29.54	17.21
	60000	30.59	28.72	23.32	34.89	20.15
	80000	35.30	33.08	28.74	38.07	24.07
	100000	39.70	37.29	35.19	40.36	32.65
GVW distribution	Sample 1	39.72	33.17	28.85	41.41	25.21
	Sample 2	23.13	22.30	18.48	25.43	15.94

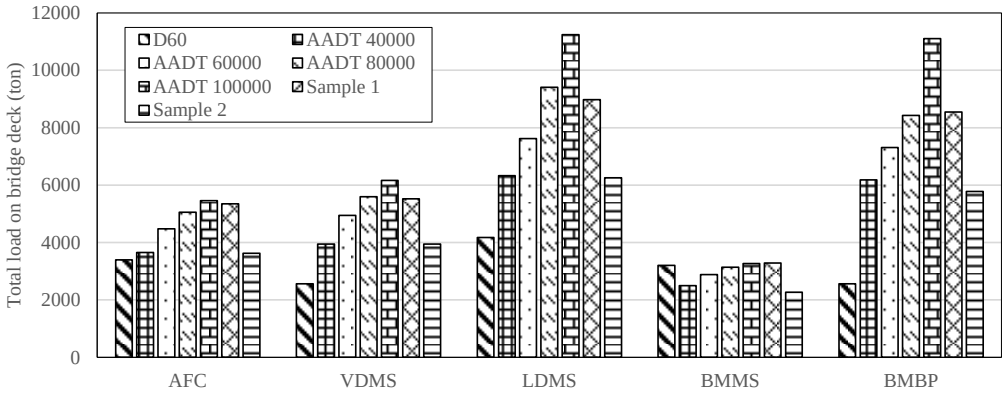

Figure 7-9 Total load on the bridge deck of the proposed traffic model and D60.

Table 7-3 Total load on bridge deck of proposed traffic model.

Total load on bridge deck (Unit: tonnes)		AFC	VDMS	LDTP	BMMS	BMBP
Code D60 loading results		3397	2560	4171	3204	2560
AADT	40000	3650	3949	6327	2494	6181
	60000	4476	4941	7624	2880	7309
	80000	5058	5592	9404	3136	8428
	100000	5461	6161	11243	3267	11106
GVW distribution	Sample 1	5343	5522	8977	3282	8547
	Sample 2	3620	3945	6251	2267	5777

7.3 Conclusions

This chapter proposes a Bayesian method for updating the spatial distribution of vehicle load level of the proposed site-specific model under time-varying traffic flow conditions. An engineering application example is given based on a natural bridge. The results show that the proposed traffic model update method based on Bayesian inference can update the random field of the spatial distribution of vehicles on bridge decks when extreme values are obtained using new WIM observations, and has advantages in describing the spatial distribution of complex traffic loads. The load form of the proposed load model is a non-uniform line load distribution, which facilitates the identification of the actual distribution of heavy vehicle loads on the bridge deck when different effects reach extreme values.

The site-specific load model presented in this chapter is only responsible for the sample WIM data. If the model is used for the feasibility assessment of new bridges, it is necessary to make a reasonable prediction of the traffic flow information at the bridge site. Based on the predicted traffic flow parameters obtained from the assessment, the CA method is applied to simulate the future traffic flow and further applied to the structural assessment of the new bridge.

The application of the updating method of the site-specific model proposed in this chapter for existing bridges can provide timely information on changes in the distribution tendency of heavy vehicles on the bridge deck. By timely learning the actual level of vehicular load distribution on the bridge deck, the changes in the structural performance induced by vehicular loads in can be assessed in real time. The structural performance assessment information can be further compared with the real-time monitored structural response to analyse the structural performance degradation or structural damage.

CHAPTER 8 Conclusions and future research

8.1 Conclusions

In this thesis, we present a probabilistic model for assessing extreme LEs on long-span bridges using a GMM method under free-flow traffic, based on WIM data. The proposed model is applied to a double-tower cable-stayed bridge case study, and its accuracy and efficiency are validated through numerical calculations using WIM data and the CA method.

The Monte Carlo method enables probabilistic modeling of complex heavy vehicle spatial distributions. Excluding light vehicles (less than 10 tonnes) from the simulation reduces computational effort without significant loss of accuracy (errors below 5%).

As neighbouring GVWs correlation increases, extreme LEs become more likely, emphasizing the importance of accurate vehicle spatial distribution modeling. The non-stationary Poisson process offers an efficient, feasible, and conservative method for this purpose.

The proposed model's results for various LEs display varying agreement with values from existing traffic load models in certain codes. This highlights the need for developing separate load models for different effects based on actual extreme response vehicle scenarios.

The developed site-specific model accurately considers extreme LEs for a specific return period, with substantial reductions in computation time compared to traditional simulations (a ratio of 2520:1 in required time).

The proposed probabilistic model's feasibility and advantages for long loaded length vehicle scenarios are demonstrated. However, due to assumptions in vehicle centroid reallocation and location simulation processes, the model may not be suitable for shorter loaded length bridge types. The appropriate load model pattern for designing or assessing long-span bridge effects can be explored based on this study's findings.

Additionally, a Bayesian inference method is proposed for updating vehicle load spatial distributions on long-span bridge decks, resulting in maximum LEs under time-varying free traffic conditions. A site-specific traffic load model is developed for different effects, along with a

probabilistic model for heavy vehicle spatial distribution, load profile updating, and load intensity calibration, based on WIM data and the CA simulation method. An application example is presented. The Bayesian inference-based traffic model updating method effectively updates on-bridge vehicle spatial distribution random fields using WIM monitoring data and is superior in describing complex spatial distributions. The proposed non-uniform distributed load shape for the traffic model enables accurate heavy vehicle load distribution recognition on the bridge deck when different effects reach extreme values, addressing limitations in traditional code models and offering insights for constructing targeted load models for various LEs.

The proposed model has been applied to other representative cable-stayed bridges apart from the one presented in the case study, with span-lengths between 200 and 1000 meters. The information of the bridges, the application process and a brief analysis of the results can be found in Appendix 3. From the study, it can be concluded a similar pattern of load distribution on the bridge deck for the extreme response scenario, although with a different load intensity, which increases as the span-length decreases. The smaller the span- length, the larger the peak load value and average load per bridge length for the same effect on the cable-stayed bridge. In contrast, the average load per bridge length under code D60 does not show significant differences between the span-specific scenarios and is not consistent with the extreme scenario case of the actual WIM data. These findings reveal the characteristics of the load levels of extreme response scenarios for different span bridges under different effects and can further guide bridge design and maintenance. In practical applications, for different long-span bridge types and spans, targeted load model can be built according to the specific loading conditions to ensure the safety of the bridge, and the extreme response scenario load model presented in this thesis can provide a powerful tool for this purpose.

Although the proposed approach is also applicable for congested traffic scenarios, the main traffic condition considered in the present paper is free-flow not congested traffic. The congestion situation is a worst-case scenario most of the time, but it is rare to occur, and daily traffic flow does not pattern in this manner. Therefore, the extreme effect value scenarios under free-flow, which occur more frequently and also can produce larger extreme effect values, are of equal value importance in the daily management and safety assessment of long-span bridges. For the safety of long-span bridges, the extreme effect scenarios generated by free-flow should not be ignored.

8.2 Future research

The proposed probabilistic model of traffic scenarios for long-span bridges is highly site-specific and can only account for the traffic sample of the bridge location. Owing to the lack of monitoring data, real-time correspondence of response and traffic scenario is not involved in the study. Likewise, due to the lack of actual congestion measurement data, the modeling of the congestion scenario is not carried out in detail in this work. The model is proposed for long-span bridges; therefore, it is not applicable to the analysis of effects with short loading length (e.g., fatigue effects). Meanwhile, the proposed model has some limitations in considering the correlation of GVWs between adjacent lanes, the consistency and variability of the scenario in terms of time and space, as well as dynamic vehicle loads. In addition, the validation of the model has been performed under free traffic flow conditions. Although also of application to congested traffic scenarios, a full study under such situation should be addressed in future research. In the thesis, only the static loading responses of vehicles are considered, and further research will be carried out on the effects of dynamic vehicle-structure interactions on the performance of long-span bridges.

The proposed traffic load model and its Bayesian inference-based approach are appropriate to obtain the maximum values of different bridge effects for long-loaded lengths under different traffic conditions in non-congested situation. These maxima correspond to critical load scenarios representing actual traffic flow conditions and they depend on the AADT and characteristics of GVW. However, the proposed model cannot depict the spatio-temporal properties of on-bridge vehicle load, as it does not consider dynamic characteristics of traffic flow, which needs further study. At the same time, distinguishing congested flow and free flow in the spatial distribution traffic model and building the corresponding updating methods is also a key content that needs attention in the future to analyze congested traffic situations and free traffic states including dynamic effects (relevant for fatigue limit state).

References

American Association of State Highway and Transportation Officials (AASHTO). (2004). *Highway Bridge Design Specifications.* Washington, DC.

Anitori, G., Casas, J.R., & Ghosn, M. (2018). Methodology for development of live load models for refined analysis of short and medium-span highway bridges. *Structure and Infrastructure Engineering*, *14*(4), 477–490.

Anitori, G., Casas, J.R, & Ghosn, M. (2017). WIM-based live-load model for advanced analysis of simply supported short- and medium-span highway bridges. *Journal of Bridge Engineering*, *22*(10), 04017062-1-04017062-11.

Bai, L. (2021). *Research on vehicle location and license plate character recognition algorithm based on deep learning*. Huazhong University of Science and Technology (Master's degree thesis): Wuhan, China. (in Chinese).

BSI BS EN 1991-2. (2003). *Eurocode 1: Actions on Structures. Part 2: Traffic Loads on Bridges.* London, UK: European Committee for Standardization.

BSI BS 5400-2. (2006). *Steel, Concrete and Composite Bridges-Part 2: Specification for Loads.* London, UK: British Standards Institution.

Buckland, P. G. (1981). Recommended design loads for bridges. *ASCE Journal of the Structural Division*, *107*, 1161–1213.

Caprani, C. C. (2012). Calibration of a congestion load model for highway bridges using traffic microsimulation. *Structural engineering international*, *22*(3), 342–348.

Caprani, C. C. (2013). Lifetime highway bridge traffic load effect from a combination of traffic states allowing for dynamic amplification. *Journal of Bridge Engineering*, *18*(9), 901–909.

Caprani, C. C., O'Brien, E. J., & Lipari, A. (2016). Long-span bridge traffic loading based on multi-lane traffic micro-simulation. *Engineering Structures*, *115*, 207–219.

Caprani, C. C., O'Brien, E. J., & McLachlan, G. J. (2008). Characteristic traffic load effects from a mixture of loading events on short to medium span bridges. *Structural Safety*, *30*(5), 394–404.

Carey, C., Caprani, C. C., & Enright, B. (2018). A pseudo-microsimulation approach for modelling congested traffic loading on long-span bridges. *Structure and Infrastructure Engineering*, *14*(2), 163–176.

Celeux, G., & Soromenho, G. (1996). An entropy criterion for assessing the number of clusters in a mixture model. *Journal of Classification*, *13*(2), 195–212.

Cheng, L., Zhang, H., & Cao, X. (2006). Vehicle weight in motion technology. *Chinese Journal of Scientific*

Instrument, *27*(8), 943–948. (in Chinese).

Chen, A., Ma, R., & Xu, Y. (2013). Vehicle loading identification and its characteristics of Sutong bridge in operation. *Journal of Chongqing Jiaotong University (Natural Science)*, *32*(S1), 729–733. (in Chinese).

Chen, B., Ye, Z., Chen, Z., & Xie, X. (2018). Bridge vehicle load model on different grades of roads in China based on Weigh-in-Motion (WIM) data. *Measurement*, *122*, 670–678.

Chen, J., Yuan, S., Sbarufatti, C., & Jin, X. (2021). Dual crack growth prognosis by using a mixture proposal particle filter and on-line crack monitoring. *Reliability Engineering & System Safety*, *215*, 107758.

Chen, S. R., & Cai, C. S. (2007). Equivalent wheel load approach for slender cable-stayed bridge fatigue assessment under traffic and wind: Feasibility study. *Journal of Bridge Engineering*, *12*(6), 755–764.

Chen, S. R., & Wu, J. (2011). Modeling stochastic live load for long-span bridge based on microscopic traffic flow simulation. *Computers & Structures*, *89*(9-10), 813–824.

Chen, W., Wang, Z., & Xu, J. (2009). A BWIM method used for steel truss bridges. *Bridge Construction*, *4*, 72–75. (in Chinese).

Chen, Z., Bao, Y., Chen, J., & Li, H. (2019). Modelling the spatial distribution of heavy vehicle loads on long-span bridges based on undirected graphical model. *Structure and Infrastructure Engineering*, *15*(11), 1485–1499.

Cooper, D. I. (2011). Development of short span bridge-specific assessment live loading. *Safety of bridges*, 64–89. Thomas Telford Publishing.

Dai, B., Xia, Y., & Li, Q. (2022). An extreme value prediction method based on clustering algorithm. *Reliability Engineering & System Safety*, *222*, 108442.

Der Kiureghian, A., & Liu, P. (1986). Structural reliability under incomplete probability information. *Journal of Engineering Mechanics*, *112*(1), 85-104.

Enright, B., Carey, C., & Caprani, C. C. (2013). Microsimulation evaluation of Eurocode load model for American long-span bridges. *Journal of Bridge Engineering*, *18*(12SI), 1252-1260.

Enright, B., & O'Brien, E. J. (2013). Monte Carlo simulation of extreme traffic loading on short and medium span bridges. *Structure and Infrastructure Engineering*, *9*(12), 1267-1282.

Fisher, RA, Tippett, LHC. (1928). Limiting forms of the frequency distribution of the largest or smallest member of a sample. *Math Proc Cambridge Philos Soc*, *24*(02), 180–90.

Frangopol, D. M., & Liu, M. (2007). Maintenance and management of civil infrastructure based on condition, safety, optimization, and life-cycle cost. *Structure and Infrastructure Engineering*, *3*(1), 29–41.

Gao, W., Li, G., Su, Q., & Han, W. (2022). Impact of rigid central clamps on longitudinal deformation of long-span suspension bridges under vehicle excitations. *Structure and Infrastructure Engineering*, *18*(6), 760–774.

Getachew, A., & O'Brien, E. J. (2007). Simplified site-specific traffic load models for bridge assessment. *Structure and Infrastructure Engineering*, *3*(4), 303-311.

Ghosn, M., Moses, F., & Wang, J. (2003). *Design of highway bridges for extreme events (No. 30)*. Transportation Research Board.

Gil, H., & Kang, S. (2015). Multiple-presence statistics of heavy trucks based on high-speed Weigh-in-Motion data. *Advances in Structural Engineering*, *18*(2), 189-200.

Gnedenko, B. V. (2017). *Theory of probability (6th ed.)*, Routledge, London, UK.

Gonçalves, M. S., Lopez, R. H., Oroski, E., & Valente, A. M. (2022). A Bayesian algorithm with second order autoregressive errors for B-WIM weight estimation. *Engineering Structures*, *250*, 113353.

Gordon, N. J., Salmond, D. J., & Smith, A. F. M. (1993). Novel approach to nonlinear/non-Gaussian Bayesian state estimation. *IEE proceedings. Part F, Radar and signal processing*, *140*(2), 107-113.

Guo, D., & Caprani, C. C. (2019). Traffic load patterning on long span bridges: A rational approach. *Structural Safety*, *77*, 18-29.

Guo, T., Li, A., & Zhao, D. (2008). Multiple-peaked probabilistic vehicle load model for highway bridge reliability assessment. *Journal of Southeast University. Natural Science Edition*, *38*(5), 763-766. (in Chinese).

Hale, D. K., Antoniou, C., Brackstone, M., Michalaka, D., Moreno, A. T., & Parikh, K. (2015). Optimization-based assisted calibration of traffic simulation models. *Transportation Research Part C: Emerging Technologies*, *55*, 100-115.

Hallenbeck, M. E., & Weinblatt, H. (2004). *Equipment for Collecting Traffic Load Data (No. 509)*. Washington, DC: The National Academies Press.

He, M., Liang, P., Liu, J., Yang, F., & Zhao, X. (2022). A new model to simulate the site-specific traffic load with consideration of precise axle load and microscopic behavior. *Structure and Infrastructure Engineering*, 1-16.

Hisada, T., & Nakagiri, S. (1985, 1985-01-01). *Role of the Stochastic Finite Element Method in Structural Safety and Reliability*. Kobe, Japan.

Hitchcock, W. A., Uddin, N., Sisiopiku, V., Salama, T., Kirby, J., & Zhao, H. (2012). *Bridge Weigh-in-Motion (B-WIM) system testing and evaluation*, FHWA/CA/OR.

Hou, R., Jeong, S., Lynch, J. P., Ettouney, M. M., & Law, K. H. (2022). Data-driven analytical load rating method of bridges using integrated bridge structural response and Weigh-in-Motion truck data. *Mechanical Systems and Signal Processing*, *163*, 108128.

Huang, W., Zhou, B., Yu, Y., & Yin, D. (2021). Vulnerability analysis of road network for dangerous goods transportation considering intentional attack: Based on Cellular Automata. *Reliability Engineering & System Safety*, *214*, 107779.

Hull, J., & White, A. (1988). The use of the control variate technique in option pricing. *Journal of Financial and Quantitative Analysis*, *23*(3), 237-251.

Hwang, E. S., Lee, K. T., & Kim, D. Y. (2012). Modeling of truck traffic for long span bridges [Proceedings Paper].

Bridge Maintenance, Safety, Management, Resilience and Sustainability, 1100-1107.

Hwang, E., & Kim, D. (2019). Live load model for long span steel cable bridges considering traffic congestion scenarios. *International Journal of Steel Structures*, *19*(6), 1996–2009.

Kelly, D. L., & Smith, C. L. (2009). Bayesian inference in probabilistic risk assessment – The current state of the art. *Reliability Engineering & System Safety*, *94*, 628–643.

Jenkinson, A. F. (1955). The frequency distribution of the annual maximum (or minimum) values of meteorological elements. *Quarterly Journal of the Royal Meteorological Society*, *81*(348), 158-171.

Jiang, X., Li, Y., Lv, Y., & Cai, Y. (2011). Design of signal acquisition system for WIM. *Electronic Design Engineering*, *19*(6), 119–121. (in Chinese).

Kennedy, D. J. L., Gagnon, D. P., Allen, D. E., & MacGregor, J. G. (1992). Canadian highway bridge evaluation: load and resistance factors. *Canadian Journal of Civil Engineering*, *19*(6), 992-1006.

Kim, J., & Song, J. (2019). A comprehensive probabilistic model of traffic loads based on Weigh-in-Motion data for applications to bridge structures. *KSCE Journal of Civil Engineering*, *23*(8), 3628-3643.

Kim, J., & Song, J. (2021). Bayesian updating methodology for probabilistic model of bridge traffic loads using in-service data of traffic environment. *Structure and Infrastructure Engineering*, 1-16.

Kioumarsi, M. M., Hendriks, M. A. N., Kohler, J., & Geiker, M. R. (2016). The effect of interference of corrosion pits on the failure probability of a reinforced concrete beam. *Engineering Structures*, *114*, 113-121.

Kitagawa, G. (1996). Monte Carlo filter and smoother for non-Gaussian nonlinear state space models. *Journal of Computational and Graphical Statistics*, *5*(1), 1-25.

Kwon, O., Kim, E., & Orton, S. (2011). Calibration of live-load factor in LRFD bridge design specifications based on state-specific traffic environments. *Journal of Bridge Engineering*, *16*(6SI), 812-819.

Leahy, C., O'Brien, E. J., Enright, B., & Hajializadeh, D. (2015). Review of HL-93 bridge traffic load model using an extensive WIM database. *Journal of Bridge Engineering*, *20*(10)

Leahy, C., O'Brien, E. J., Enright, B., & Power, R. T. (2015). *Estimating characteristic bridge traffic load effects using Bayesian statistics*. Paper presented at the 12th International Conference on Applications of Statistics and Probability in Civil Engineering (ICASP12), Vancouver, Canada.

Leahy, C., O'Brien, E., & O Connor, A. (2016). The effect of traffic growth on characteristic bridge load effects. *Transportation Research Procedia*, *14*, 3990-3999.

Lin, Y., & Jiao, X. (2021). Adaptive Kernel Auxiliary Particle Filter Method for Degradation State Estimation. *Reliability Engineering & System Safety*, *211*, 107562.

Lipari, A., Caprani, C. C., & O'Brien, E. J. (2017). A methodology for calculating congested traffic characteristic loading on long-span bridges using site-specific data. *Computers & Structures*, *190*, 1-12.

Liu, C., Cowles, G. W., Zemeckis, D. R., Fay, G., Le Bris, A., & Cadrin, S. X. (2019). A hardware-accelerated particle

filter for the geolocation of demersal fishes. *Fisheries Research*, *213*, 160-171.

Liu, P., & Der Kiureghian, A. (1991). Finite element reliability of geometrically nonlinear uncertain structures. *Journal of Engineering Mechanics*, *117*(8), 1806-1825.

Li, D., Tang, X., Phoon, K., Chen, Y., & Zhou, C. (2013). Bivariate simulation using copula and its application to probabilistic pile settlement analysis. *International Journal for Numerical and Analytical Methods in Geomechanics*, *37*(6), 597-617.

Li, Q., Wang, C., & Zhang, H. (2016). A probabilistic framework for hurricane damage assessment considering non-stationarity and correlation in hurricane actions. *Structural Safety*, *59*, 108-117.

Li, S., Fang, H., & Shi, B. (2021). Remaining useful life estimation of Lithium-ion battery based on interacting multiple model particle filter and support vector regression. *Reliability Engineering & System Safety*, *210*, 107542.

Lu, N., Beer, M., Noori, M., & Liu, Y. (2017). Lifetime deflections of long-span bridges under dynamic and growing traffic loads. *Journal of Bridge Engineering*, *22*(11)

Mahadevan, S., & Haldar, A. (1991). Practical random field discretization in stochastic finite element analysis. *Structural Safety*, *9*(4), 283-304.

Maruyama, O., & Hoshiya, M. (2008). Stochastic interpolation of spatial random fields by BF/MCF-ISM. *Journal of Engineering Mechanics*, *134*(2), 198-205.

Micu, E. A., Malekjafarian, A., OBrien, E. J., Quilligan, M., McKinstray, R., Angus, E., … Catbas, F. N. (2019). Evaluation of the extreme traffic load effects on the Forth Road Bridge using image analysis of traffic data. *Advances in Engineering Software*, *137*(December 2018), 102711.

Ministry of Communications and Transportation (MOCAT). (2015). *General Code for Design of Highway Bridges and Culverts JTG D60*. Beijing: China Communications Press. (in Chinese).

Moses, F. (1979). Weigh-in-motion system using instrumented bridges. *Transportation Engineering Journal of ASCE*, *105*(3), 233-249.

Noh, Y., Choi, K. K., & Du, L. (2008). Reliability-based design optimization of problems with correlated input variables using a Gaussian copula. *Structural and Multidisciplinary Optimization*, *38*(1), 1-16.

Nowak, A. S., Lutomirska, M & Ibrahim, F. I. (2010). The development of live load for long span bridges. *Bridge Structures*, *6*(1, 2), 73–79.

Nowak, A. S. (1993). Live load model for highway bridges. *Structural Safety*, *13*(1), 53-66.

Nowak, A. S. (1994). Load model for bridge design code. *Canadian Journal of Civil Engineering*, *21*(1), 36-49.

Nowak, A. S. (1995). Calibration of LRFD bridge code. *Journal of Structural Engineering (New York, N.Y.)*, *121*(8), 1245-1251.

O'Brien, E. J., Bordallo-Ruiz, A., & Enright, B. (2014). Lifetime maximum load effects on short-span bridges subject to growing traffic volumes. *Structural Safety, 50*, 113-122.

O'Brien, E. J., Hayrapetova, A., & Walsh, C. (2012). The use of micro-simulation for congested traffic load modeling of medium- and long-span bridges. *Structure and Infrastructure Engineering*, *8*(3), 269-276.

O'Brien, E. J., Lipari, A., & Caprani, C. C. (2015). Micro-simulation of single-lane traffic to identify critical loading conditions for long-span bridges. *Engineering Structures*, *94*, 137-148.

O'Brien, E. J., Schmidt, F., Hajializadeh, D., Zhou, X. Y., Enright, B., Caprani, C. C., Wilson, S., & Sheils, E. (2015). A review of probabilistic methods of assessment of load effects in bridges. *Structural Safety, 53*, 44-56.

O'Brien, E. J., & Enright, B. (2013). Using Weigh-in-Motion data to determine aggressiveness of traffic for bridge loading. *Journal of Bridge Engineering*, *18*(3), 232-239.

Pang, Z., Si, X., Hu, C., Du, D., & Pei, H. (2021). A Bayesian inference for remaining useful life estimation by fusing accelerated degradation data and condition monitoring data. *Reliability Engineering & System Safety, 208*, 107341.

Paszek, E. (2007). *Introduction to Statistics*. Publisher: Connexions, Web site: https://archive.org/details/ost-math-col10343.

Roberts, J. E., & Shepard, R. (2000). Bridge management for the 21st century. *Transportation Research Record*, *1696*(1), 197-203.

Ruan, X., Zhou, J., Shi, X., & Caprani, C. C. (2017). A site-specific traffic load model for long-span multi-pylon cable-stayed bridges. *Structure and Infrastructure Engineering*, *13*(4), 494-504.

Ruan, X., Zhou, J., Tu, H., Jin, Z., & Shi, X. (2017). An improved cellular automaton with axis information for microscopic traffic simulation. *Transportation Research Part C: Emerging Technologies*, *78*, 63-77.

Soriano, M., Casas, J.R., & Ghosn, M. (2017). Simplified probabilistic model for maximum traffic load from weigh-in-motion data. *Structure and Infrastructure Engineering*, *13*(4), 454-467.

Tian, J., Li, G., Treiber, M., Jiang, R., Jia, N., & Ma, S. (2016). Cellular automaton model simulating spatiotemporal patterns, phase transitions and concave growth pattern of oscillations in traffic flow. *Transportation Research Part B: Methodological, 93*, 560-575.

Tulsyan, A., Bhushan Gopaluni, R., & Khare, S. R. (2016). Particle filtering without tears: A primer for beginners. *Computers & Chemical Engineering, 95*, 130-145.

Wang, F., & Xu, Y. (2019). Traffic load simulation for long-span suspension bridges. *Journal of Bridge Engineering*, *24*(5)

Wang, N., Ren, W., & Wan, H. (2013). Bridge weigh-in-motion and its optimization algorithm based on dynamic strain. *Journal of Vibration and Shock, 32*(4), 116–120. (in Chinese).

Xiao, Q. (2014). Evaluating correlation coefficient for Nataf transformation. *Probabilistic Engineering Mechanics*,

37, 1-6.

Xia, Y., Li, F., Gu, Y., Yuan, W., & Zhou, Z. (2014). Study on vehicular fatigue load spectrum expressway bridge based on WIM system. *Journal of Highway and Transportation Research and Development*, *31*(3), 56–64. (in Chinese).

Xiong, W., Cai, C. S., Kong, B., & Ye, J. (2017). Overturning-collapse modeling and safety assessment for bridges supported by single-column piers. *Journal of Bridge Engineering*, *22*(11)

Xu, Y., Chen, Z., & Xia, Y. (2012). Fatigue assessment of multi-loading suspension bridges using continuum damage model. *International Journal of Fatigue*, *40*, 27-35.

Yang, Y., Wang, Y., Wang, C., & Xue, C. (2006). Sensor design and finite element analysis for Weigh-in-Motion (WIM) system for vehicles. *Instrument Technique and Sensor*, *12*, 4–8. (in Chinese).

Yang, Y., Wu, W., Wang, B., & Li, M. (2020). Analytical reformulation for stochastic unit commitment considering wind power uncertainty with Gaussian mixture model. *IEEE Transactions on Power Systems*, *35*(4), 2769-2782.

Yuan, Y., Han, W., Huang, P., Zhao, J., Li, Y., & Zhang, J. (2017). Structure safety assessment under heavy traffic based on weigh in motion and simulation analysis. *Advances in Structural Engineering*, *20*(12), 1864-1878.

Yu, Q. (2021). *Research on moving vehicle detection and tracking algorithm based on video processing*. Southeast University (Master's degree thesis): Nanjing, China. (in Chinese).

Yu, Y., Cai, C. S., He, W., & Peng, H. (2019). Prediction of bridge maximum load effects under growing traffic using non-stationary Bayesian method. *Engineering Structures*, *185*, 171-183.

Yu, Y., & Cai, C. S. (2019). Prediction of extreme traffic load effects of bridges using Bayesian method and application to bridge condition assessment. *Journal of Bridge Engineering*, *24*(3), 4019003.

Zang, Y., Shangguan, W., Cai, B., Wang, H., & Pecht, M. G. (2021). Hybrid remaining useful life prediction method. A case study on railway D-cables. *Reliability Engineering & System Safety*, *213*, 107746.

Zhao, L., Zhou, Z., Song, Y., Meng, M., & Huang, Q. (2020). Uncertainty quantification of MEMS devices with correlated random parameters. *Microsystem Technologies*, *26*(5), 1689-1696.

Zhou, J., Caprani, C. C., & Zhang, L. (2021). On the structural safety of long-span bridges under traffic loadings caused by maintenance works. *Engineering Structures*, *240*, 112407.

Zhou, J., Ruan, X., Shi, X., & Caprani, C. C. (2019). An efficient approach for traffic load modelling of long span bridges. *Structure and Infrastructure Engineering*, *15*(5), 569-581.

Zhou J. (2018). *Methods and Application of Modeling, Prediction and Assessment of Traffic Load Effects on Long Span Bridges*. Tongji University (PhD's degree thesis): Shanghai, China. (in Chinese).

Zhu, R. (2017). *Studies of establishment methodology for scenario-specific vehicle load models of medium-small span bridges*. Tongji University (PhD's degree thesis): Shanghai, China. (in Chinese).

Zivkovic, Z. (2004). Improved adaptive Gaussian mixture model for background subtraction. Proceedings of the 17th International Conference on Pattern Recognition, 2, 28-31.

Appendix 1. List of acronyms

Acronyms	Significance
AADT	Annual average daily traffic volume
AASHTO	Highway Bridge Design Specifications of America
AFC	Axial force of the longest cable (Effect 1)
BMBP	Bending moment at the bottom of the pylon (Effect 5)
BMMS	Bending moment at mid-span of the main span (Effect 4)
BS 5400	Specification for Loads of Britain
CA	Cellular automata
CDF	Cumulative distribution function
D60	General code for design of highway bridges of China
GEV	Generalized extreme value distribution
GMM	Gaussian mixture model
GVW	Gross vehicle weight
IID	Independent and identically distributed
IL	Influence line
LDTP	Longitudinal displacement at the top of the pylon (Effect 3)
LE(s)	Load effect(s)
MCS	Monte Carlo simulation
PDF	Probability density function
PF	Particle filter
RNDGT	Road networks for dangerous goods transportation
SSM	State space model
VDMS	Vertical deflection at mid-span of the main span (Effect 2)
WIM	Weigh-in-motion

Appendix 2. Results for each effect in the case study

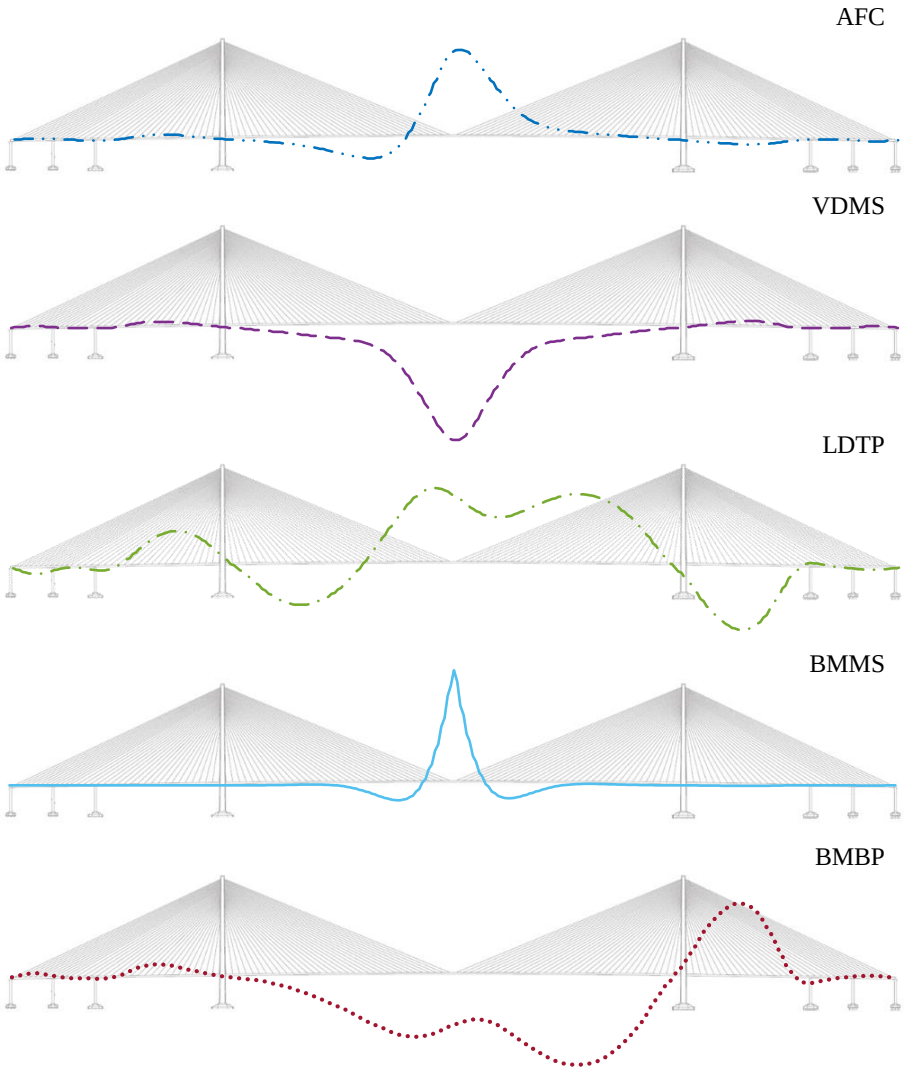

Figure A-1 Structural effects and influence lines in Sutong bridge.

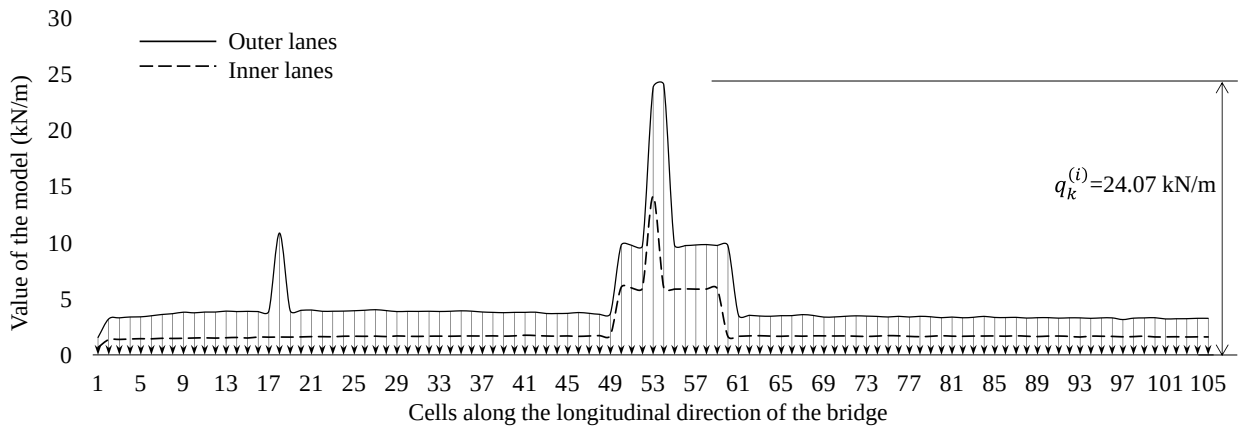

Figure A-2 Extreme response scenario load model of AFC.

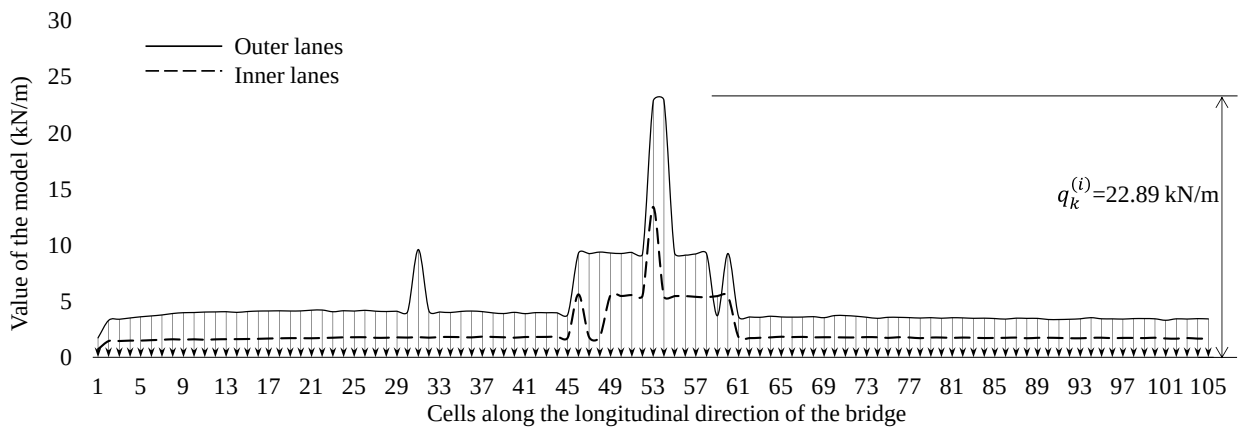

Figure A-3 Extreme response scenario load model of VDMS.

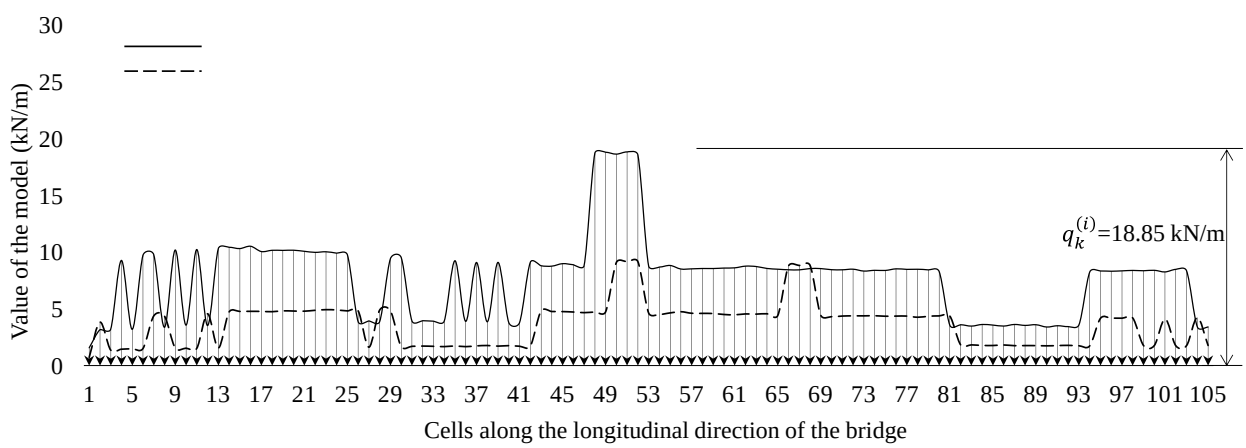

Figure A-4 Extreme response scenario load model of LDTP.

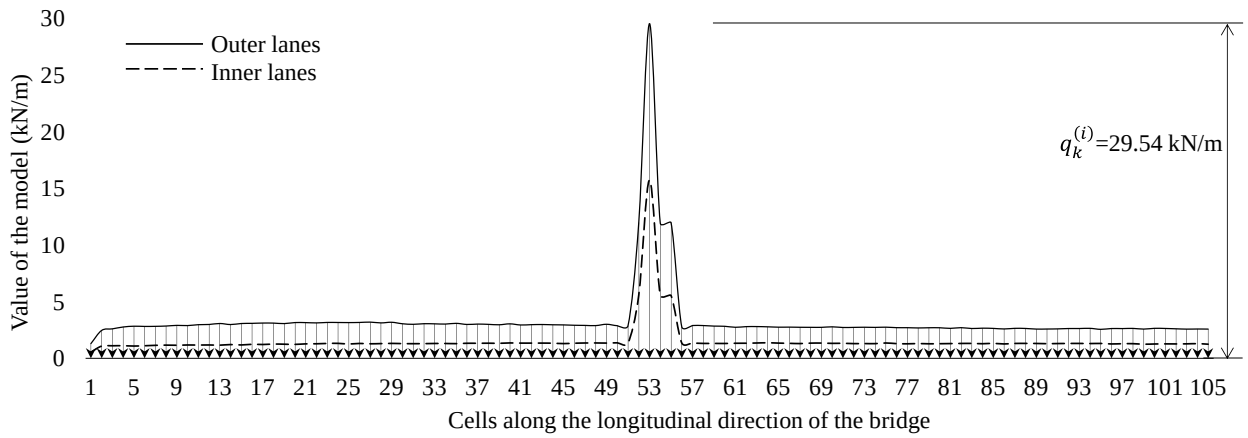

Figure A-5 Extreme response scenario load model of BMMS.

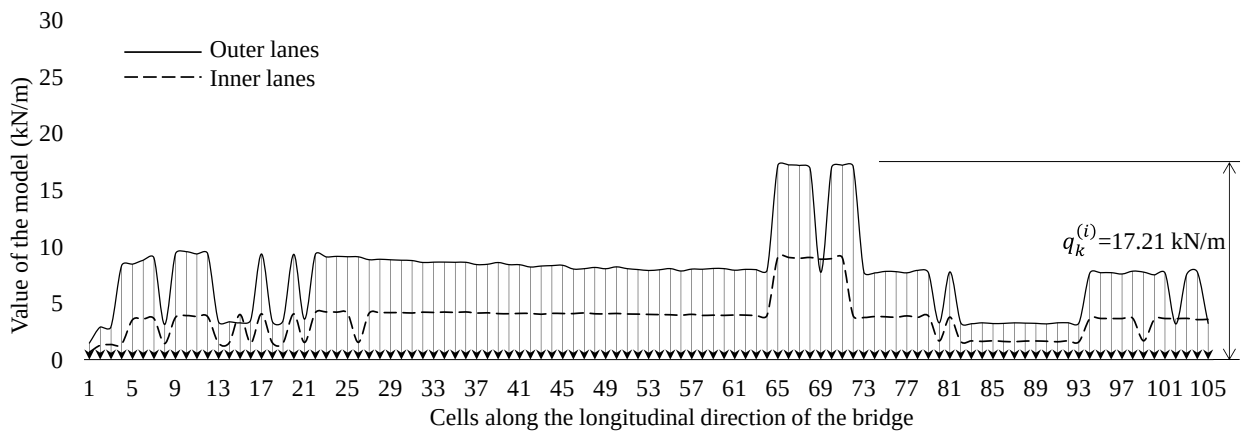

Figure A-6 Extreme response scenario load model of BMBP.

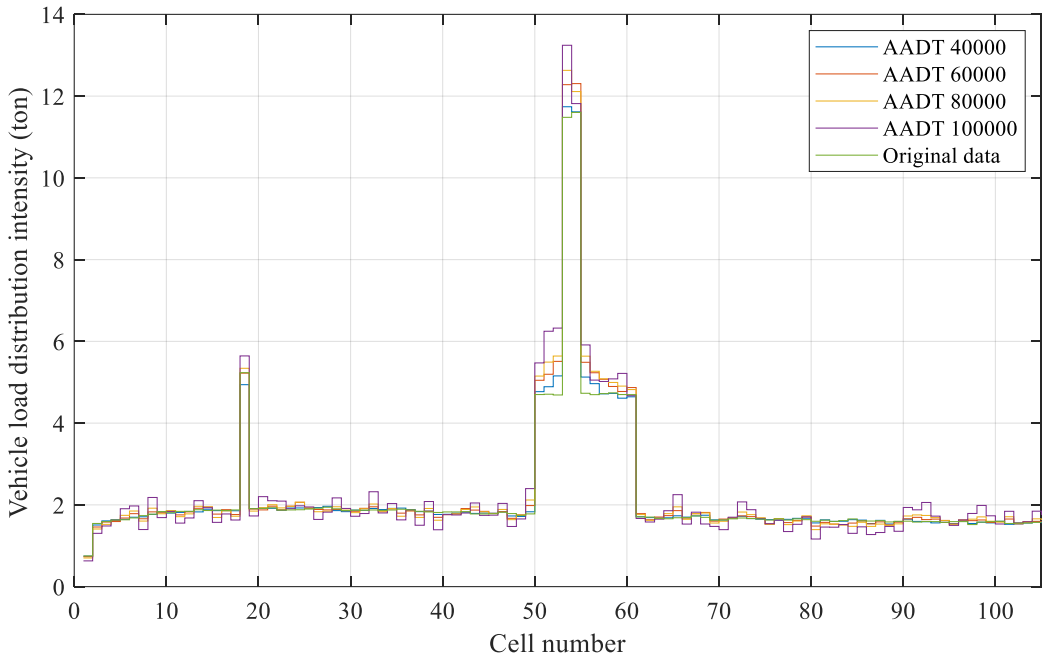

Figure A-7 Distribution of vehicle load intensity for outer lane before and after updating using four traffic states for AFC.

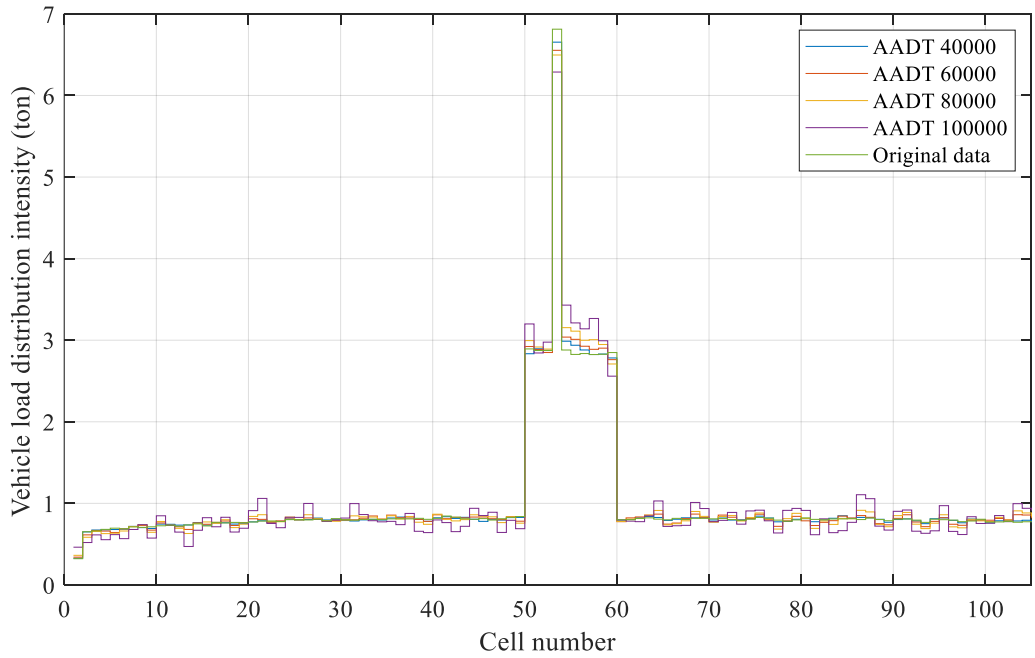

Figure A-8 Distribution of vehicle load intensity for inner lane before and after updating using four traffic states for AFC.

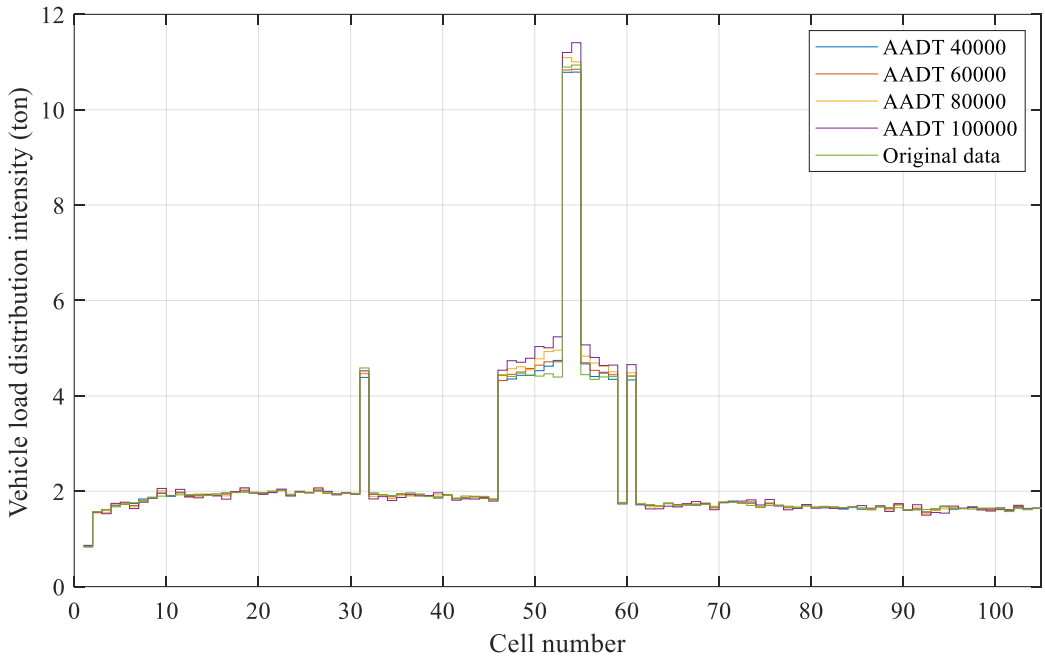

Figure A-9 Distribution of vehicle load intensity for outer lane before and after updating using four traffic states for VDMS.

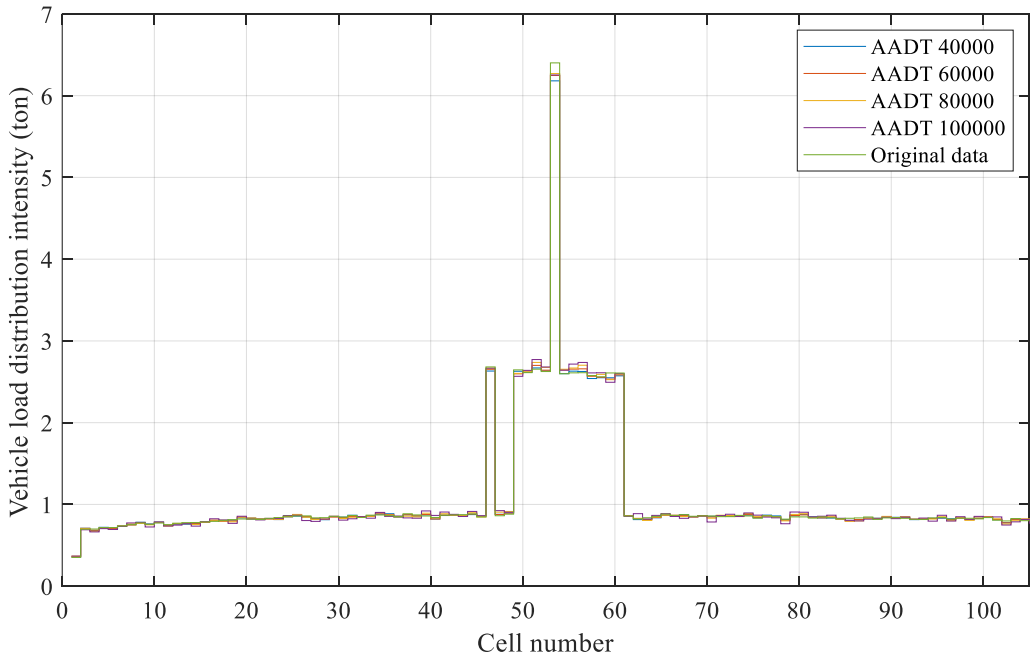

Figure A-10 Distribution of vehicle load intensity for inner lane before and after updating using four traffic states for VDMS.

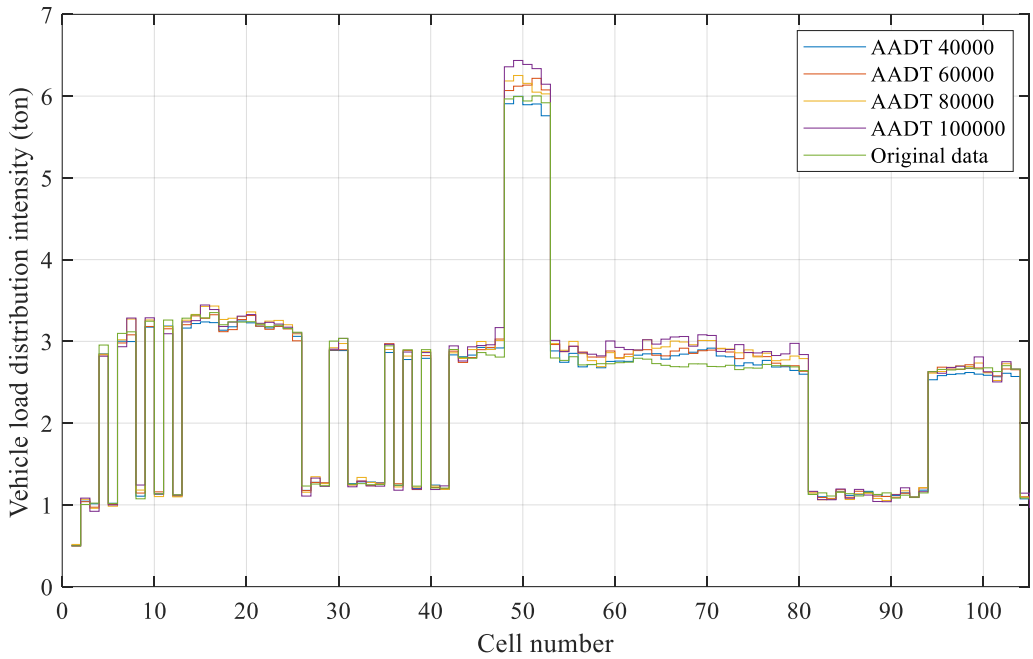

Figure A-11 Distribution of vehicle load intensity for outer lane before and after updating using four traffic states for LDTP.

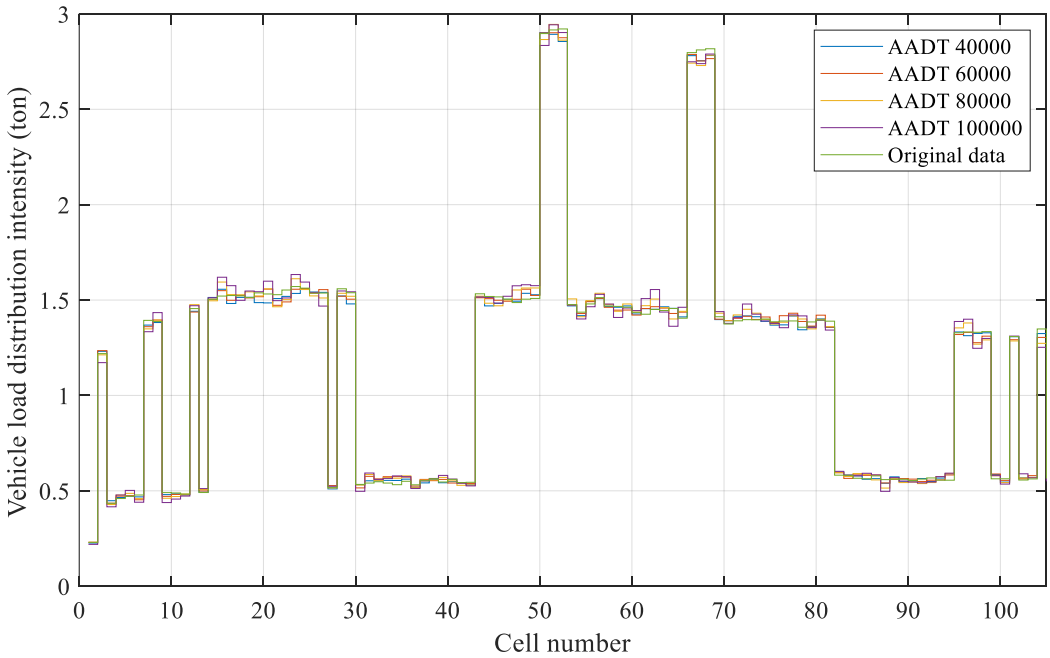

Figure A-12 Distribution of vehicle load intensity for inner lane before and after updating using four traffic states for LDTP.

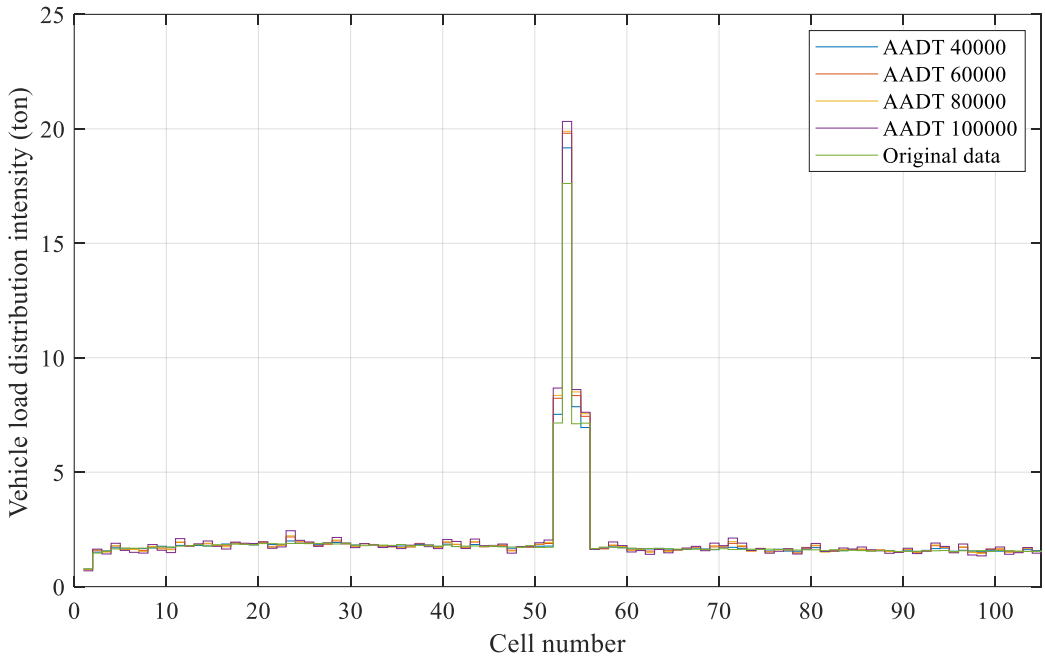

Figure A-13 Distribution of vehicle load intensity for outer lane before and after updating using four traffic states for BMMS.

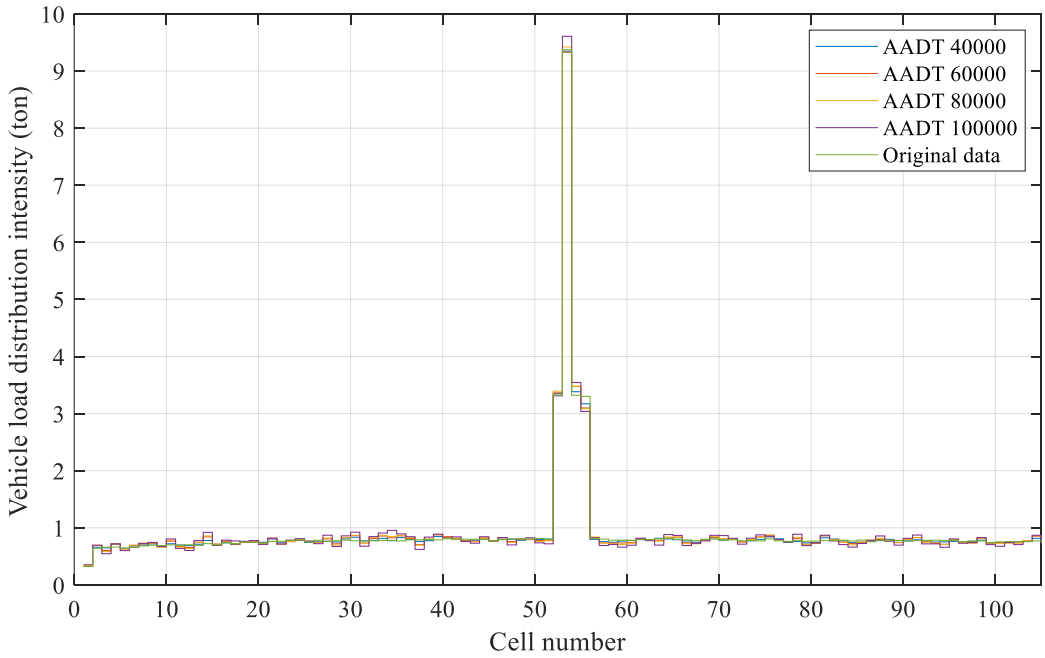

Figure A-14 Distribution of vehicle load intensity for inner lane before and after updating using four traffic states for BMMS.

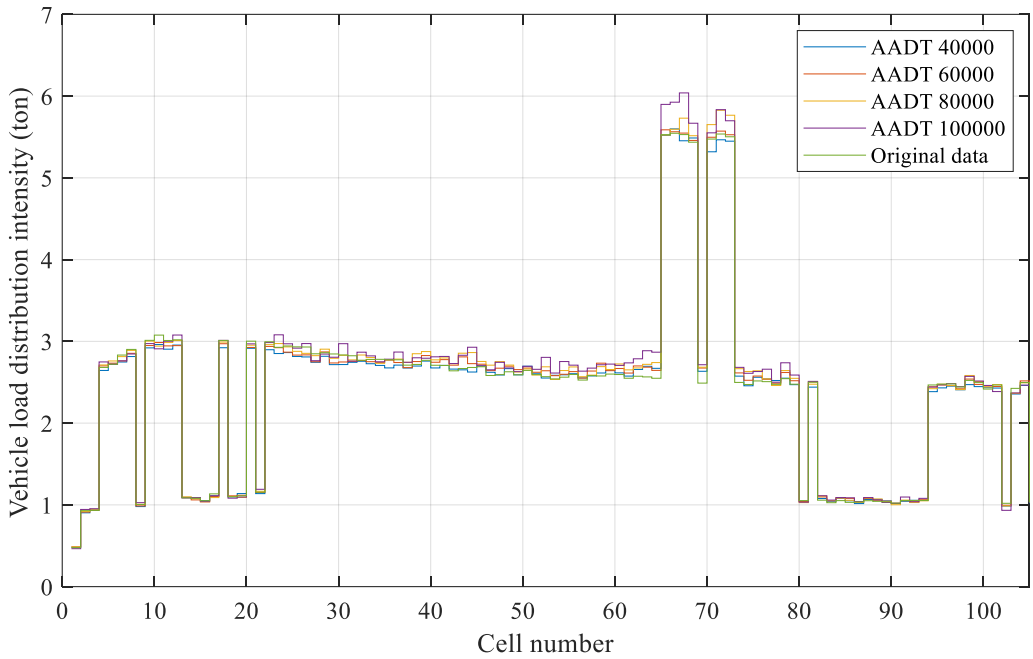

Figure A-15 Distribution of vehicle load intensity for outer lane before and after updating using four traffic states for BMBP.

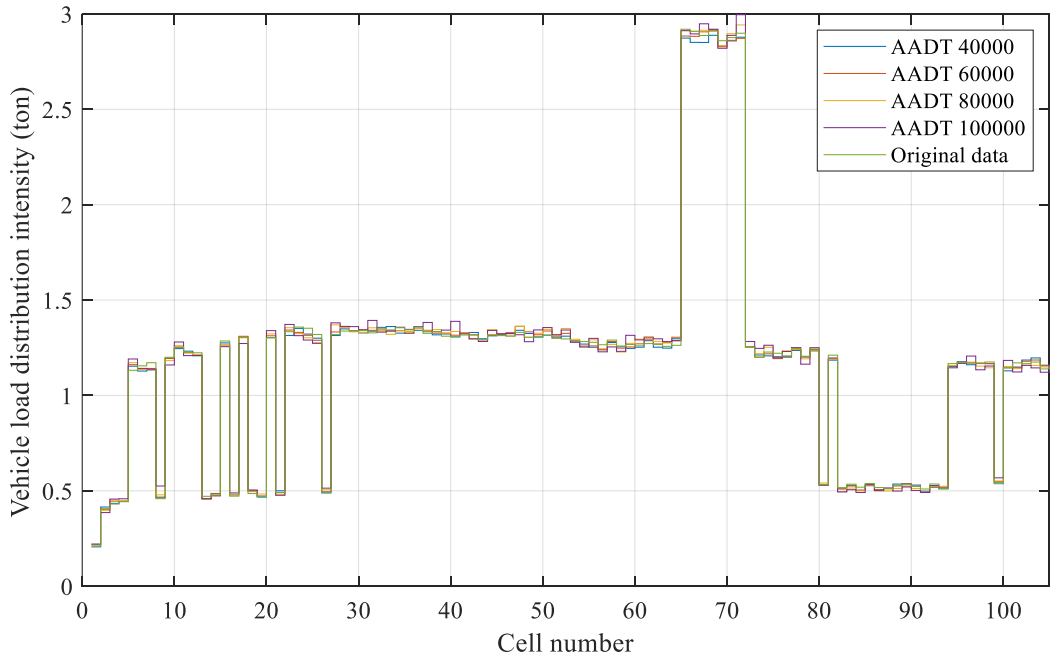

Figure A-16 Distribution of vehicle load intensity for inner lane before and after updating using four traffic states for BMBP.

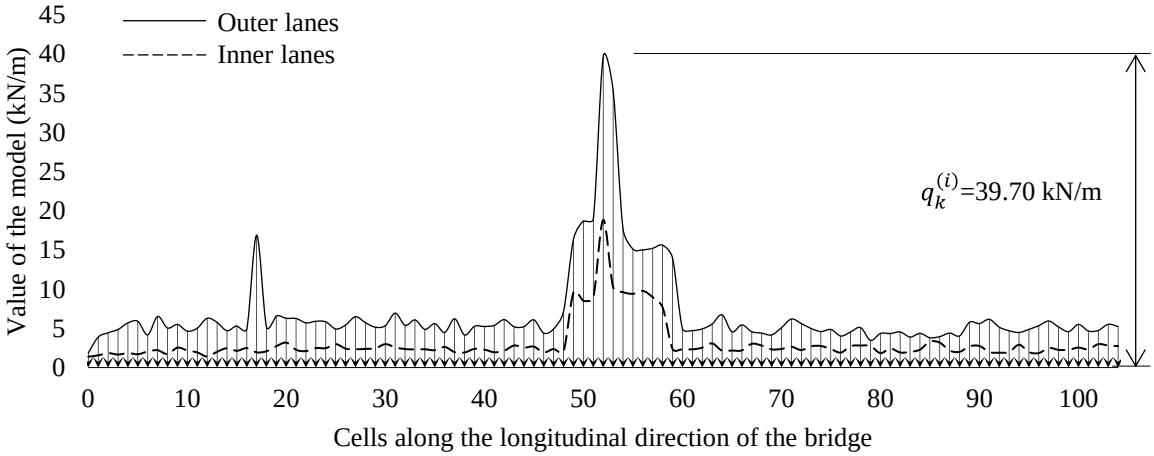

Figure A-17 Updated extreme response scenario load model under AADT = 100000 of AFC.

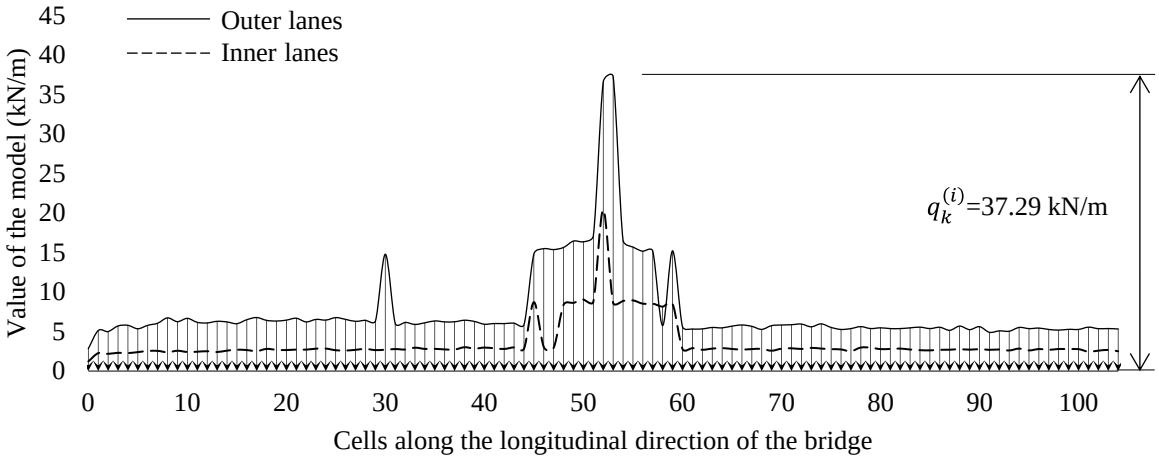

Figure A-18 Updated extreme response scenario load model under AADT = 100000 of VDMS.

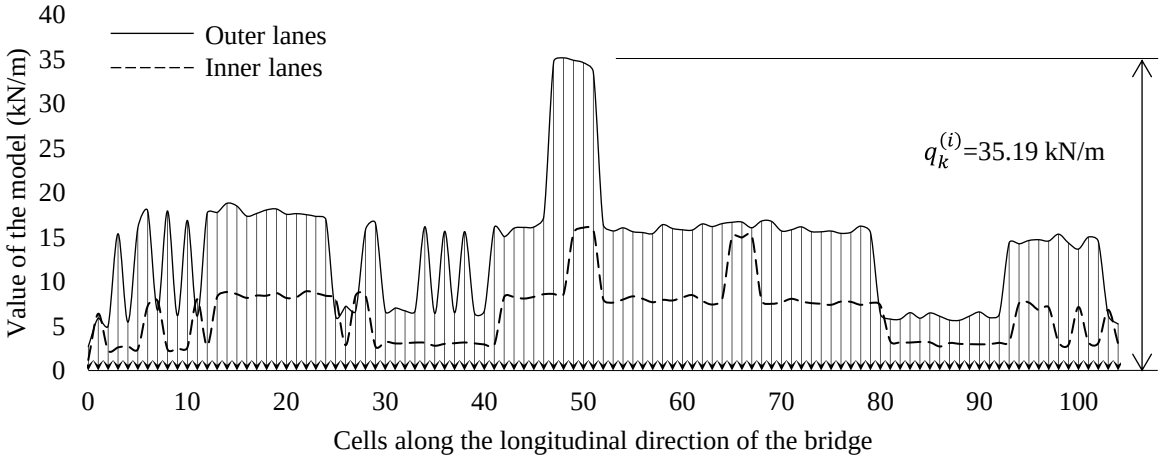

Figure A-19 Updated extreme response scenario load model under AADT = 100000 of LDTP.

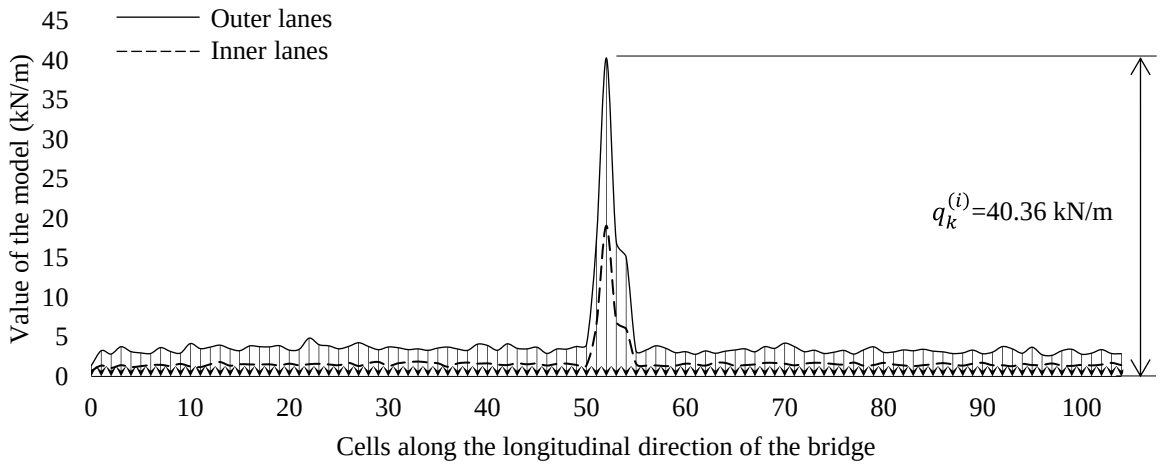

Figure A-20 Updated extreme response scenario load model under AADT = 100000 of BMMS.

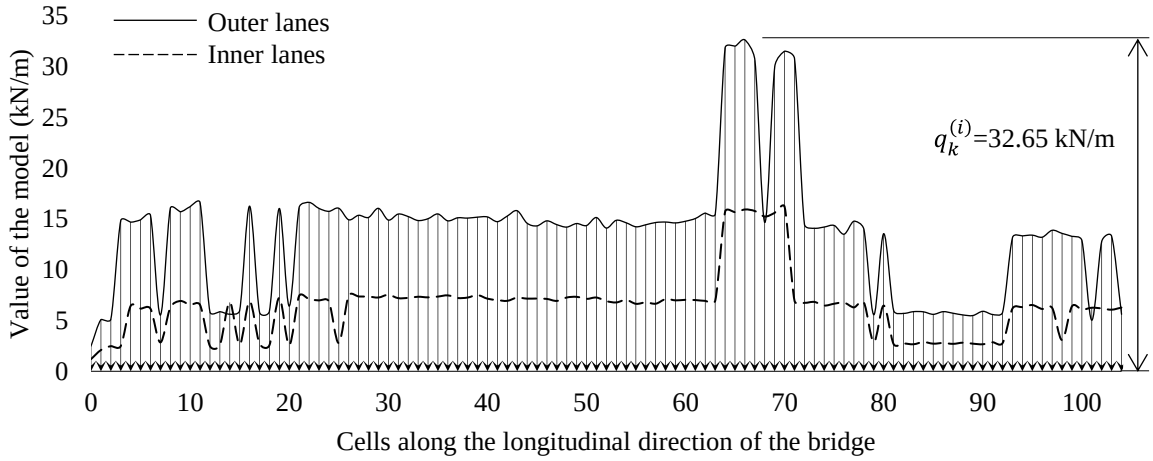

Figure A-21 Updated extreme response scenario load model under AADT = 100000 of BMBP.

Table A-1 The parameters of Poisson processes for vehicle location model of AFC (veh).

λ of Poisson process		Cell number		
		1-49, 59-105	50-52, 54-58	53, 54
Outer lanes	Stationary		4.6537	
	Non-stationary	3.6820	13.2221	29.3900
λ of Poisson process		Cell number		
		1-49, 59-105	50-52, 54-58	53, 54
Inner lanes	Stationary		1.9356	
	Non-stationary	1.4658	6.0453	14.1579

where outer lanes include lane 1 and 6, inner lanes include lane 2 to lane 5.

Table A-2 The parameters of Poisson processes for vehicle location model of VDMS (veh).

λ of Poisson process		Cell number		
		1-30,32,35-45,62-105	31,33,34,46-52,55-61	53,54
Outer lanes	Stationary		4.8593	
	Non-stationary	3.5690	8.9435	25.6294
λ of Poisson process		Cell number		
		1-29,31,32,34-41,43,45,47,48,61-67,70,71,73-105	30,33,42,44,46,49-51,55-60,68-69,72	52-54
Inner lanes	Stationary		2.0491	
	Non-stationary	1.4258	3.5664	11.1082

where outer lanes include lane 1 and 6, inner lanes include lane 2 to lane 5.

Table A-3 The parameters of Poisson processes for vehicle location model of LDTP (veh).

λ of Poisson process		Cell number		
		1-15,19,23-43,58,77-95,97-105	16-18,20-22,44-47,49,52-57,59-76,96	48,50,51
Outer lanes	Stationary		5.2128	
	Non-stationary	3.1498	8.2225	14.4799
λ of Poisson process		Cell number		
		1-13,23-44,56,58,78-105	14-22,45-49,53-55,57,59-65,69-77	50-52,66-68
Inner lanes	Stationary		2.2252	
	Non-stationary	1.2507	3.4222	5.9988

where outer lanes include lane 1 and 6, inner lanes include lane 2 to lane 5.

Table A-4 The parameters of Poisson processes for vehicle location model of BMMS (veh).

λ of Poisson process		Cell number		
		1-50, 56-105	51, 52, 54, 55	53
Outer lanes	Stationary		4.2139	
	Non-stationary	3.4082	14.4592	43.8121
λ of Poisson process		Cell number		
		1-50, 56-105	51, 52, 54, 55	53
Inner lanes	Stationary		1.7169	
	Non-stationary	1.3584	5.9885	20.4787

where outer lanes include lane 1 and 6, inner lanes include lane 2 to lane 5.

Table A-5 The parameters of Poisson processes for vehicle location model of BMBP (veh).

λ of Poisson process		Cell number		
		1-32,34-38,57,79-95,97-105	33,39-56,58-64,66-70,72-78,96	65,71
Outer lanes	Stationary		5.2459	
	Non-stationary	3.1339	8.2774	13.7145
λ of Poisson process		Cell number		
		1-37,39,42,44,53,55-59,61,78-95,97-105	38,40,41,43,45-52,54,60,62-64,72-77,96	65-71
Inner lanes	Stationary		2.2553	
	Non-stationary	1.4550	3.5579	6.2500

where outer lanes include lane 1 and 6, inner lanes include lane 2 to lane 5.

Table A-6 Parameter of simulated GMM of Effect AFC (tonnes).

GMM *i*-th component	Mean value of Outer lane	Mean value of Inner lane
1	16.98	17.02
2	29.60	29.56
3	60.80	60.66
4	99.71	101.13

Table A-7 Parameter of simulated GMM of Effect VDMS (tonnes).

GMM *i*-th component	Mean value of Outer lane	Mean value of Inner lane
1	16.82	17.18
2	28.96	29.80
3	53.02	61.02
4	78.64	103.81

Table A-8 Parameter of simulated GMM of Effect LDTP (tonnes).

GMM *i*-th component	Mean value of Outer lane	Mean value of Inner lane
1	18.04	16.45
2	45.79	27.69
3	54.97	59.22
4	85.25	97.82

Table A-9 Parameter of simulated GMM of Effect BMMS (tonnes).

GMM *i*-th component	Mean value of Outer lane	Mean value of Inner lane
1	17.77	18.09
2	47.29	51.88
3	84.83	86.82
4	105.44	161.91

Table A-10 Parameter of simulated GMM of Effect BMBP (tonnes).

GMM *i*-th component	Mean value of Outer lane	Mean value of Inner lane
1	18.24	16.93
2	46.88	29.60
3	52.27	59.89
4	88.06	103.54

Appendix 3. Extended application of the proposed extreme response scenario probabilistic model

Five representative long-span cable-stayed bridges with main spans range from 200 to 1000 meters are selected as the research objects to study the influence of the span length on maximum values of representative load effects and respective loading patterns and load intensities. They are all typical cable-stayed bridges with two towers and multiple lanes. A finite element software is used to model and analyze these bridges, calculate their influence lines of five effects and to obtain their maximum values according to the Chinese code D60 and the actual traffic flow loading. The span information and actual size comparison of the bridges are shown in **Figure A-22**. In the research, the following effects are selected as the more representative: the axial force of the longest cable (AFC, Effect 1), the vertical deflection of the main girder at mid-span of the main span (VDMS, Effect 2), the longitudinal displacement at the top of the pylon (LDTP, Effect 3), the bending moment of the main girder at mid-span of the main span (BMMS, Effect 4), and the bending moment at the bottom of the pylon (BMBP, Effect 5).

Based on the extreme response scenario model proposed in the thesis, the values and forms of the load models constructed for the five effects of the four other bridges (not included in chapter 5) based on the same measured WIM data, with an AADT of 40000 vehicles are shown in **Table A-11**, **Figures A-23** to **A-42**. It can be seen that the same effect for different spans of cable-stayed bridges has an approximate pattern of load distribution on the bridge deck for the extreme response scenario, mainly because of the similarity on the respective influence lines as presented in **Figures A-44** to **A-48**. In summary, the extreme response scenario load distribution for the BMMS (Effect 4) tends to be concentrated near the center of the span, while the LDTP (Effect 3) and BMBP (Effect 5) tend to have a more dispersed load distribution. Comparing the load values $q_k^{(i)}$, it can be seen that the smaller the span-length, the larger the peak load value for the same effect on the cable-stayed bridge. This is in accordance to several traffic load model codes that recommend to decrease the load intensity as the span-length increases.

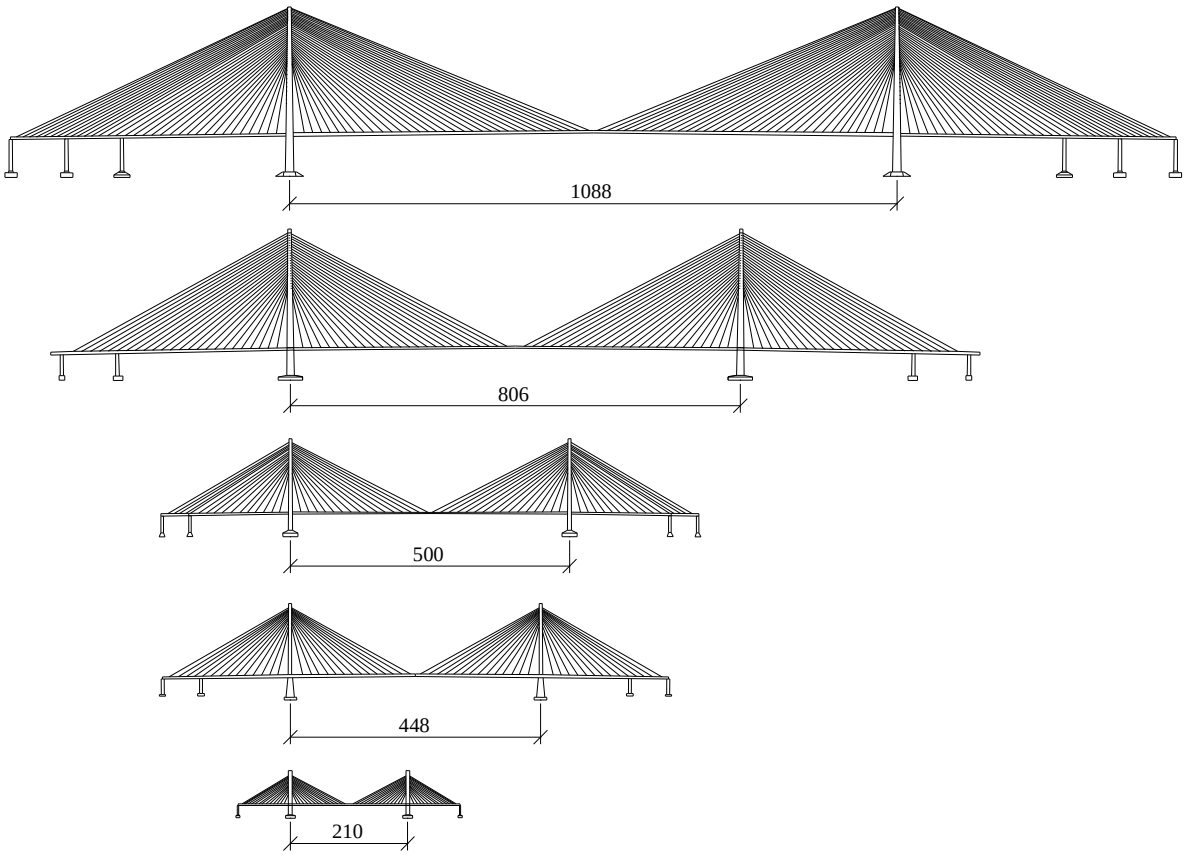

Figure A-22 Five long-span cable-stayed bridges with different span lengths (m).

Table A-11 Load intensity and load form schematic diagram of traffic model for different structural effects of different bridges (AADT= 40000).

Bridge and span length		AFC	VDMS	LDTP	BMMS	BMBP
Load intensity $q_k^{(i)}$ (Unit: kN/m)		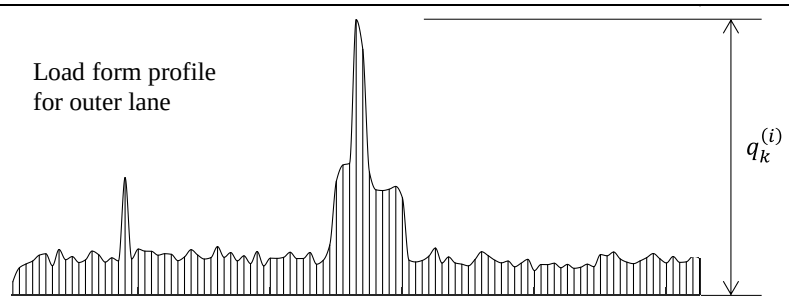				
Bridge 1	1088 m	24.07	22.89	18.85	29.54	17.21
Bridge 2	806 m	33.83	29.38	11.05	45.56	14.11
Bridge3	500 m	36.84	31.39	16.61	72.76	23.50
Bridge4	448 m	37.66	43.37	18.04	85.66	16.27
Bridge5	210 m	46.39	47.38	37.25	79.13	34.65

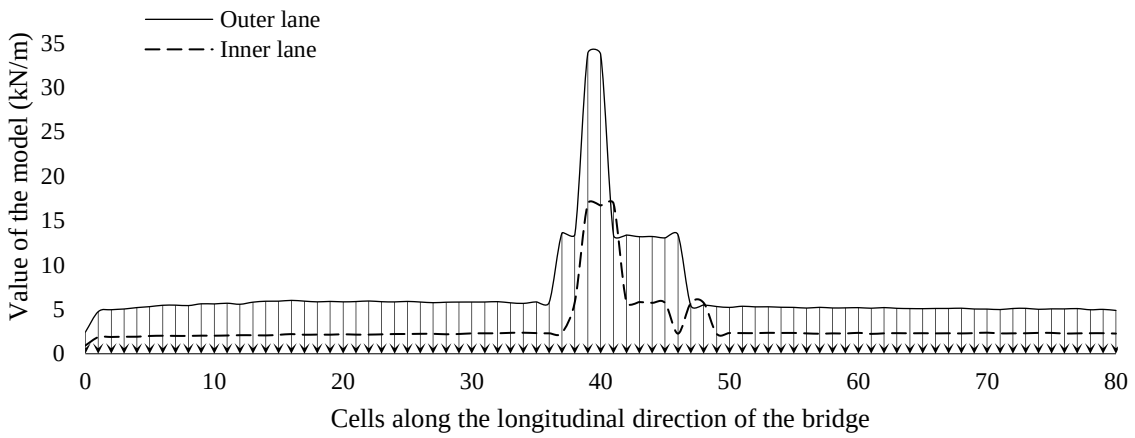

Figure A-23 Extreme response scenario load model of AFC for Bridge 2.

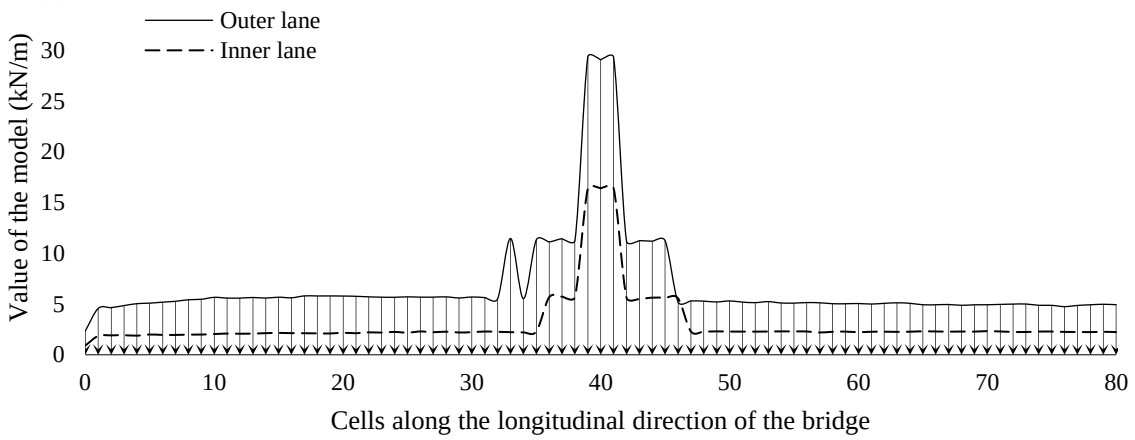

Figure A-24 Extreme response scenario load model of VDMS for Bridge 2.

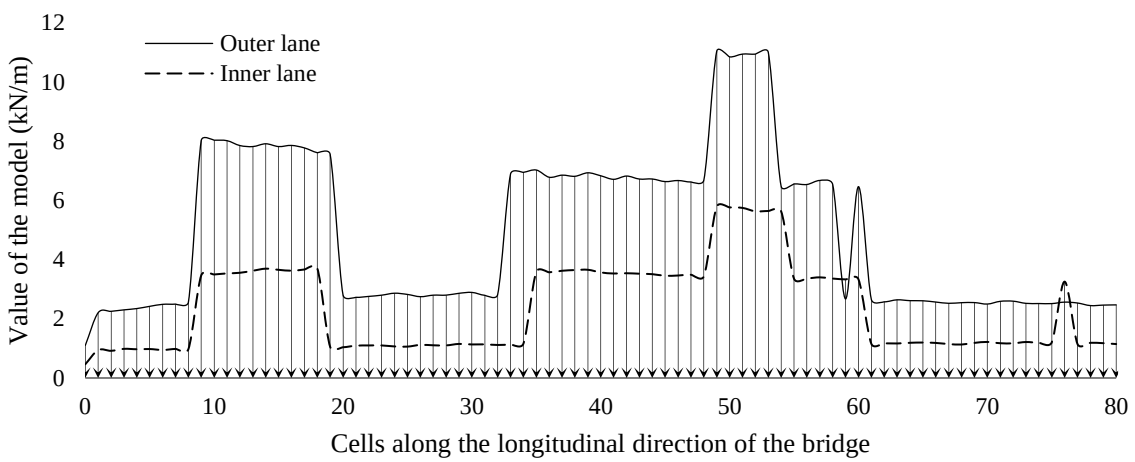

Figure A-25 Extreme response scenario load model of LDTP for Bridge 2.

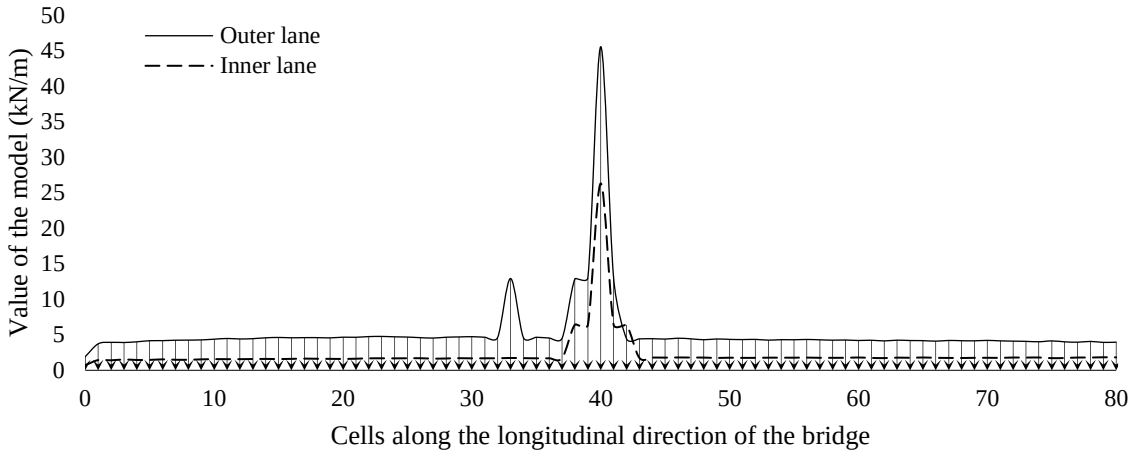

Figure A-26 Extreme response scenario load model of BMMS for Bridge 2.

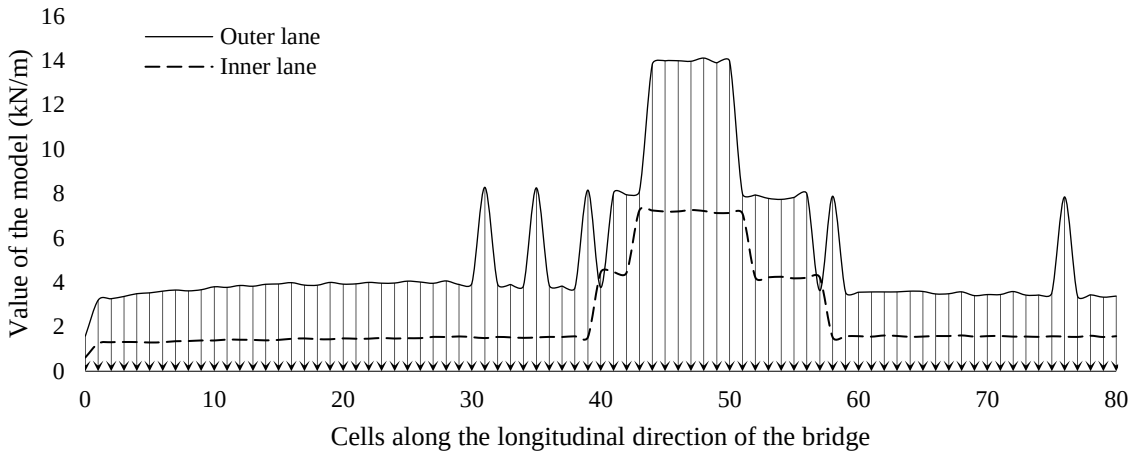

Figure A-27 Extreme response scenario load model of BMBP for Bridge 2.

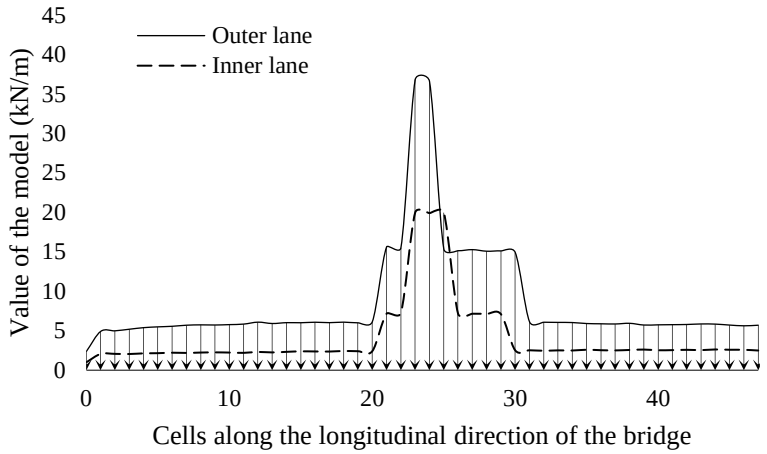

Figure A-28 Extreme response scenario load model of AFC for Bridge 3.

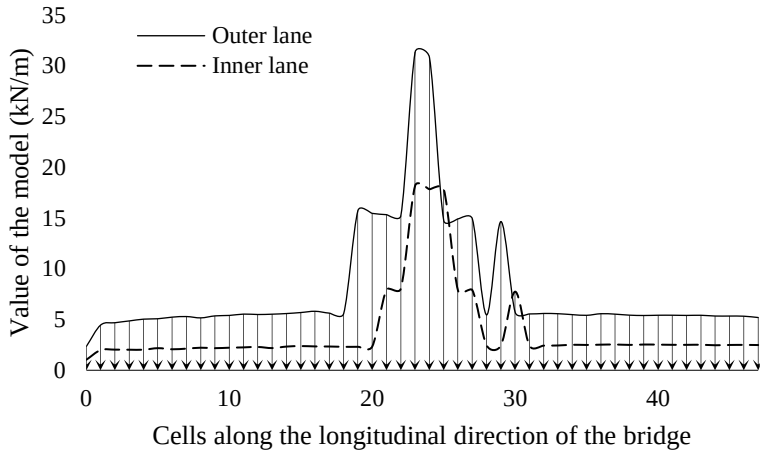

Figure A-29 Extreme response scenario load model of VDMS for Bridge 3.

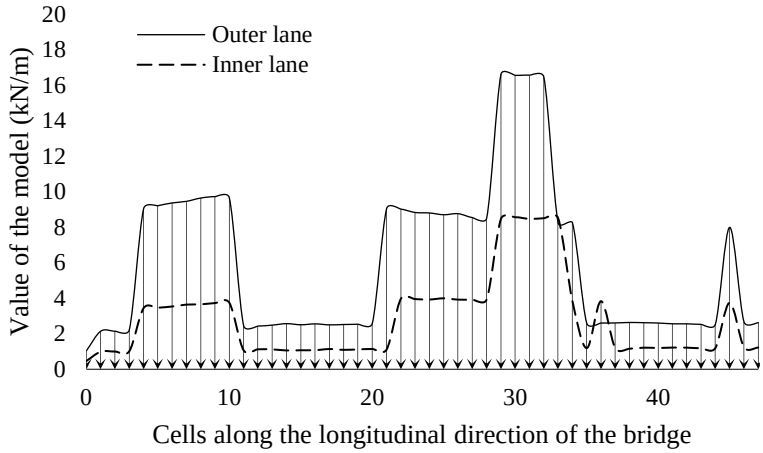

Figure A-30 Extreme response scenario load model of LDTP for Bridge 3.

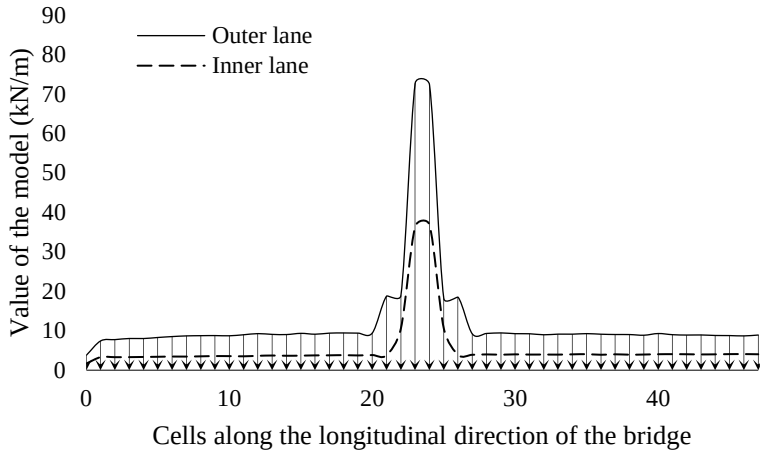

Figure A-31 Extreme response scenario load model of BMMS for Bridge 3.

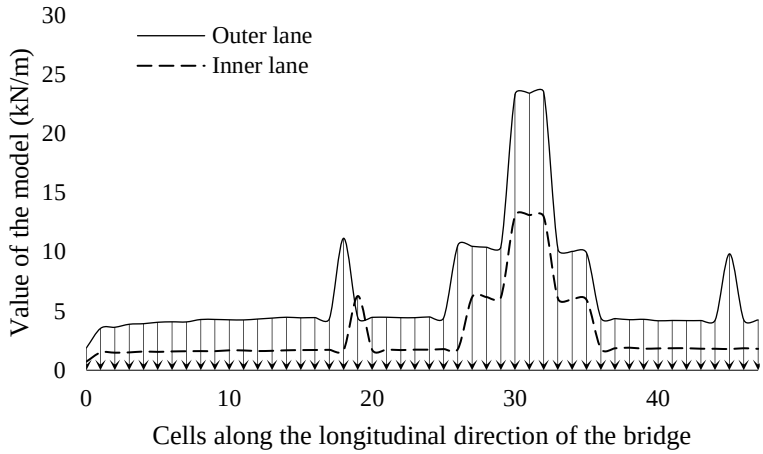

Figure A-32 Extreme response scenario load model of BMBP for Bridge 3.

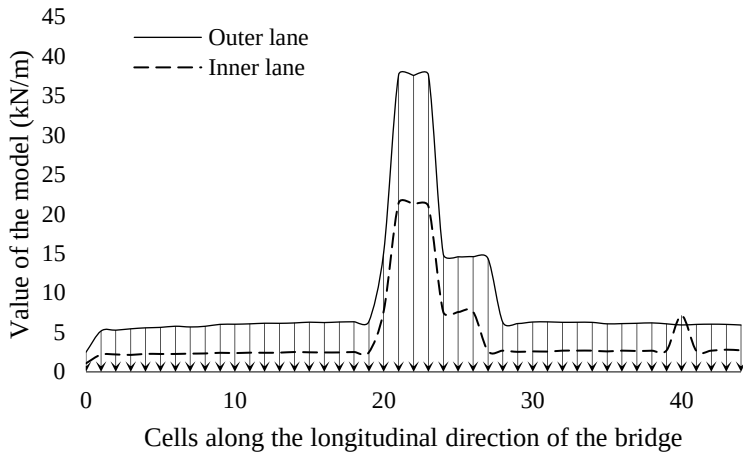

Figure A-33 Extreme response scenario load model of AFC for Bridge 4.

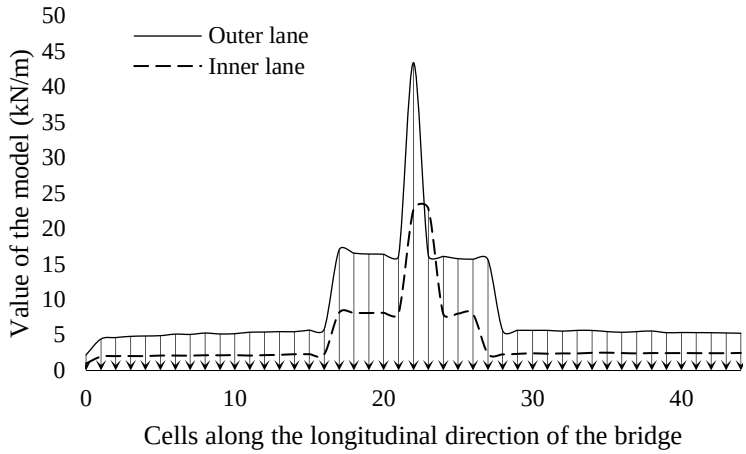

Figure A-34 Extreme response scenario load model of VDMS for Bridge 4.

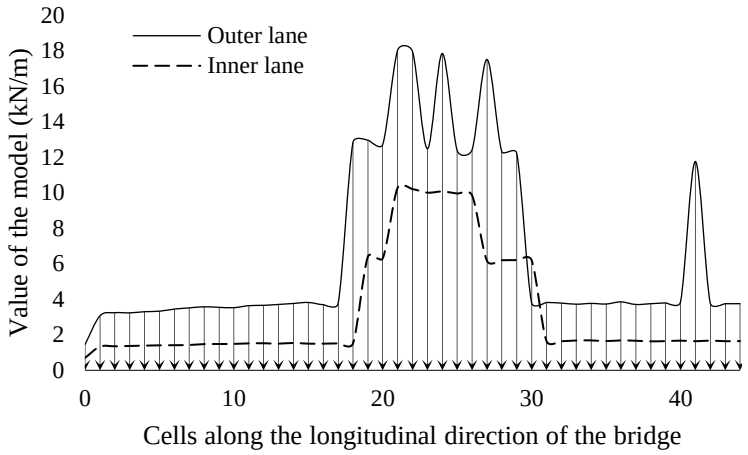

Figure A-35 Extreme response scenario load model of LDTP for Bridge 4.

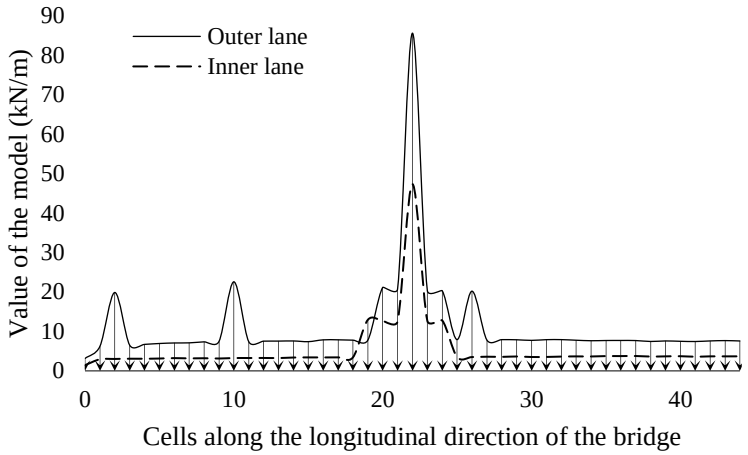

Figure A-36 Extreme response scenario load model of BMMS for Bridge 4.

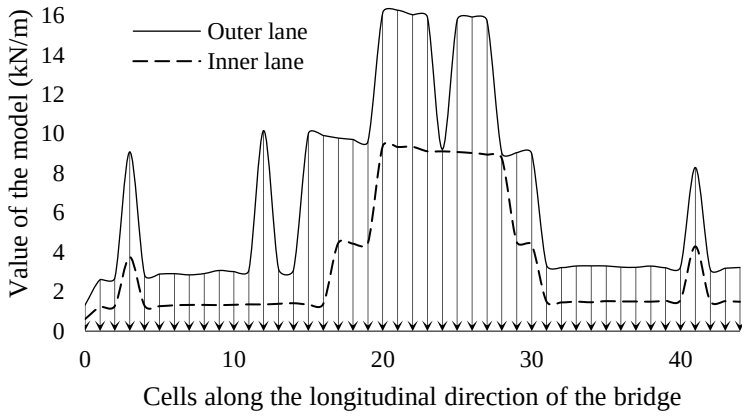

Figure A-37 Extreme response scenario load model of BMBP for Bridge 4.

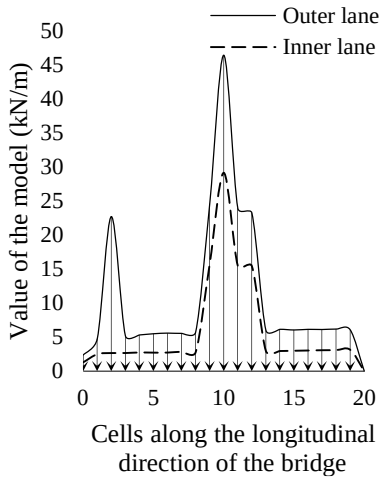

Figure A-38 Extreme response scenario load model of AFC for Bridge 5.

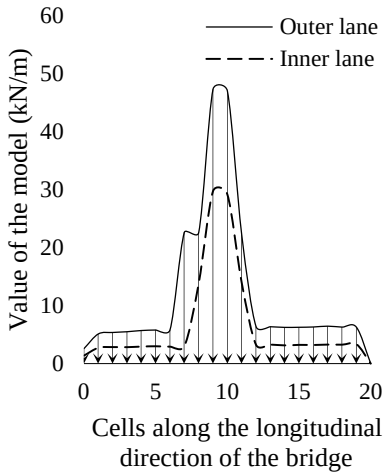

Figure A-39 Extreme response scenario load model of VDMS for Bridge 5.

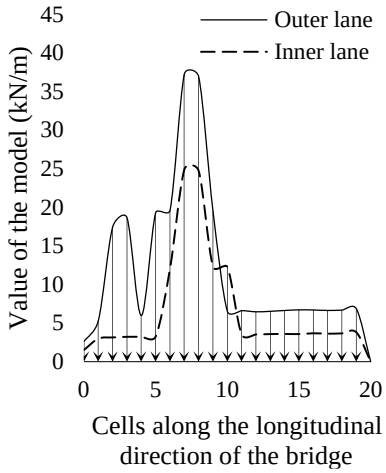

Figure A-40 Extreme response scenario load model of LDTP for Bridge 5.

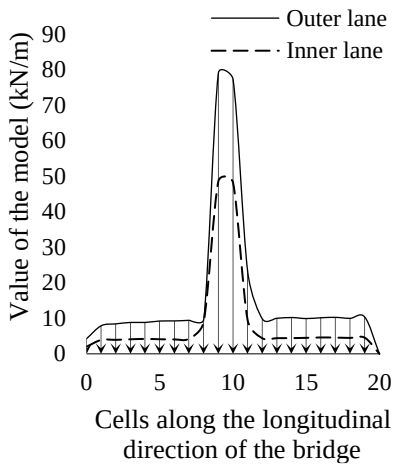

Figure A-41 Extreme response scenario load model of BMMS for Bridge 5.

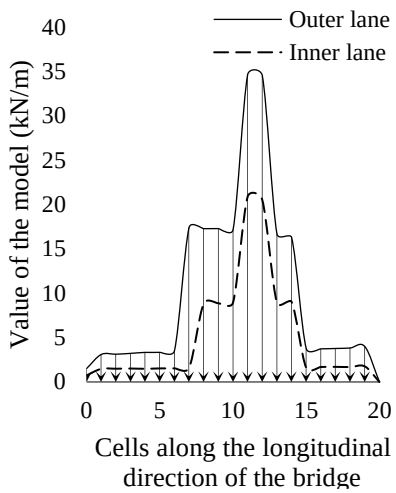

Figure A-42 Extreme response scenario load model of BMBP for Bridge 5.

Table A-12 and **A-13** show the total load on the bridge deck for the extreme response scenario model and the code D60, and **Table A-14** and **A-15** give the average load per unit bridge length for the extreme response scenario model and D60. The ratio of the load per unit bridge length between the extreme scenario model and D60 is also plotted in **Figure A-43**. Based on the tables and figure, the average load per unit bridge length for different spans with different effects is discussed. As the bridge span decreases, the average load per unit bridge length shows an overall increasing trend.

In summary, we can conclude that for most of the effects, the extreme scenarios for the shorter span bridges are subjected to relatively larger average loading per unit length. This may be due to the higher randomness of the traffic loads, where heavy vehicle aggregation and queuing situations

in the traffic flow are the ones more likely to cause extreme values of structural effects. However, heavy vehicle aggregations of less than ten vehicles are relatively common, while heavy vehicle aggregations of a dozen or more vehicles are uncommon (except in congestion, and the proportion of heavy vehicles in congestion is usually much smaller than in normal free flow). If a specific bridge length is used to frame the traffic flow, it is easier for the shorter bridge to obtain a segment of traffic where the whole length of the bridge is congested with heavy vehicles, while it is more difficult to obtain a segment of traffic where the whole length of the bridge is congested with heavy vehicles for longer bridges. Therefore, for long-span bridges of different lengths, the longer the bridge length, the smaller the average load of the extreme response scenario. It is important to note that the above analyses are all discussed for the site-specific extreme response scenario, which represents the extreme scenario when the actual WIM data is applied and is the true load scenario that the bridge may be subjected to during operation. In contrast, the average load per bridge length under code D60 (**Table A-14**) does not show significant differences between the span-specific scenarios and is not consistent with the extreme scenario case of the actual WIM data. These findings reveal the characteristics of the load levels of extreme response scenarios for different span bridges under different effects and can further guide bridge design and optimization. In practical applications, for different bridge types and spans, targeted load model can be built according to the specific loading conditions to ensure the safety of the bridge, and the extreme response scenario load model presented in this thesis can provide a powerful tool for this purpose.

Table A-12 Total load on the bridge deck of D60 (tonnes).

i-th bridge	Span (m)	AFC	VDMS	LDTP	BMMS	BMBP
Bridge 1	1088	3397	2560	4171	3204	2560
Bridge 2	806	3173	2587	3238	1049	2652
Bridge 3	500	2110	1312	1910	1312	1445
Bridge 4	448	1777	1511	1844	979	1445
Bridge 5	210	922	787	1191	384	855

Table A-13 Total load on the bridge deck of the proposed model (tonnes).

i-th bridge	Span (m)	AFC	VDMS	LDTP	BMMS	BMBP
Bridge 1	1088	3650	3949	6327	2494	6181
Bridge 2	806	4196	4169	3129	3123	3291
Bridge 3	500	3196	3020	2246	4412	2418
Bridge 4	448	3167	3036	2370	3967	2432
Bridge 5	210	1854	2070	2084	2801	1692

Table A-14 Load per unit bridge length on the bridge deck of D60 (tonnes/m).

i-th bridge	Span (m)	AFC	VDMS	LDTP	BMMS	BMBP
Bridge 1	1088	1.62	1.22	1.99	1.53	1.22
Bridge 2	806	1.96	1.60	2.00	0.65	1.64
Bridge 3	500	2.20	1.37	1.99	1.37	1.50
Bridge 4	448	1.97	1.68	2.05	1.09	1.61
Bridge 5	210	2.30	1.97	2.98	0.96	2.14

Table A-15 Load per unit bridge length on the bridge deck of the proposed model (tonnes/m).

i-th bridge	Span (m)	AFC	VDMS	LDTP	BMMS	BMBP
Bridge 1	1088	1.74	1.88	3.01	1.19	2.94
Bridge 2	806	2.59	2.57	1.93	1.93	2.03
Bridge 3	500	3.33	3.15	2.34	4.60	2.52
Bridge 4	448	3.52	3.37	2.63	4.41	2.70
Bridge 5	210	4.63	5.18	5.21	7.00	4.23

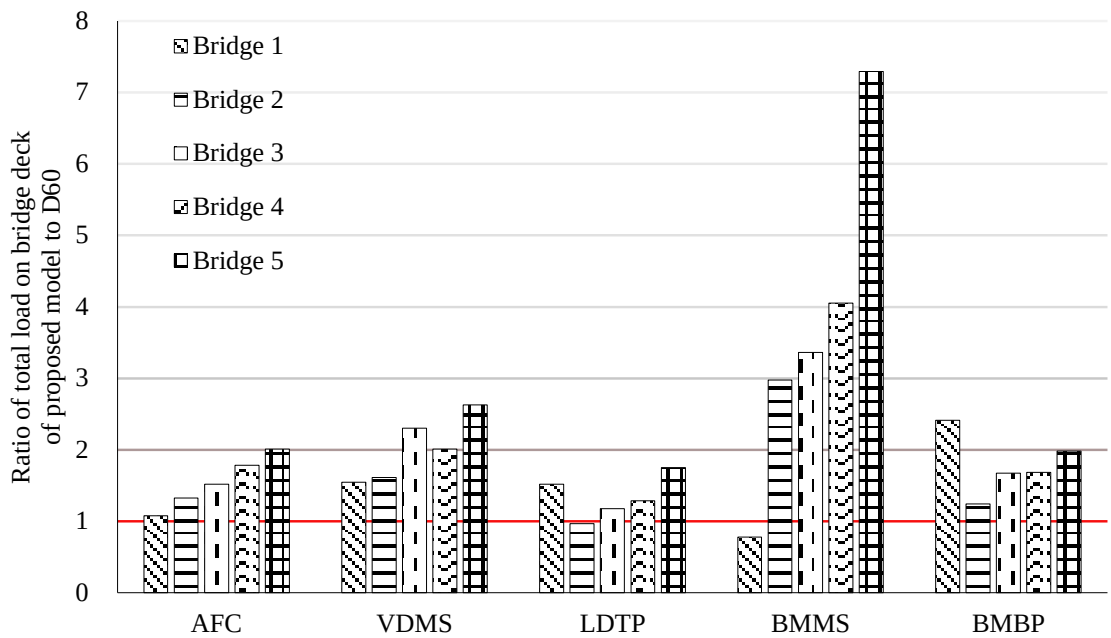

Figure A-43 Ratio of total load on the bridge deck of the proposed traffic model to D60.

Figure A-44 to **A-48** show the influence line shapes of the five bridges from Effect 1 to Effect 5. The influence lines of the five bridges of each effect are normalized by length and maximum value and then placed in the same figure to compare their trends. It can be seen that except for the influence line of bridge 5 in Effect 3, the influence lines of other effects all show similar shape trends. The influence lines of Effect 1 and Effect 2 are generally similar, and the peak of the influence line appears in the mid-span area, and the peak area is wider. The influence lines of

Effect 3 and Effect 5 are generally similar, and the influence values are distributed with large values in the whole bridge length. In Effect 4, the peak of the influence line appears in the mid-span area, and the peak area is narrow.

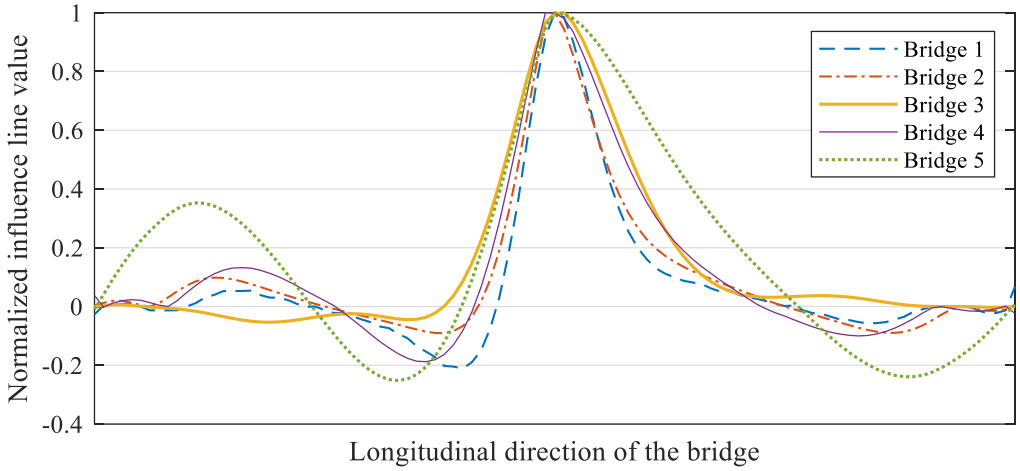

Figure A-44 Influence line shapes of AFC for five bridges.

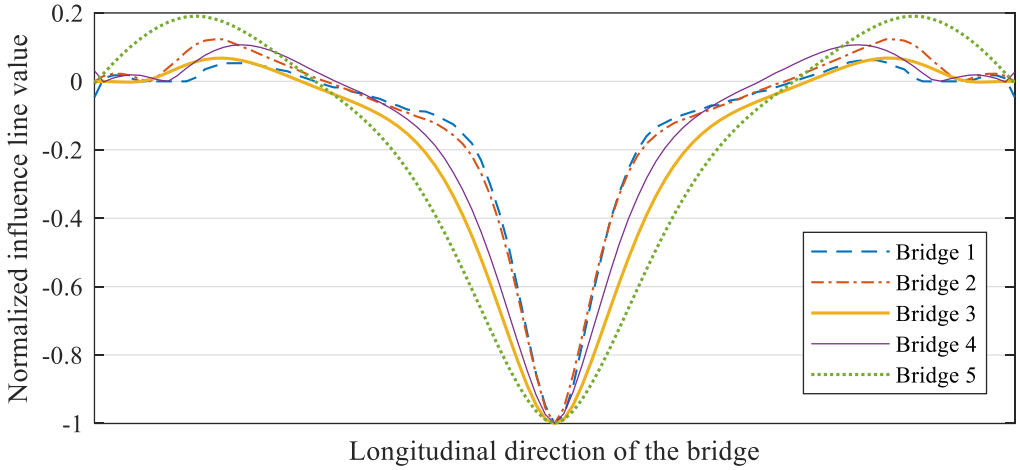

Figure A-45 Influence line shapes of VDMS for five bridges.

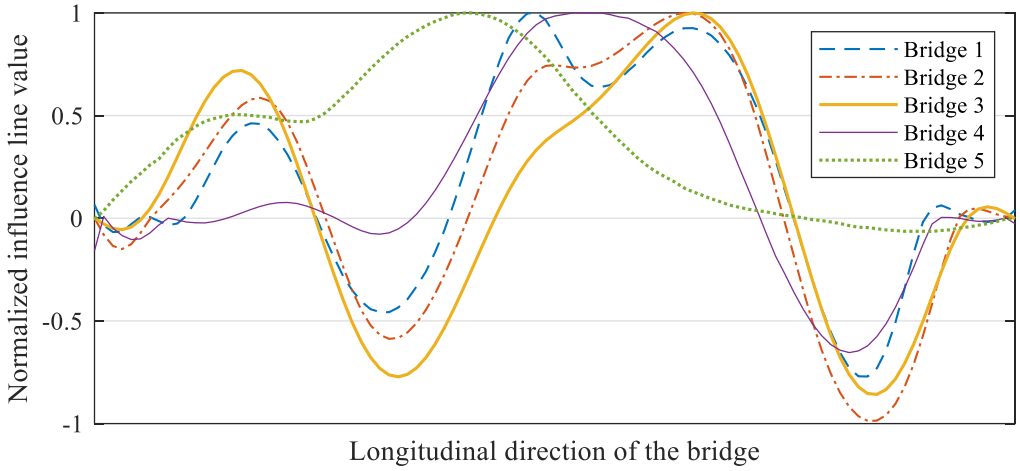

Figure A-46 Influence line shapes of LDTP for five bridges.

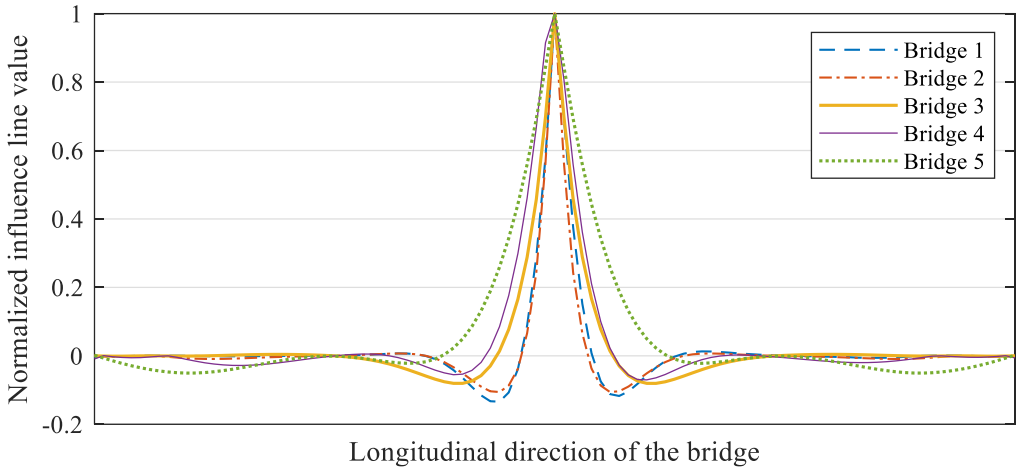

Figure A-47 Influence line shapes of BMMS for five bridges.

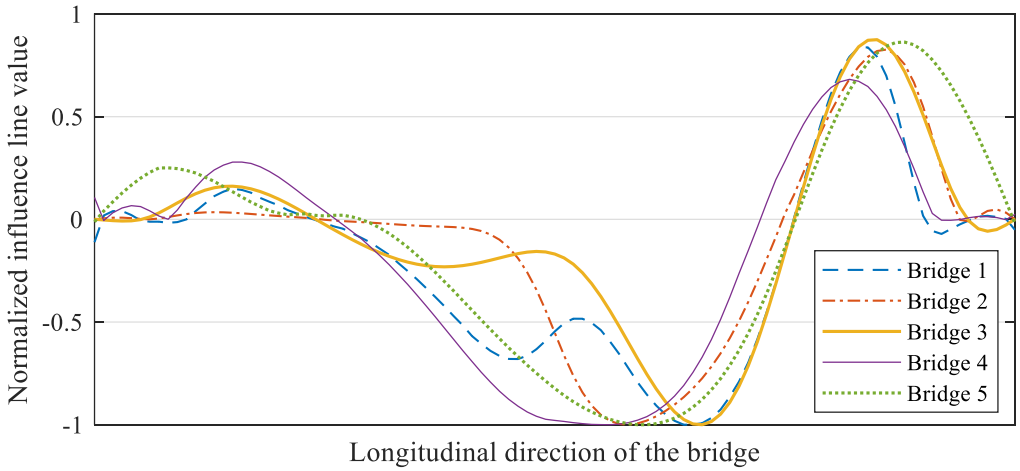

Figure A-48 Influence line shapes of BMBP for five bridges.